AD-A148 480 STRUCTURE OF SOLIDS SURFACES IN WEAR SITUATIONS(U) 1/2
RENSSELAER POLYTECHNIC INST TROY N Y DEPT OF MECHANICAL
ENGINEERING J L LAUER 17 OCT 84 AFOSR-TR-84-0970
UNCLASSIFIED AFOSR-81-0005 F/G 11/8 NL

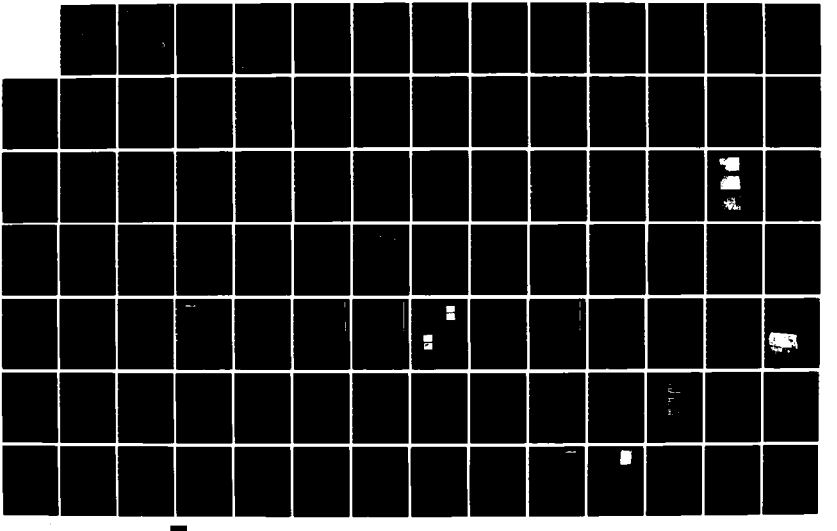

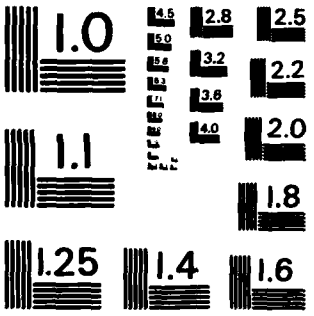

MICROCOPY RESOLUTION TEST CHART
NATIONAL BUREAU OF STANDARDS - 1963 - A

UNCLASSIFIED

SECURITY CLASSIFICATION OF THIS PAGE (When Data Entered)

OCT 84

(13)

REPORT DOCUMENTATION PAGE	READ INSTRUCTIONS BEFORE COMPLETING FORM
1. REPORT NUMBER AFOSR-TR- 84-0970	2. GOVT ACCESSION NO. / 3. RECIPIENT'S CATALOG NUMBER
4. TITLE (and Subtitle) Structure of Solids Surfaces in Wear Situations	5. TYPE OF REPORT & PERIOD COVERED Final Report
	6. PERFORMING ORG. REPORT NUMBER
7. AUTHOR(s) James L. Lauer	8. CONTRACT OR GRANT NUMBER(s) AFOSR-81-0005
9. PERFORMING ORGANIZATION NAME AND ADDRESS Dept. of Mechanical Engineering Rensselaer Polytechnic Institute Troy, NY 12180-3590	10. PROGRAM ELEMENT, PROJECT, TASK AREA & WORK UNIT NUMBERS 61102F 2303/A2
11. CONTROLLING OFFICE NAME AND ADDRESS Directorate of Chemical Sciences Air Force of Scientific Res. (AFSC) Bolling Air Force Base, DC 20332	12. REPORT DATE October 17, 1984
	13. NUMBER OF PAGES 121
14. MONITORING AGENCY NAME & ADDRESS(if different from Controlling Office) AD-A148 480	15. SECURITY CLASS. (of this report) Unclassified
	15a. DECLASSIFICATION/DOWNGRADING SCHEDULE

16. DISTRIBUTION STATEMENT (of this Report)

Approved for public release; distribution unlimited.

17. DISTRIBUTION STATEMENT (of the abstract entered in Block 20, if different from Report)

DTIC ELECTE DEC 10 1984 S E D

18. SUPPLEMENTARY NOTES

19. KEY WORDS (Continue on reverse side if necessary and identify by block number)

Interference microspectrometry, Ellipsometry, Speckle contrast, Wear, Surface Profilometry, Auger electron spectroscopy, Jet Fuel Deposits, Infrared emission spectroscopy, Surface Analysis, Surface oxidation

20. ABSTRACT (Continue on reverse side if necessary and identify by block number)

Identification and understanding of the surface phenomena involved in lubrication and wear are necessary if failures are to be avoided or at least mitigated. Failure of lubrication and high wear rates can be very costly to both civilian and military machinery.

While many new methods of surface analysis have been developed in recent

DD FORM 1 JAN 73 1473

UNCLASSIFIED

SECURITY CLASSIFICATION OF THIS PAGE (When Data Entered)

DTIC FILE COPY

84 11 16 024

years, their requirements of ultrahigh vacuum and of electron bombardment make these methods destructive. Furthermore they mostly furnish only elemental analysis and then their spatial resolution is not high. For some of our work we have been fortunate in having access to a scanning Auger electron spectrophotometer (AES); its best spatial resolution of about 50 μm is rather high. However, most of our analyses were carried out with spatial resolutions better than 20 μm and they made use of (i) a phase-locked interference microscope (PLIM), (ii) an electronic Faraday-modulated ellipsometer (EFME), (iii) speckle-contrast (SC), and (iv) friction and lubricant thickness measurements with a ball-on-plate sliding contact. All this apparatus was of our ultimate design and it was assembled and completed in the search for significant surface changes in a bearing operated on its way to failure except--for SC, which was studied for applicability to metal-gas reactions. The design and construction of the PLIM and EFME are major accomplishments to this project.

A realistic system was selected for these wear studies; an operating bearing contact consisting of a loaded M-50 bearing steel ball-on-plate mock-bearing and lubricants simulating MIL 23699 and its additives, i.e. a most common heavily loaded bearing system. The mock-bearing had dimensions such that the width of the wear track was amenable to our surface analyses.

Significant changes were found (i) in the changes of the surface profile within the wear track over the course of bearing operation for different lubricants, (ii) in the rate of oxidation of the steel bearing surface within and without the wear track, (iii) in the rate of the change of optical profile within and without the wear track after a brief exposure to dilute hydrochloric acid, and (iv) in the friction for different lubricants. Common surface additives in lubricants, such as tricresylphosphate (antiwear) and benzotriazole (anticorrosion), produced larger profile changes then other common lube additives. Invariably these changes could be associated with the more rapid formation of surface oxides within than without the wear track.

The hydrochloric acid probe reaction changing the surface profile could become a convenient and useful test for bearing surface reliability.

The PLIM and EFME instruments developed for this work will prove to be useful in many different applications, not only in the analysis of metal and metal oxide surfaces. The applicability of SC to reaction studies will, however, remain limited to gross changes. For these it can be used from large distances.

As part of this project, but in a separate investigation, jet fuel deposits formed on surfaces of a Jet Fuel Oxidation Tester (JFTOT) were analyzed by infrared emission Fourier microspectrophotometry, a technique we developed under a previous AFOSR grant.

STRUCTURE OF SOLID SURFACES IN WEAR SITUATIONS

FINAL REPORT ON

Grant No. AFOSR-81-0005

to the Air Force Office of Scientific Research

by

JAMES L. LAUER

Department of Mechanical Engineering,
Aeronautical Engineering & Mechanics
Rensselaer Polytechnic Institute
Troy, NY 12180-3590

October 17, 1984

TABLE OF CONTENTS

COMPLETED PROJECT SUMMARY

1. TITLE: Structure of Solid Surfaces in Wear Situations

2. PRINCIPAL INVESTIGATOR: Dr. James L. Lauer
Department of Mechanical Engineering,
Aeronautical Engineering and Mechanics
Rensselaer Polytechnic Institute
Troy, NY 12181

3. INCLUSIVE DATES: 1 December 1981 - 30 June 1984

4. GRANT NUMBER: AFSOR-81-0005

5. COSTS AND FY SOURCE: $85,555, FY81; $101,995, FY82;
$89,000, FY83

6. SENIOR RESEARCH PERSONNEL: Dr. J. L. Lauer

7. JUNIOR RESEARCH PERSONNEL:

S.S. Fung
P. Vogel
M. Marxer
M. Mailloux

8. PUBLICATIONS: see pages 20-22

9. ABSTRACT OF OBJECTIVES AND ACCOMPLISHMENTS: (see following page)

ABSTRACT OF OBJECTIVES AND ACCOMPLISHMENTS

Identification and understanding of the surface phenomena involved in lubrication and wear are necessary if failures are to be avoided or at least mitigated. Failure of lubrication and high wear rates can be very costly to both civilian and military machinery.

While many new methods of surface analysis have been developed in recent years, their requirements of ultrahigh vacuum and of electron bombardment make these methods destructive. Furthermore they mostly furnish only elemental analysis and then their spatial resolution is not high. For some of our work we have been fortunate in having access to a scanning Auger electron spectrophotometer (AES); its best spatial resolution of about 50 μm is rather high. However, most of our analyses were carried out with spatial resolutions better than 20 μm and they made use of (i) a phase-locked interference microscope (PLIM), (ii) an electronic Faraday-modulated ellipsometer (EFME), (iii) speckle-contrast (SC), and (iv) friction and lubricant thickness measurements with a ball-on-plate sliding contact. All this apparatus was of our ultimate design and it was assembled and completed in the search for significant surface changes in a bearing operated on its way to failure except--for SC, which was studied for applicability to metal-gas reactions. The design and construction of the PLIM and EFME are major accomplishments to this project.

A realistic system was selected for these wear studies; an operating bearing contact consisting of a loaded M-50 bearing steel ball-on-plate mock-bearing and lubricants simulating MIL 23699 and its additives, i.e. a most common heavily loaded bearing system. The mock-bearing had dimensions such that the width of the wear track was amenable to our surface analyses.

Significant changes were found (i) in the changes of the surface profile within the wear track over the course of bearing operation for different lubricants, (ii) in the rate of oxidation of the steel bearing surface within and without the wear track, (iii) in the rate of the change of optical profile within and without the wear track after a brief exposure to dilute hydrochloric acid, and (iv) in the friction for different lubricants. Common surface additives in lubricants, such as tricresylphosphate (antiwear) and benzotriazole (anticorrosion), produced larger profile changes then other common lube additives. Invariably these changes could be associated with the more rapid formation of surface oxides within than without the wear track.

The hydrochloric acid probe reaction changing the surface profile could become a convenient and useful test for bearing surface reliability.

The PLIM and EFME instruments developed for this work will prove to be useful in many different applications, not only in the analysis of metal and metal oxide surfaces. The applicability of SC to reaction studies will, however, remain limited to gross changes. For these it can be used from large distances.

As part of this project, but in a separate investigation, jet fuel deposits formed on surfaces of a Jet Fuel Oxidation Tester (JFTOT) were analyzed by infrared emission Fourier microspectrophotometry, a technique we developed under a previous AFOSR grant.

1. INTRODUCTION

While many new methods of surface analysis have been developed in recent years, their requirements of ultrahigh vacuum and of electron bombardment make these methods destructive. Furthermore they mostly furnish only elemental analysis and then their spatial resolution is not high. For some of our work we have been fortunate in having access to a scanning Auger electron spectrophotometer (AES); its best spatial resolution of about 50 μm is rather high. However, most of our analyses were carried out with spatial resolutions better than 20 μm and they made use of (i) a phase-locked interference microscope (PLIM), (ii) an electronic Faraday-modulated ellipsometer (EFME), (iii) speckle-contrast (SC), and (iv) friction and lubricant thickness measurements with a ball-on-plate sliding contact. All this apparatus was of our own ultimate design and assembled and brought to bear in the search for significant surface changes of a loaded ball-plate sliding contact operated on its way to failure except for SC, which was studied for applicability to metal-gas reactions.

A realistic system was selected for these laboratory studies; an operating contact consisting of a loaded M-50 bearing steel ball-on-plate of the same material mock-bearing and lubricants simulating MIL 23699 and its additives, i.e. a most common heavily loaded bearing system. The mock-bearing had dimensions such that the width of the wear track was amenable to our surface analyses.

Significant changes were found (i) in the changes of the surface profile within the wear track over the course of bearing operation for different lubricants, (ii) in the rate of oxidation of the steel bearing surface within and without the wear track, (iii) in the rate of change of optical profile within and without the wear track after a brief exposure to dilute hydrochloric acid, and (iv) in the friction for different lubricants. Common surface additives in lubricants, such as tricresyl-phosphate (antiwear) and benzotriazole (anticorrosion), produced larger profile changes than other common lube additives. Invariably these changes could be associated with the more rapid formation of surface oxides within than without the wear track.

The hydrochloric acid probe reaction changing the surface profile could become a convenient and useful test for bearing surface reliability.

The PLIM and EFME instruments developed for this work will prove to be useful in many different applications, not only in the analysis of metal and metal oxide surfaces. The applicability of SC to reactions studies will, however, remain limited to gross changes. For these it can be used from large distances.

As part of this project, but in a separate investigation, jet fuel deposits formed on surfaces of a Jet Fuel Oxidation Tester (JFTOT) were analyzed by infrared emission Fourier microspectrophotometry, a technique we developed under a previous AFOSR grant.

All of the following comments are taken from papers published or in process of publication with the exception of the speckle work which is communicated here for the first time.

2. MATERIALS

The lubricants were trimethylol propane triheptanoate base stock either alone or with one or all of the following (i) benzotriazole (0.0203% corrosion inhibitor, BTZ), (ii) dioctyldiphenylamine and (iii) phenyl-alpha-naphthylamine (both 1.036% and antioxidants, DODPA and PANA), and (iv) tricresylphosphate (2.55% TCP antiwear additive). The fully formulated oil is equivalent to MIL-L-23699 (G-MIL-99).

The probe solution was 0.04 M hydrochloric acid in ethanol.

The ball and the plate were hardened (62-63RC) martensitic M-50 steel (0.8% C, 4.1% Cr, 1.0% V, 4.25% Mo).

The speckle contrast (SC) experiments were also carried out with M-50 steel plates. The bromine reagent used for the etching was Analytical Reagent grade.

The jet fuel deposits were supplied on their original support, i.e. the tubes from the Jet Fuel Thermal Oxidation Tester (JFTOT), by Mr. Robert Morris, Fuels Branch, Fuels and Laboratory Division, Aero Propulsion Laboratory, Department of the Air Force, Air Force Wright Aeronautical Laboratories, Wright Patterson Air Force Base, OH 45433.

3. APPARATUS AND EXPERIMENTAL CONDITIONS

3.1 Ball/Plate Sliding Contact

In this rig an M-50 bearing ball of 20.6 mm diameter could be rotated by a horizontal shaft supported by two bearings and driven by an electric motor. The ball was loaded from the top by an M-50 plate supported by linear bearings on a horizontal loading platform in such a way that the friction force developed in the contact could be determined from the strain generated in a leaf spring connecting the plate with the loading platform. The load could be varied by hanging weights on the loading platform. The lubricants were injected into the contact from a reservoir at ambient temperature by a peristaltic pump.

The maximum Hertzian pressure was 0.1 GPa in all the experiments reported here. The ball speed was 220 revolutions per minute, corresponding to 0.2 m/s linear speed. The duration of every run was 30 minutes at which time the traction force had reached a near-steady value.

No attempt was made to control the contact temperature or to measure it. However, an estimate of the maximum surface temperature rise based on Winer's calculations [1] indicated that the temperature could have exceeded 220°C, the critical temperature for TCP/surface reaction according to Faut and Wheeler [2].

3.2 AC Phase-Locked Interference Microscope (PLIM)

This instrument, schematically shown in Fig. 1, is basically a Michelson interferometer with a laser source and microscope objectives facing two mirrors at almost equal distances from the beamsplitter. One of these mirrors is the reference mirror which is vibrated piezoelectrically at 20 KHz. The other "mirror" is the sample surface, which can be translated horizontally to bring surface features of different heights into the field of view. Reflected radiations from these mirrors are recombined at the beamsplitter and passed through another microscope objective to bring enlarged interference fringes onto a photodetector. If the two beamsplitter-to-mirror distances are equal, the photodetector is "locked" into the peak of a fringe and the 20 kHz amplitude vanishes. If they are not equal, an error signal is generated, resulting in a d.c. potential on the piezoelectric crystal to shift its plane in such a way as to make the distances equal. A plot of d.c. potential against the horizontal sample position results in the "optical" profile of a surface. It is the optical profile rather than the true physical profile because in reality phases and not distances are compared and phases depend on the optical constants of the surface layer and its thickness as well as on the optical properties of the substrate. For this reason the profiles obtained with different laser wavelengths are different when different surface layers, e.g. oxides on steel, are present. From these differencies the nature and thickness of the oxides can be deduced provided some of the optical constants are independently known, e.g. ellipsometrically.

3.3 Faraday-Modulated Electronic Recording Scanning Ellipsometer (ESE)

A schematic diagram of the Faraday-modulated ellipsometer is shown in Fig. 2. This is the ellipsometer originally designed by Monin and Boutry [3], which was modified first by Sullo and Moore at the University of Rochester [4] and now

by us. Radiation from the laser source S is polarized by the polarizer P, whose azimuth of vibration with respect to the plane of incidence is θ. On reflection from the sample surface M the plane-polarized radiation has become elliptically polarized. The angle of the semi-major axis of the ellipse and the plane of incidence is γ. CF is a Faraday modulator consisting of a solenoidal coil with a Faraday glass cylinder at its axis. The magnetic field generated by the coil causes the azimuth of polarized radiation of the light traveling along the axis of the cylinder to be changed proportionally to the magnitude of the magnetic field and to the length of the cylinder, the proportionality constant being called the Verdet constant. This phenomenon is known as the Faraday effect. The coil is driven by a 500 Hz oscillator, causing the magnetic field to vary with that frequency. By the Faraday effect the inclination angle of the polarization ellipse with respect to the plane of incidence is also varied with the same frequency. The radiation from the Faraday modulator is passed through the polarization analyzer A of azimuth β and is finally detected by the photocell or photomultiplier PM.

Our instrument uses a 10 cm long, 0.6 cm diameter Faraday glass cylinder (three times as long as Sullo's) in order to obtain a large amplitude of modulation. The current in the coil is modulated with a 500 Hz frequency. If the analyzer angle β is equal to the true azimuth γ, the radiation detected at the 500 Hz frequency by a phase-sensitive electronic detector is zero and the electronic system is "locked". At the same time, the amplitude of the first harmonic (1000 Hz) is monitored to make sure it is non-zero. If, however, the amplitude detected at 500 Hz is nonzero, an error signal is used to turn the analyzer by an angle appropriate to make it zero. This is done by an electro-optic transducer and control circuitry capable of resolving 0.01 degrees of arc.

Scanning of a sample surface is done by moving the sample M parallel to its plane while the polarizer is rotated at an essentially constant speed with a DC motor and the analyzer is being continuously reset at corresponding azimuths. Plots of polarizer versus analyzer angle look like the curve of Fig. 3. One method of obtaining the ellipsometric parameters ψ and Δ from this curve is graphically as shown in the figure. However, our computerized curve fitting program is much more accurate, because all the data points on the curve are used, not just a few selected ones. Furthermore, many such curves can be traced and averaged in a short time. Once Δ and ψ are known, the index of refraction n and the film thickness can be calculated, but since n is complex, consisting of two variables, more than two measurements are needed, e.g. at more angles of incidence (not just at 45^{o}), different wavelengths, etc. The computations can become quite extensive, but are easily performed on a small laboratory computer.

By placing a microscope objective forming a real image of the sample surface ahead of the detector, sample areas as small as 20 μm in diameter can be resolved ellipsometrically. Most of the energy reflected of the surface is lost, but sufficient energy remains to make the measurements.

Since the design and operation of our ellipsometer is unique and not jet published, a detailed description of the present apparatus is presented in Appendix I.

3.4 Apparatus for Speckle Measurements

Fig. 4 shows the setup schematically. A helium-neon laser of low power (2 milliwatts) was used as the source. Its wavelength (6328 Å) allows measurements of only low roughness. The thought was to replace it later by an infrared source

when an appropriate detector will be available. The mirror arrangement allows variation of the angle of incidence. The entire setup was mounted rigidly on a steel plate sitting on a home-made optical table.

The samples were M-50 steel heat-treated for use in bearings, polished with 600 grade silicon carbide paper.

A Yashica FRI camera body (no lens) was used with fine-grain Kodak Panatonic-X, ISO 32, FX 135 film. The size of the illuminated area could be varied with the exit lens of the spatial filter. For this work the average spot diameter was 2 mm. Observation was in the far field (L = 5m, so that $(D^2/4\lambda) = 1.58m$).

3.5 Apparatus for Jet Fuel Deposit Analysis

The Fourier emission infrared microspectrophotometer used in this work was developed under a previous AFOSR grant and is well described in the appended publications [5,6].

4. RESULTS

4.1 Tractions and Surface Roughness. Effect of the Acid Probe

Figure 5 shows traction curves for the different lubricants after the ball and plates were soaked in them for three hours at ambient temperature. The operating conditions were such that scoring or scuffing would occur very soon for the fully formulated oil, thereby allowing us to maximize the differences with respect to scoring or scuffing for the additives. Differences between the bearing surfaces for the antioxidants and TCP with and without soaking were found. The surface roughnesses (standard CLA roughness) were determined from the optical profiles and plotted in Fig. 6. The antioxidants DODPA and PANA show the least change over the measured time period within the error limits. DODPA and PANA are also the only lubricants giving a significant reduction of roughness in the initial phase of operation when the acid probe was applied (Fig. 7). Since these measurements were made in separate experiments, the consistency of the traction, roughness, and acid probe data must be significant. Another interesting observation is the sharp increase in relative roughness change after acid treatment for both BLZ and TCP (Fig. 6) in the final stage of the ball plate run, while the roughness change remained about constant during most of the run.

A closer examination of Fig. 6 reveals some interesting correlations. Since the vertical scale is arbitrary and the curves were displaced by arbitrary amounts to avoid confusion, only trends are significant. The fully formulated oil (G-MIL-99) and the two amine additives PANA and DODPA gave rise to roughness peaks at about 20 seconds. The fully formulated oil, the base oil and BTZ, the anticorrosion additive, had roughness peaks at about 80 seconds. Only TCP shows a descending slope beyond 100 seconds. These differences might be related to the formation of different surface oxides.

The two surface additives TCP and BTZ had the highest traction while the antioxidants had the lowest. All the surfaces were soaked for three hours in the respective lubricants, cleaned and dried, and then immediately used in the traction test with clean base oil (Fig. 5).

4.2 Ellipsometry of Wear Tracks

In Fig. 7, the changes of slope, $\cos \Delta / \tan \psi$, were plotted across the wear track for the samples of Fig. 5. It will be noted that TCP, which had the highest traction in Fig. 5, also shows the greatest variation over the traverse. The sharp positive and negative peaks correspond to a spot on the wear track (between 100 and 500 μm on the abscissa), which is clearly visible under the microscope. The half-widths of these peaks is about 20 μm. The slope changes for the other materials inside the wear track were much smaller. Outside the wear track the slope variations were minimal; the bottom curve for DODPA shows the characteristic behavior there. Clearly, the nature of the surface is different inside the wear track. The change is not caused by a change of reflecting angle, for the reflected laser beam is very restricted by apertures. When the angles and corresponding azimuths were changed in order to compute the film thickness and the optical constants, the former came out to be about 60 Å at the maximum and the latter correspond roughly to Fe_2O_3 by comparison with the data of Leberknight and Lustman [7]. The identification is tentative and not unique for lack of reference data, which will be obtained later.

The preferential production of a thin oxide layer on wear tracks would seem to be general, but is strongest for those produced in the presence of TCP.

It should be pointed out that the collection of data such as those of Fig. 7 presents problems different from those encountered when ellipsometry is used with dielectric substrates [8]. Most ellipsometric work today refers to dielectrics and semiconductors. The most important difference is reflectivity - high for metals and low for dielectrics and semiconductors. Furthermore, metals have a complex index of refraction (two optical constants), dielectrics only a real index of refraction.

4.3 Auger Electron Spectrograms

The plates were analyzed after the ball experiments with every lubricant. Three areas were selected, two within the wear track and one outside of it for reference. After the ball experiment, the specimens were washed with lots of alcohol and allowed to dry and not handled or treated prior to their introduction into the Auger spectrometer. As a control, a polished M-50 plate not used in a ball/plate experiment was included in the set of Auger analyses.

All the lubricants and the reference gave about the same spectra in the as received condition. However, after six minutes of ion bombardment, all the spectra from outside the wear scar as well as from the reference plate were essentially free of O and C while those from inside the wear scar, notably those from TCP and perhaps also from BTZ had a higher O and C content.

In order to show the effect of ion bombardment on elemental composition, the plots of Fig. 8 were drawn for two position within the wear scar. They present the ratios of the O and C peaks to one of the Fe peaks as a function of time. A sharp change of slope after two-to-four minutes probably signifies the removal of a surface layer.

From these observations, the following deductions would seem to be reasonable:

1. The high C-ratios and O-ratios in the outermost surface layer are probably atmospheric contamination. They are present even in the reference.

2. TCP and GMIL (also containing TCP) have an oxide layer under the atmospheric contamination layer. BTZ is likely to have one as well. The reference, however, does not have such a layer within our error of measurement, but the other materials might have a weak oxide layer.

3. A carbide layer might also underly the atmospheric contamination layer.

4.4 Determination of the Rate of Etching of M-50 Steel by Bromine Vapor by the Use of Speckle Contrast

4.4.1 Background

This reaction was chosen as an example rather than liquid state reactions which proceed at the metal-lubricant boundary because gas-solid reactions are more easily controlled. While we realized all the time that interference microscopy was a more sensitive and reliable tool than laser speckle, the greater simplicity,

larger viewing area and larger distance of observation are clearly favoring laser speckle. The primary purpose of the experiment was to establish feasibility.

While this reaction was not the first to be monitored optically, it was probably the first to be monitored by speckle contrast. Burland, Bjorkland, and Alvarez [9] and later Burland and Brauchle [10] used holography to determine photochemical reaction rates on surfaces. The most frequently used kinetic technique, measurement of the disappearance of the reactants or the appearance of products by following changes in their optical absorption, is of low sensitivity because of the difficulties involved in detecting small absorption changes. The change of speckle contrast is of very high sensitivity even though it is not a zero-background technique as holography is in the detection of photochemical reactions. (In the holographic application the photochemical change itself stores the hologram).

Speckle interferometry was tried at first, but it proved to be difficult to obtain reproducible data. Here, it will be recalled, the speckle pattern before the chemical change is compared with the pattern after the change in such a way that visible fringes are observed. The probable reason for our failure was the non-uniform reaction rate of the surface area viewed, although mechanical movement could not be excluded. Speckle contrast averages over a fairly large area, is non-destructive, can be measured in real time (although we used slow photographic recording) and from a considerable distance and can be made very sensitive to changes of surface roughness when the surface is very smooth. Under these conditions the optical reflectivity would be close to unity and insensitive to small changes. The speckle method therefore complements reflectivity. It also happens that the chemical reactivity of a highly polished bearing surface is much more informative than that of a well-worn one.

4.4.2 Theory

The article by Welford [11] is an excellent review of the relation between laser speckle and surface roughness. It deals with speckle produced in transmission while our work dealt exclusively with reflected speckle. However, the basic ideas are very much the same.

For example, when a surface is illuminated by coherent light from a laser beam, a large number of points on the surface will scatter the radiation and sets of interference fringes will be formed by pairs of scattering points, because the scattered radiation originated from the same laser beam and is coherent. Therefore the speckle pattern is a coherent sum (or a sum of complex amplitudes) of sets of two-beam interference fringes of different spacings, directions, amplitudes, etc.

This qualitative explanation suggests how the random pattern occurs but it does not explain why the contrast is so great. Many complicated theoretical expressions have been derived for this purpose, but Goodman's [12] is probably the easiest to grasp, for he likens the chaotic jumble of "speckles" to a random-walk phenomenon. He points out that the complex amplitude of the radiation field at (x,y,z) in the plane in which the speckles are observed may be regarded as resulting from the sum of contributions from many scattering areas on the rough surface. Assuming now that the amplitude and phases of the elementary scattering areas are statistically independent of each other and are equally likely to lie anywhere in the primary interval $(-\pi, \pi)$, i.e. the surface is rough compared with a wavelength, and that the number of the elementary contributions is large, the probability density function of I, the irradiance in the speckle observation plane is of the form

$$p(I) = \begin{cases} \frac{1}{\bar{I}} e^{-\frac{I}{\bar{I}}} & I \geq 0 \\ 0 & \text{otherwise,} \end{cases}$$

where $\bar{I}$ is the mean or expected irradiance. The probability that the irradiance exceeds a certain threshold I_t is then

$$p\,(I > I_t) = e^{-\frac{I_t}{\bar{I}}}, \quad I_t \geq 0$$

A fundamentally important characteristic of the negative exponential distribution is that its standard deviation precisely equals its mean. Thus, the contrast of a polarized speckle pattern, as defined by

$$C = \frac{\sigma_I}{\bar{I}}$$

is always unity. Once the surface has a roughness sufficient to produce phase excursions compariable to 2π rad, negative exponential statistics result, and further increases of roughness produce no perceptible changes of irradiance statistics. Therefore, all surfaces that are rough on the scale of a wavelength produce the same form of irradiance statistics, regardless of just how much rougher than this limit they may be.

Accordingly it would seem that surface roughnesses estimates on the basis of speckle contrast are limited to surface roughness of the order of a wavelength or less. For this reason our original proposal called for infrared speckle, for the infrared extends over a large wavelength range, say 1-25 μm, even without the use of a vacuum. Furthermore, it would seem possible to decrease the observed surface roughness by variation of the observation angle.

Having realized that speckle contrast can be a measure of surface roughness only for effective roughnesses of the order of a laser wavelength or less, a model for the speckle/roughness relation at smaller roughness should be developed. The thin phase screen model of Welford [11] serves this purpose. The following assumptions are made:

(a) The metal surface is assumed to be a perfect reflector without phase change at all angles of incidence.

(b) The surface slopes are assumed to be small enough to permit ignoring problems of shadowing.

(c) The general shape is smooth compared to the wavelength of the light, i.e. no sharp peaks or angles.

(d) There are no polarization effects.

The thin phase screen model is a plane surface of 100% reflectivity with appropriately varying phase change on reflection at different points. In effect, the thin phase screen model is analogous to a reflection grating "randomly ruled." If $z(x,y)$ is the rms surface roughness (peak height distribution measured from the center line average, CLA), then the phase change on reflection associated

with it is $\phi\ (x,y) = \frac{2\pi}{\lambda}\ z(x,y)\cdot 2\cos\phi$ where ϕ is the angle of incidence and reflection (measured from the surface normal). This equation shows that oblique reflecttion ($0 < \phi < \frac{\pi}{2}$) reduces the phase and permits larger roughness to be measured (as shown below).

To obtain a heuristic relation between speckle contrast and phase, Asakura [5] proceeded as follows:

The speckle intensity distribution in the observation plane is

$$I(\vec{r}') = |\int K(\vec{r},\vec{r}')|^2 = |\int K(\vec{r},\vec{r}')\ O(\vec{r})\ d\vec{r}\ |^2$$

where $\vec{r}$ (equivalent to x,y) refers to the object plane (surface) and $\vec{r}'$ to the speckle observation plane by the usual intensity $\sim$ (amplitude)^2 relation. $K(\vec{r},\vec{r}')$ is the point spread function which indicates a spreading amplitude distribution at the observation plane due to a point at the object plane. The point amplitude distributions within an extended area of $K(\vec{r},\vec{r}')$ contribute to forming the speckle intensity at an arbitrary point $\vec{r}'$ of the observation plane. The thin phase screen model equates

$$O(\vec{r}) = e^{-i\phi(\vec{r})}$$

so that $I(\vec{r}') = |\int K(\vec{r},\vec{r}')e^{-i\phi(\vec{r}')}\ d\vec{r}|'$

Thus the intensity at a point $\vec{r}'$ in the observation plane is given by superposition of phase variations over light waves within an extended area of $K(\vec{r},\vec{r}')$. As the phase variations over that area increase, the intensity variation at the observation plane increases, thus yielding an increase of the contrast in the speckle pattern. To quantitatively specify the speckle intensity variations, the average contrast V, defined by a normalized standard deviation of speckle intensity variations at the observation plane, is introduced

$$V = \frac{\langle \Delta 0 I^2\rangle^{\frac{1}{2}}}{\langle I\rangle} = [\langle I^2(\vec{r}')\rangle - \langle I(\vec{r}')\rangle^2]/\langle I(\vec{r}')\rangle$$

where the brackets indicate ensemble average.

By determining V for samples of known roughness (rms roughness by a stylus profilometer), the roughness of an unknown surface can be found, provided it is in the accessible range (smooth to a wavelength of the laser reflected from it).

4.4.3 Apparatus for the Etching Experiment

One reason bromine etching was used in the preliminary experiments was the relative ease with which it could be applied. The apparatus of Figure 9 served very well. The water bath temperature was kept constant at 100°C and the amount of bromine contacting the sample was controlled by the time the valve was kept open. After every exposure the sample steel specimen was returned to the same position for the speckle experiment. Some tests were made for the reproducibility of the speckle pattern after loading in the etching apparatus and repositioning the speckle apparatus and no changes could be detected.

In Figure 10 three speckle patterns as obtained on photographic film are shown. They correspond to total etching times of zero, 15, and 75 seconds. The increase

in contrast with exposure time is very apparent. Careful comparison of these photographs will also show that exactly the same region was illuminated and "speckled" and that the central region (somewhat below center in these prints) has spread out and become lighter.

4.4.4 Speckle Intensities

The speckle intensities were obtained with a microphotometer scanning the developed photographic film. Some of the densitometer tracings are shown in Figures 11 and 12. The differences are very pronounced. For calibration the speckle patterns of steel specimens of known roughness were obtained and evaluated as shown in Figure 13. A curved CLA had to be used in the evaluation of the traces. Some of the original profilometer traces (TALYSURF) are shown in Figure 14.*

It should be pointed out that in addition to having the available roughness range limited by the physics of speckle we had the further limitation of the latitude of the photographic film. To overcome this problem the exposure times had to be changed and the data were evaluated with the help of the H&D curve supplied for this film. In most cases repeat exposures had to be run and photometered.

4.4.5 Results of the Speckle Experiments

The data of Table I and Figures 15 and 16 show the results. The contrast increases very rapidly at first, comes to a plateau and then reaches the level of maximum contrast (Figure 8). There is, however, a further gradual decrease of contrast noticeable over a much longer time period. The normalized central peak intensity in the speckle observation plane, which, according to Welford [11] is given by

$$R = e^{-g^2},$$

where g^2 is the variance of the phase of the wavefront from the scatterer, i.e.

$$g^2 = \langle \phi^2 \rangle - \langle \phi \rangle^2$$

is plotted in Figure 16. It shows a rapid decrease at first, followed by a break and a much slower decrease. The break occurs at about the same exposure time as the maximum contrast (50 seconds).

At the end of the etching experiment the steel specimen was seen to be irregularly coated with a thin, reddish-brown layer. The layer could be rubbed off very easily with tissue paper. The specimen was then found to be just as smooth with respect to speckle contrast as it was before the etching. Unfortunately no weights were determined so that the mass per unit area of the layer remains unknown.

4.5 Analysis of Jet Fuel Deposits

Since a detailed report was written on this work [17], only a few words are necessary here. Fourier infrared emission microspectrophotometry was used. The deposit spectra reflect the jet fuel composition, especially when nitrogen and sulfur compounds are present.

The "peacock" rings which have been frequently observed on JFTOT deposits were found to correspond to infrared emission maxima and infrared spectra exhibiting inverted bands and must therefore consist of real matter and not merely of optical interference. The deposition of material in these rings probably has its origin in reduced fluid flow which is caused by instabilities in the laminar boundary layer. Similar rings were observed previously, but without thermal gradients which "fix" deposits on the tube walls by the thermal cracking of the fuel. The particles in these rings are likely to be uniform and can appear to be brightly colored just as the gold particles in thin gold films. It is therefore suggested that deposit formation on JFTOT and also aircraft fuel tubes can be reduced by deliberately producing turbulent flow, for example by the interposition of screens.

5. DISCUSSION AND CONCLUSIONS

5.1 Wear of Bearing Surfaces

In our previous publications [13],[14] the difference in the effect of dilute hydrochloric acid (our acid probe) on causing contour changes within and outside a wear track was described, this difference being especially great when scuffing conditions were approached. It was also found that the presence of the antiwear additive TCP in the lubricant would enhance this difference. Then the question was raised why scuffing could occur so suddenly, apparently without warning, even though operating conditions could have been far from those postulated by the Blok temperature criterion. An objective was to try to explain the behavior of the acid probe in the hope that an answer there would also help toward arriving at an answer to the latter question.

Differences in the optical profile at different wavelengths, ellipsometry, and Auger electron spectroscopy have now been shown to discriminate between the surface within the wear track on M-50 steel and outside of it. The evidence points to a higher concentration of an oxide, most likely iron oxide, within the wear track than outside. Interestingly enough, it would seem that TCP promotes the formation of such an oxide. Such an oxide would react much faster chemically with acid than the alloy steel itself. Thus, the oxide would explain the behavior of the hydrochloric acid probe. The oxide is more likely to be formed in the wear track than outside of it because of the higher surface temperature in the wear track. It would also reduce friction at higher temperatures, though not at low ones and explain both our data of Fig. 5 and the results of Faut and Wheeler [2]. Although such an iron oxide layer on the surface could conceivably promote the formation of friction polymer--whose formation was reported to be enhanced by TCP also--it is more likely that the same oxidizing conditions that lead to the formation of the oxide also lead to the formation of friction polymer. Since friction polymer is, in turn, related to acid sludge and the acid is likely to react quickly with the basic iron oxide, provided the temperature is high enough, a case could be made for a mechanism of scuffing, viz. removal of the oxide layer by reaction with acids in the lubricant exposing the nascent metal and allowing metal-to-metal welds. Work now in progress in our laboratory will test this idea.

A new metallurgical phase for M-50 steel was also found and reported in our publication [14]. Its etching characteristics seemed to identify it as a carbide. The higher carbon contents found in the wear track below the surface, expecially for TCP, are consistent with this identification.

The sharp initial decrease in the ball experiment of acid probe reactivity of the two amine antioxidants can be explained by the initial formation of an amine surface film and subsequent exposure of the original alloy steel surface, i.e., the lack of a surface oxide. Since the metal reacts more slowly than the oxide--which was prevented from forming--the probe reaction slows down. Once the amine antioxidant is exhausted, the reaction speeds up again, however, thus explaining the increased activity later. The amine surface film could also be instrumental in reducing traction.

The behavior of BTZ, the anticorrosion additive, has been found to be similar to TCP in some ways. Its low oil solubility requires its small concentration. By the same token, it is more likely to come out of solution and coat the bearing surfaces with an anodic [15] layer. However, as Parkins [15] admits, the behavior of these materials is still not well understood, even by electrochemists, though

they have been used for a long time.

Recently we found that the formation of surface oxide on M-50 steel following scoring is influenced by surface roughness especially in the presence of TCP. For this reason the hardness and surface texture of the steel used in our experiments required exact control. Our results confirm observations by Yamamoto et al. [16], who used a paraffin oil with no additives and show a much greater effect when additives are present.

Thus, it would seem that leads have been generated to help in the design of lubricating materials to reduce traction and scuffing failure. Their chemical interaction with the bearing surfaces, i.e., the formation of oxide and perhaps other layers is an important key.

5.2 Discussion of the Speckle Experiment

Since this series of experiments was carried out primarily to demonstrate the feasibility of speckle contrast for chemical reaction rate measurements, some ancillary data necessary for interpretation of the results were not obtained. For example weight and thickness data and chemical analyses of the deposit layer would have been very helpful. However, even so the data show that surface reaction occurs over small patches (speckle contrast rapidly increases), which then grow slowly (contrast slightly decreases). Central speckle intensity data are consistent with the contrast data; the intensity drops rapidly at first and then continuously at a slow rate. It would seem that the reaction takes place at active centers on the surface; once they are saturated no new centers are formed and the reaction stops except for some slight diffusion-controlled increase. Since the surface cover is discontinuous and the areas of contract between the reaction product and the original metal surface are small and scattered, it is not surprising that the product rubs off easily and that no change of the surface roughness was then observed.

I think this result is interesting from the point of view of friction and lubrication as well. Our microscope profile data (and so have profilometer data by others) have shown little correlation of surface roughness with approach to scuffing failure, yet chemical reactivities of the surface have been found to change (see next section). The active reaction centers are not asperities--at least not of significant size--but different chemical structures of the metal surface itself, such as metal atoms bound or not bound to carbon atoms, in cubic or hexagonal structures or on different crystal planes, etc. This idea is not new; different reactivites on different crystal faces have been measured, but I am not aware of such measurements in a polycrystalline and multiphase environment such as that of M-50.

Perhaps the so called "lack of recovery" problem is also related. When two bodies in contact under pressure are made to slide over each other by a tangential force (frictional force), the minute displacements occurring prior to overall motion are not fully reversible when the tangential force is removed. The prevailing theories (Mindlin, Cattaneo, Beilby) assume plastic deformation near the contact or a microcrystalline layer. A material of different chemical structure, similar to the bromides or oxides of our experiment, formed only at dispersed centers, could well account for it as well and provide a mechanism for such "non-recovery" in the presence of a lubricant.

5.3 Discussion of Jet Fuel Deposit Analysis

Evidence points to changes in deposition mechanism (more and different oxidation) with deposition time. A detailed discussion is presented in Reference [17].

6. STATUS

Thus the achievements of the project can be summarized as follows:

(i) An scanning electronic interference microscope and a scanning electronic ellipsometer have been built allowing surface profiling to ±20 Å in depth and about ±1 μm in width. These tools make possible the determination of dielectric or semiconducting surface layers, i.e. not merely elemental composition, given suitable standards, as well as layer depth and patch location.

(ii) Surfaces of an alloy steel were shown to oxidize when scored and more so in the presence of lubricating oil additives that strongly adsorb to the surfaces. Such oxides may have higher chemical reactivity especially toward acids than the alloy steel and promote the failure of bearings.

(iii) The formation of fuel deposits on simulated jet aircraft surfaces occurs in stages (at least two), the later ones being more influenced by oxygen-containing free radicals than the earlier ones.

7. REFERENCES

1. Ausherman, V.K., Nagaraj, H.S., Sanborn, D.M., and Winer, W.O., "Infrared Temperature Mapping in Elastohydrodynamic Lubrication," Transactions ASME, F, 98, 236 (1976).

2. Faut, O.D., and Wheeler, D.R., "On the Mechanism of Lubrication by Tricresylphosphate (TCP) - The Coefficient of Friction as a Function of Temperature for TCP on M-50 Steel," ASLE Transactions, 26, 3, 344-350 (1983).

3. Monin, J., and Boutry, G.-A., "Concept, Realization and Performance of a New Ellipsometer," Nouv. Rev. Optique, 4, 159-169 (1973).

4. Sullo, Nancy J., "Measurement of Absolute Refractive Index Profiles in Gradient Index Materials Using Modulation Ellipsometry." M.S. Thesis, Institute of Optics, University of Rochester, supervised by Professor Duncan T. Moore.

5. "Oxidized Aircraft Fuel Deposits on Metal Surfaces by Polarization-Modulated Infrared Fourier Emission Microspectrophotometry," James L. Lauer and Leonhard E. Keller, Application of Surface Science, 15, 50-65 (1983).

6. "Emission FTIR Analyses of Thin Microscopic Patches of Jet Fuel Residues Deposited on Heat Metal Surfaces," James L. Lauer and Peter Vogel, Applications of Surface Science, 18, (1984) 182-206.

7. Leberknight, C.E., and Lustman, B., "An Optical Investigation of Oxide Films on Metals," J. Opt. Soc. Am., 29, 59-66 (1939).

8. Vedam, K., The Characterization of Materials in Research: Ceramics and Polymers. J.J. Burke and V. Weiss, eds. Syracuse University Press, 1975, pp. 503-537.

9. Burland, D.M., Bjorkland, G.C., and Alvarez, D.C., "Use of Holographic Interferometry Holography to Investigate Photochemical Reactions," J. Am. Chem. Soc., 102, 7117-19 (1980).

10. Burland, D.M., and Brauchle, Chr., "The Use of Holography to Investigate Complex Photochemical Reactions," J. Chem. Phys. 76 (9), 4502-4512 (1982).

11. Welford, W.T., "Laser Speckle and Surface Roughness," Contemporary Physics, 21 (4), 401-412 (1980).

12. Goodman, J.W., "Some Fundamental Properties of Speckle," J. Opt. Soc. Am., 66 (11), 1145-50 (1976).

13. Lauer, J .L., and Fung, S.S., "Microscopic Contour Changes of Tribological Surfaces by Chemical and Mechanical Action," ASLE Transactions, 26, 430-436 (1983).

14. Lauer, J.L., Fung, S.S., and Jones, W.R. Jr., "Topological Reaction Rate Measurements Related to Scuffing," ASLE Preprint No. 83-LC-2B-1. Presented at the ASME/ASLE Lubrication Conference in Hartford, CT, October 18-20, 1983.

15. Parkins, R.N.: Corrosion Inhibition, in Comprehensive Treatise of Electrochemistry, Vol. 4, Electrochemical Materials Science, J. O'M Bockris, B.E. Conway,

E. Yeager, and R.E. White, eds., Plenum Press, New York, 1981, pp. 313-315.

16. Yamamoto, Y., Hirano,F., and Hashimoto, M., "The Effect of Surface Roughness on Scoring, Part 3 In the Case of Hardened Carbon Steel." Bulletin of the Japanese Society of Mechanical Engineering, 23 (186), 2132-2138 (1980).

17. "Analysis of Jet Fuel Deposits," James L. Lauer and Peter Vogel, AFOSR Report, 77 pages, December 28, 1983.

8. PUBLICATIONS AND PRESENTATIONS

1. "Analysis of Aircraft Fuel Line Deposits by Polarization Infrared Fourier Microemission Spectrophotometry." Invited paper presented at the 3rd Symposium on Applied Surface Analysis, University of Dayton, OH, June 3, 1981.

2. "Analysis of Infrared Emission From Thin Particulate Adsorbates," James L. Lauer and L.E. Keller. Presented at the 1981 International Conference on Fourier Transform Infrared Spectroscopy, University of South Carolina, Columbia, June 8, 1981.

3. "Pit Growth on Scuffed Bearing Surfaces," James L. Lauer, Simon Fung, and Duncan T. Moore. Presented at the Dallas, TX, Meeting of the American Physical Society, March 8-12, 1982, at the Symposium on Chemical Processes at Surfaces (Division of Chemical Physics), Paper No. DO 9. Bulletin of the American Physical Society, 27, (3), 226 (1982).

4. "Microscopic Contour Changes of Tribological Surfaces by Chemical and Mechanical Action," James L. Lauer, and Simon Fung. Presented at the ASME/ASLE Lubrication Conference, Washington, DC, October 5-7, 1982. Preprint No. 82-LC-3B-3.

5. "Infrared Emission Spectrophotometric Study of the Changes Produced by TiN Coating of Metal Surfaces in an Operating EHD Contact." James L. Lauer, Leonhard Keller, and William R. Jones, Jr. Presented at the ASME/ASLE Lubrication Conference, Washington, DC, October 5-7, 1982. Preprint No. 82-LC-3C-3.

6. "Phenomena at Moving Phase Boundaries," Invited speaker (J.L. Lauer) at the 1982 Gordon Research Conference on Friction and Lubrication, June 4, 1982.

7. Alignment of Fluid Molecules in an EHD Contact." by James L. Lauer, Leonhard E. Keller, Frank H. Choi, and Vincent W. King, ASLE Transactions, 25, 3, 329-336, (July 1982).

8. "Analysis of Aircraft Fuel Line Deposits by Polarization Infrared Fourier Micro-Emission Spectrophotometry," James L. Lauer and L.E. Keller, Application of Surface Science, 9, 175-189 (1982).

9. "Topological Reaction Rate and Thickness Measurements with a Phase-Locked Interference Microscope." James L. Lauer and Simon S. Fung. Presented at the Pittsburgh Conference in Atlantic City in March 1983. Paper No. 789.

10. "In Situ Analysis of Deposits Formed on Jet Fuel Oxidation Test (JFTOT) Tubes by Polarization Modulated Infrared Fourier Emission Microspectrophotometry." James L. Lauer and Peter Vogel. Presented at the Pittsburgh Conference in Atlantic City in March 1983. Paper No. 060.

11. "Composition and Profiles of Patches Formed on Metal Surfaces by Polarization-Modulated Infrared Emission Fourier Microspectrophotometry and by Phase-Locked Laser Interference Microscopy." Invited Lecture by J.L. Lauer at the 1982 AFOSR Molecular Dynamics and Surface Chemistry Contractors' Conference on December 1-3, 1982 at the USAF Academy in Colorado Springs, CO.

12. "Infrared Emission Spectrophotometric Study of the Changes Produced by TiN Coating of Metal Surfaces in an Operating EHD Contact." ASLE Preprint No. 82-LC-3C-3. James L. Lauer, L.E. Keller, and William R. Jones, Jr. Presented paper at the ASME/ASLE Lubrication Conference in Washington, DC, October 5-7, 1982. Revised text published in ASLE Transactions, Vol 26(4), 437-444 (1983).

13. "Microscopic Contour Changes of Tribological Surfaces by Chemical and Mechanical Action." James L. Lauer and Simon S. Fung. ASLE Preprint No. 82-LC-3B-3. Presented at the ASME/ASLE Lubrication Conference in Washington, DC, October 5-7, 1982. Revised text published in ASLE Transactions, Vol. 26, 430-436 (1983).

14. "Oxidized Aircraft Fuel Deposits on Metal Surfaces by Polarization-Modulated Infrared Fourier Emission Microspectrophotometry." Application of Surface Science, 15, 50-65 (1983).

15. "Emission FTIR Analyses of Thin Microscopic Patches of Jet Fuel Residues Deposited on Heated Metal Surfaces." Presented by J.L. Lauer at the 5th Symposium on Applied Surface Analysis, June 8-10, 1983, at the University of Dayton, Dayton, OH, 45469.

16. "Analyses of Thin Microscopic Patches of Jet Fuel Residues Deposited on heated Metal Surfaces by Emission FTIR," James L. Lauer and Peter Vogel. Presented at the 1983 International Conference on Fourier Transform Spectroscopy, September 5-9, 1983, University of Durham, England.

17. "Topological Reaction Rate Measurements Related to Scuffing." James L. Lauer and Simon Fung (RPI) and William R. Jones, Jr. (NASA-Lewis). Preprint No. 83-LC-2B-1. Presented at the ASLE/ASME Lubrication Conference in Hartford, CT, October 18-20 (1983).

18. "Surface Changes Preceding Bearing Failure." Presented by J.L. Lauer at the 1984 Pittsburgh Conference, March 5-9, 1984 in Atlantic City, NJ.

19. "Analysis of Microscopic Deposits Intitially Formed on Active Centers of Metal Surfaces by Infrared Emission Spectroscopy." Presented by J.L. Lauer at the Third International Conference on Infrared Physics (CIRPS), Zurich, Switzerland, July 23-27, 1984.

20. "Optical and Other Properties Changes of M-50 Bearing Steel Surfaces for Different Lubricants and Additives Prior to Scuffing," James L. Lauer, Norbert Marxer, and William R. Jones, Jr., to be presented at the ASME/ASLE Joint Lubrication Conference in San Diego, CA, Oct. 23-25, 1984. ASLE Preprint No. 84-LC-2A-3.

21. "Emission FTIR Analyses of Jet Fuel Deposits," James L. Lauer and Peter Vogel, invited paper presented at the "Stability and Compatibility of Alternate Fuels," Symposium of the Division of Petroleum Chemistry at the 188th National American Chemical Society (ACS) Meeting in Philadelphia, PA, August 26-31, 1984. Preprints-Symposia, General Papers. Vol 29, No. 4, p. 1015-1026.

22. "Analysis of Patchy Microscopic Depositions from Jet Fuels on Stainless Steel and Aluminum by IR Emission," James L. Lauer and Peter Vogel, presented at the Third International Conference on Infrared Physics held at the ETH, Zurich, Switzerland, July 23-27, 1984. Proceedings of the Third International Conference on Infrared Physics, W. Ruegsegger and F.K. Kneubuhl, eds., pp. 678-680 (1984).

    At this conference Dr. J.L. Lauer was a session presider. The paper will subsequently be published in Infrared Physics

23. "Changes Produced on Lubricated Bearing Surfaces during Operation Under High Loads," James L. Lauer and Norbert Marxer, presented at the 6th Symposium on Applied Surface Analysis at the University of Dayton, Dayton, OH, on June 6-8, 1984. The paper will subsequently be published in Application of Surface Science.

24. "Infrared Emission Study of Fuel Deposit Formation on Heated Metal Surfaces." James L. Lauer and Peter Vogel, presented at the 31st Canadian Spectroscopy Symposium, September 20 to Oct. 3 at the Gray Rocks Inn, St. Jovite, Quebec, Canada.

25. "Emission FTIR Analyses of Thin Microscopic Patches of Jet Fuel Residues Deposited on Heated Metal Surfaces," James L. Lauer and Peter Vogel, Applications of Surface Science, 18, (1984) 182-206.

26. "Characterization of Lubricated Bearing Surfaces Operated under High Loads," to be presented at the International Tribology Conference, Tokyo, Japan, July 1985.

TABLE I

RESULTS OF THE BROMINE ETCHING EXPERIMENTS
Sample: M-50 Steel

Etching Period	Cumulative Etching Time	CLA Roughness (Area Above CLA divided by distance scanned)	Normalized Central Peak Intensity
0	0	14.6	1
5 s	5.s	31.5	11.0×10^{-6}
10 s	15.s	29.3	8.4
20 s	35.s	30.6	9.8
40 s	75.s	49.3	2.5
1 m	2.25 m	45.8	2.9
1 m	3.25 m	49.4	2.9
2 m	6.25 m	48.8	1.6
3 m	9.25 m	--	1.0
5 m	14.25 m	--	0.35
7 m	21.25 m	44.6	0.14

LIST OF FIGURES

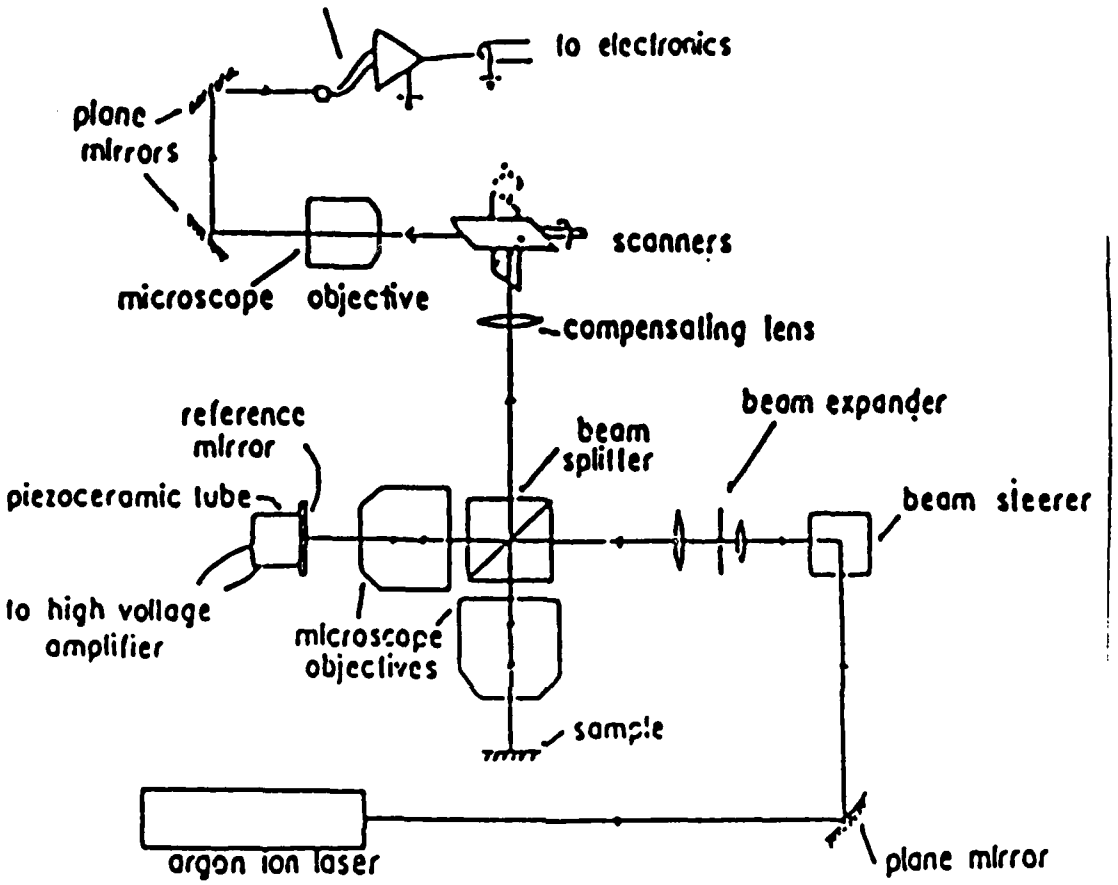

Fig. 1 Schematic drawing of laser interferometer

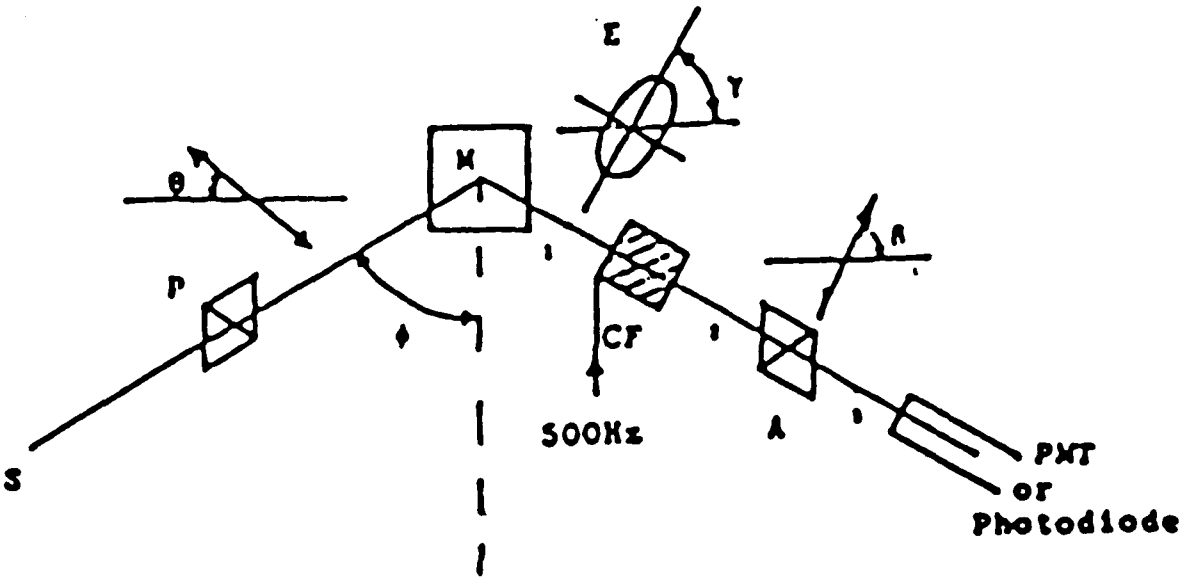

Fig. 2 Schematic drawing of ellipsometer

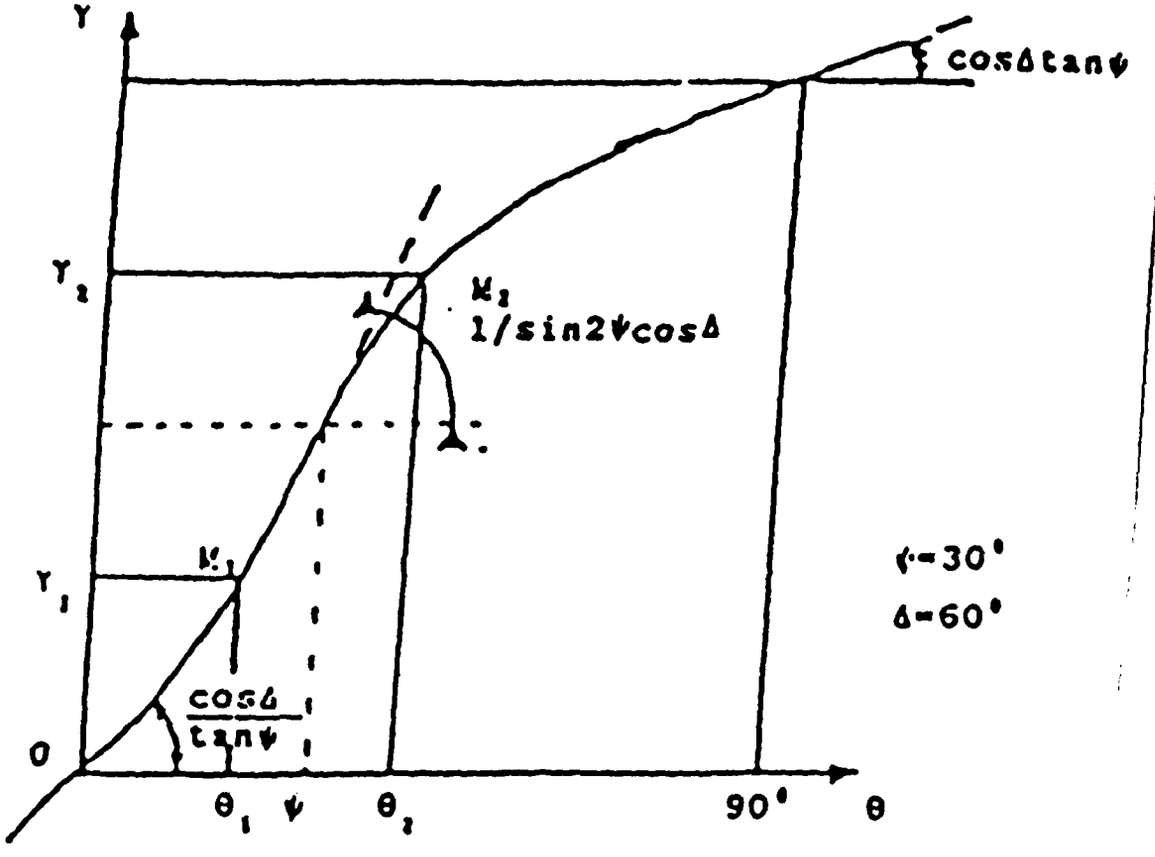

Fig. 3 Determination of the ellipsometer parameters

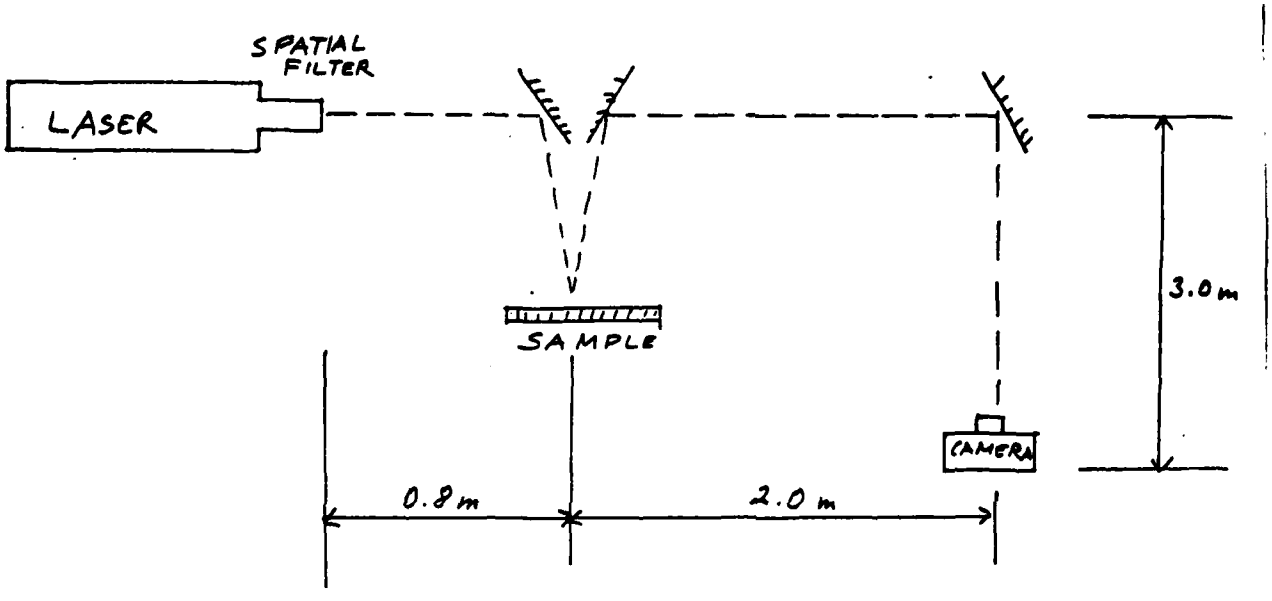

Fig. 4 Experimental setup for speckle measurements

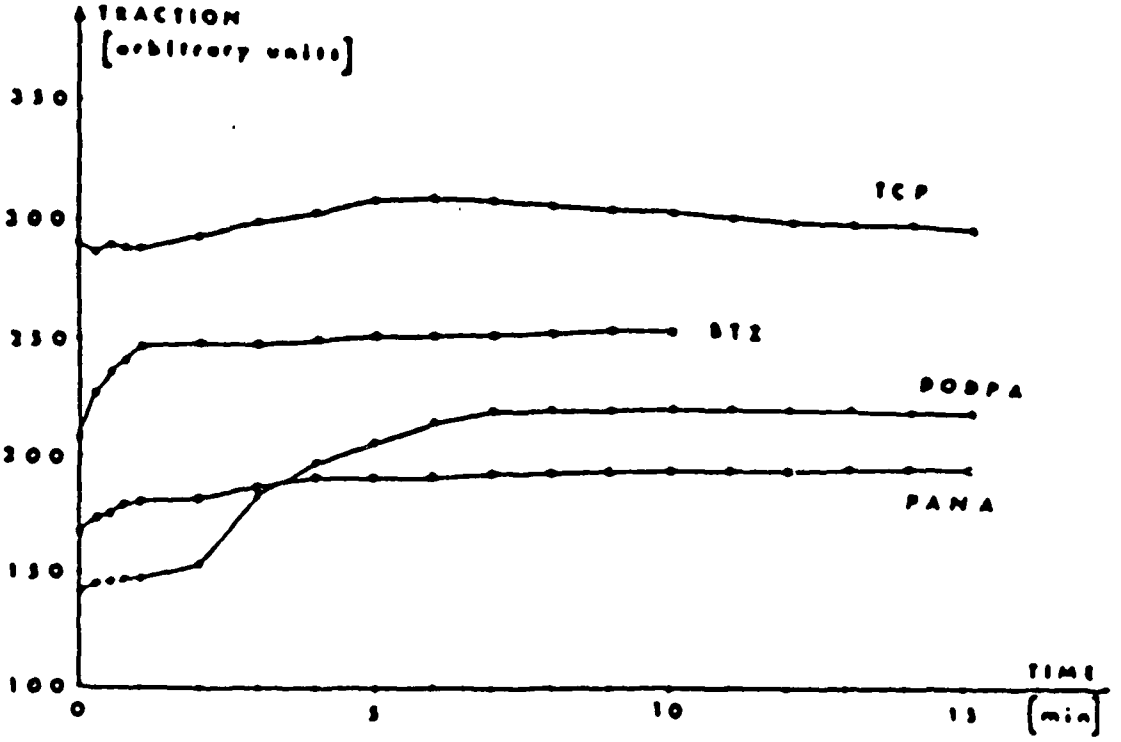

Fig. 5 Traction for different lubricants

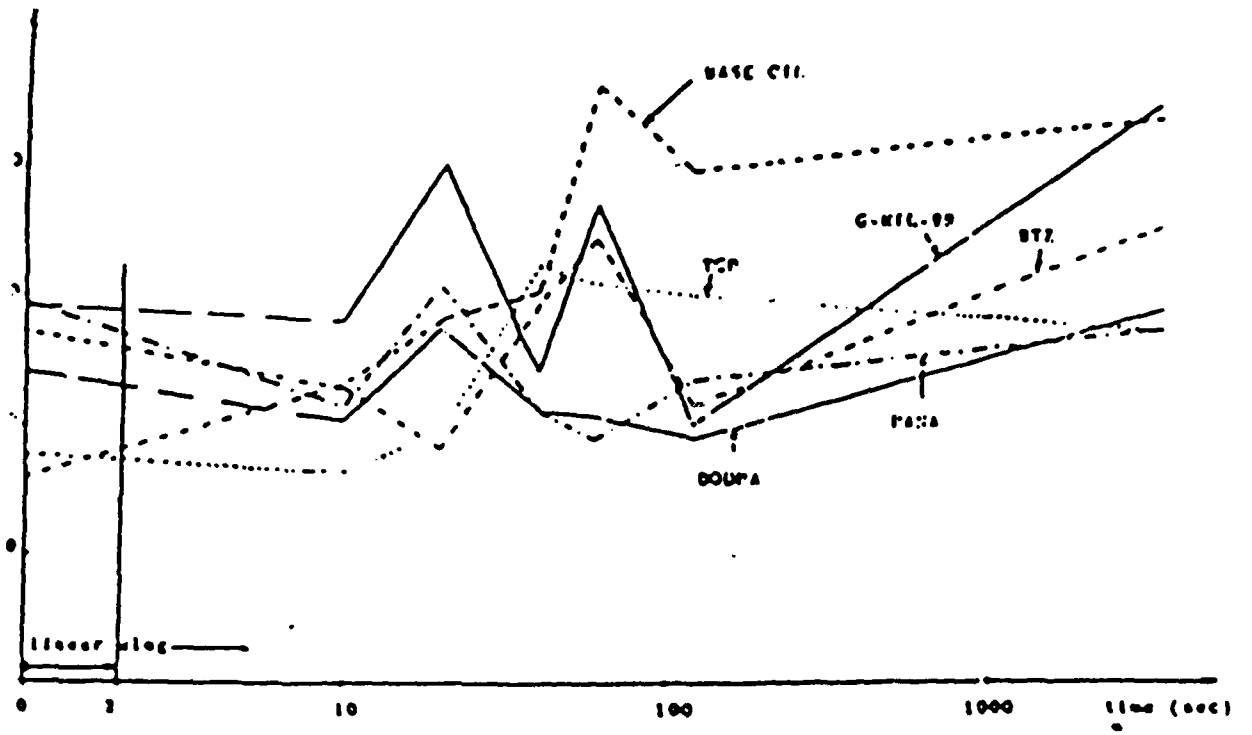

Fig. 6 Roughness changes with operating time

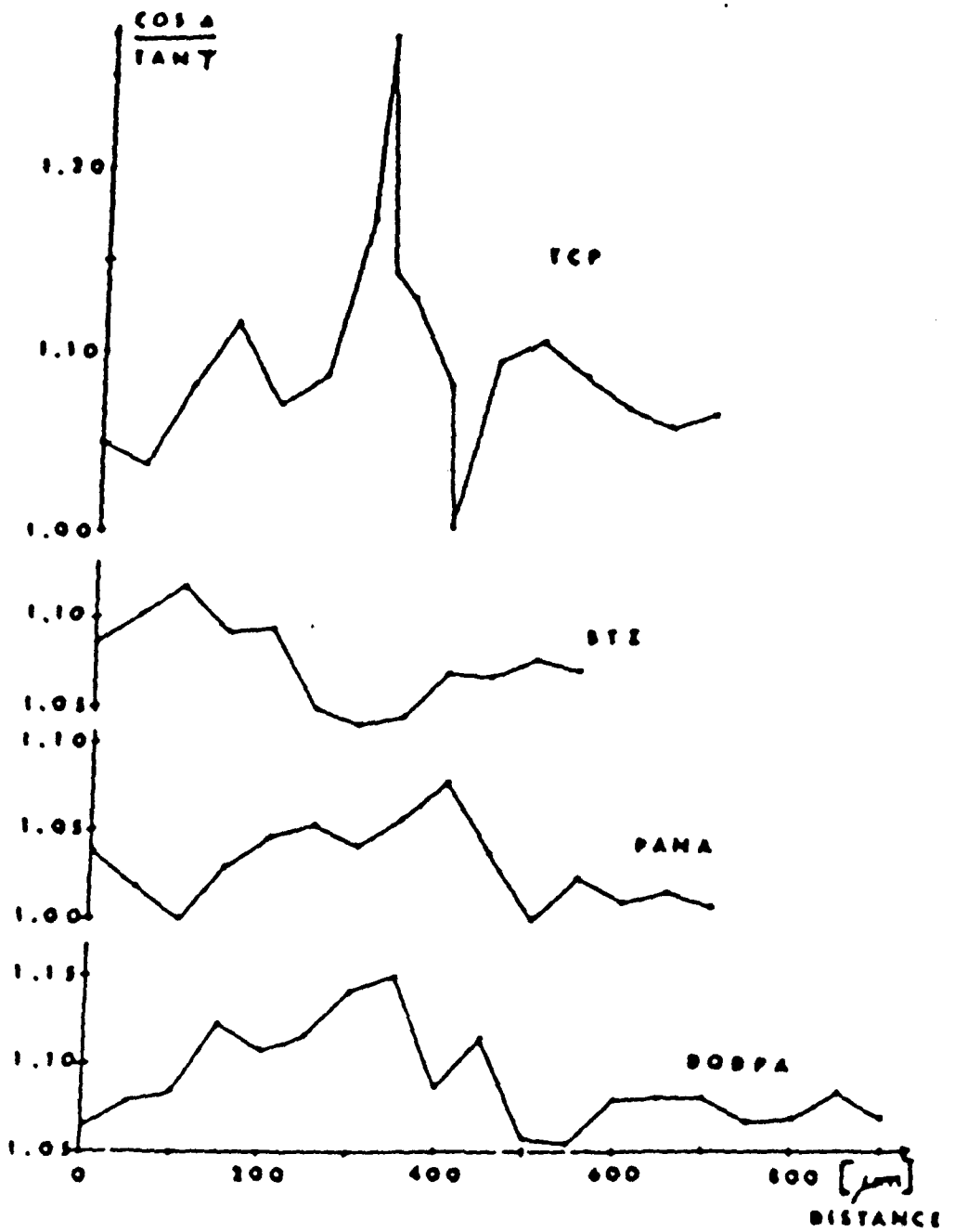

Fig. 7 Ellipsometric slopes over a wear track traverse for different lubricants

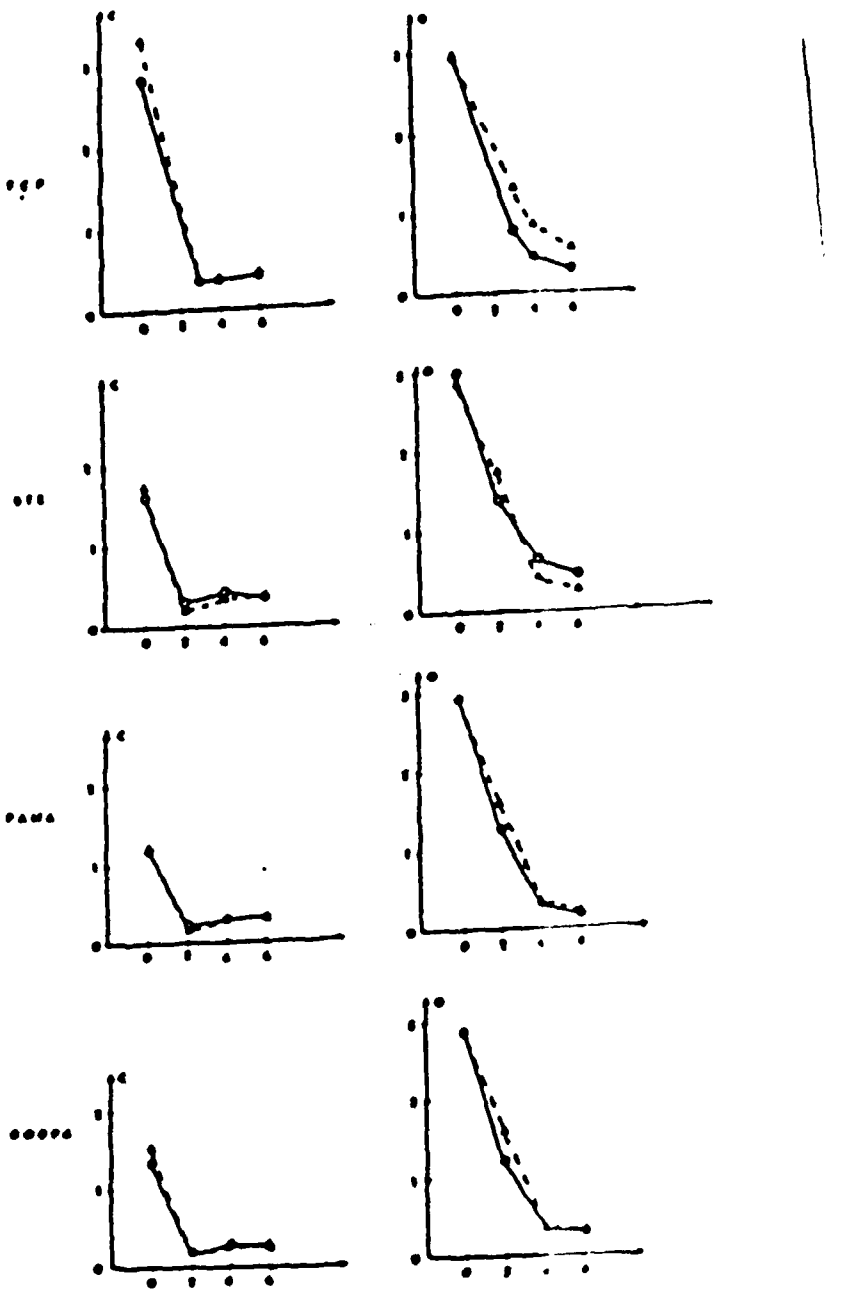

Fig. 8 Ratio of a carbon to an iron Auger peak (le[illegible] of an oxygen to the same iron peak (right) for ion bomba[illegible] zero to six minutes (10 Å are removed per minute[illegible] and broken lines refer to two different spots [illegible] the wear track.

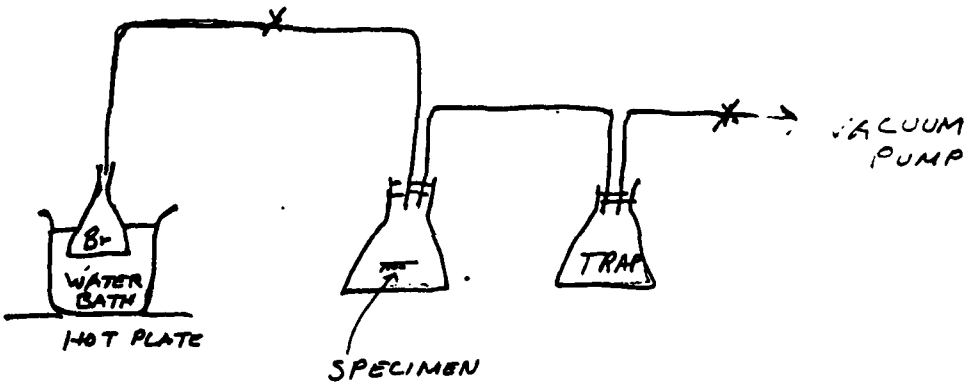

Fig. 9 Apparatus used for the etching experiment

(a)

(b)

(c)

Fig. 10 Comparison of three speckle patterns from the etching experiment, (a) before etching, (b) after 15 seconds of exposure to bromine vapor and (c) after 75 seconds of exposure of bromine vapor

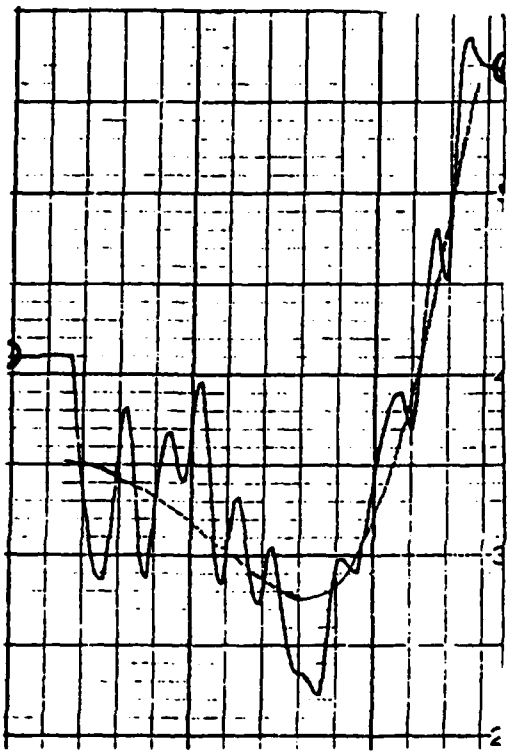

Fig. 11a Before etching
CLA = 69 nm

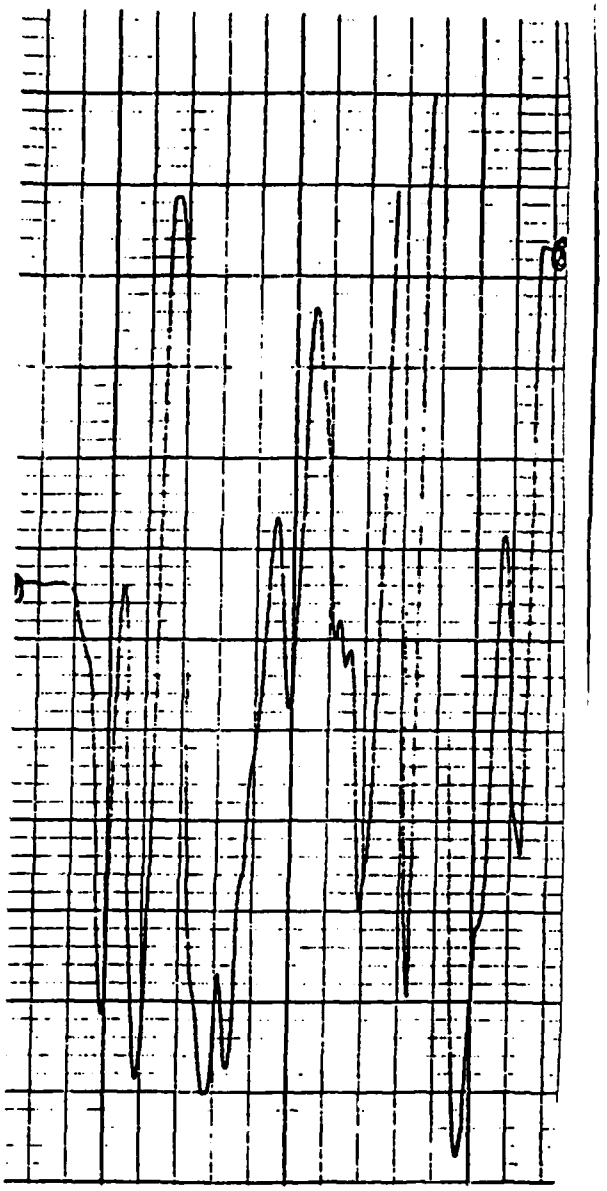

Fig. 11b After vapor etching
with bromine

Fig. 11 Densitometer traces of speckle pattern before and after bromine etching (75 seconds)

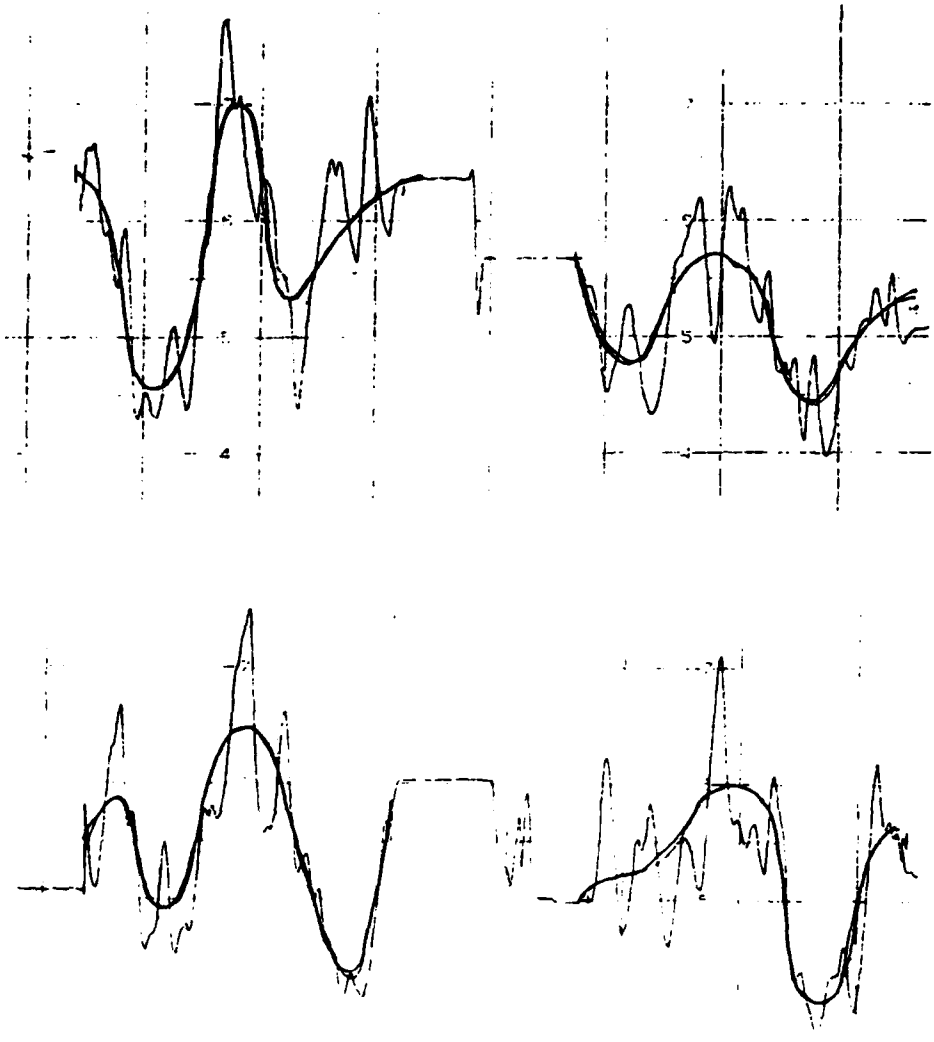

Before etching

Fig. 12a A series of densitometer traces of speckle patterns obtained after different periods of etching with bromine vapor

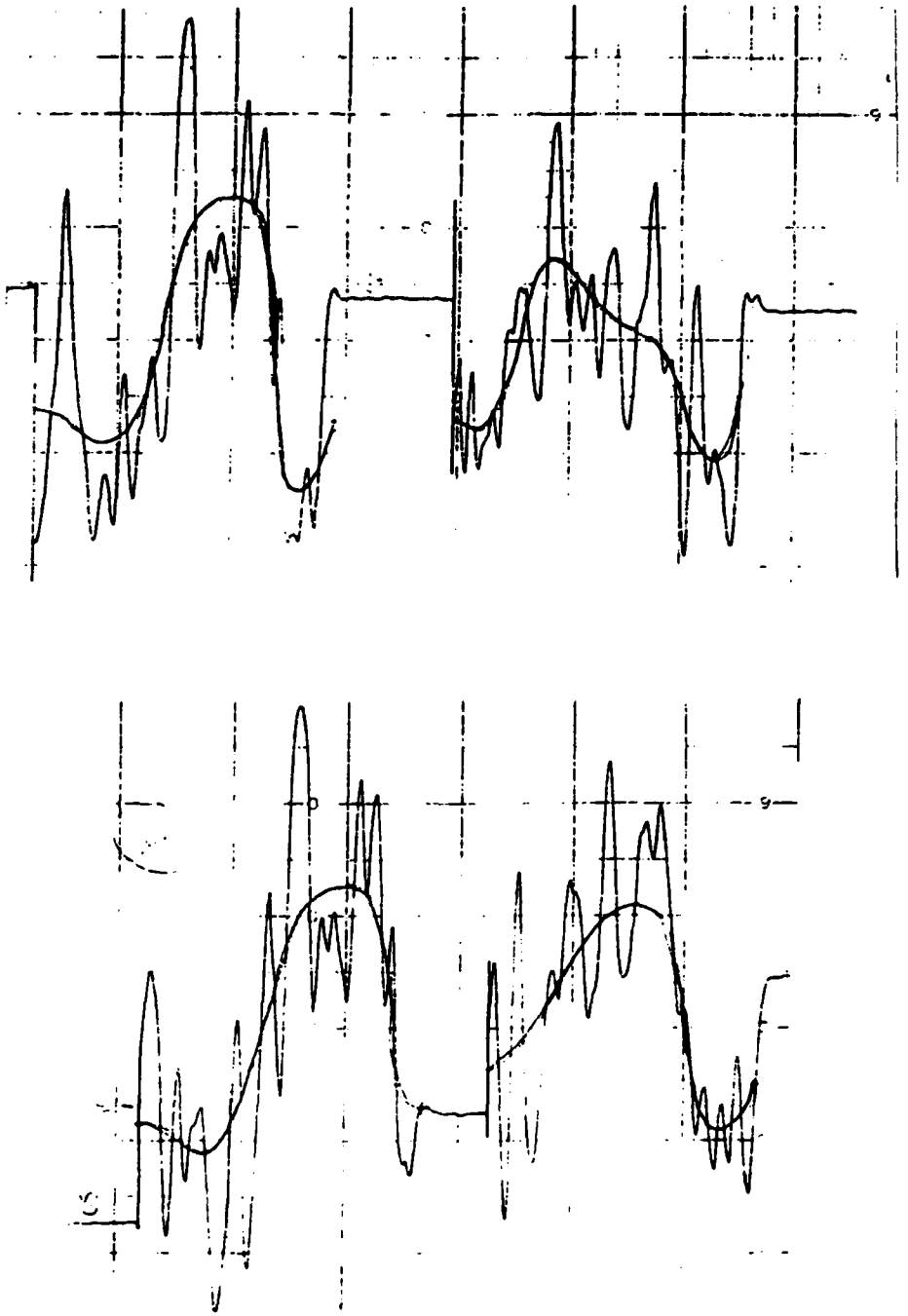

15 sec

Fig. 12b A series of densitometer traces of speckle patterns obtained after different periods of etching with bromine vapor

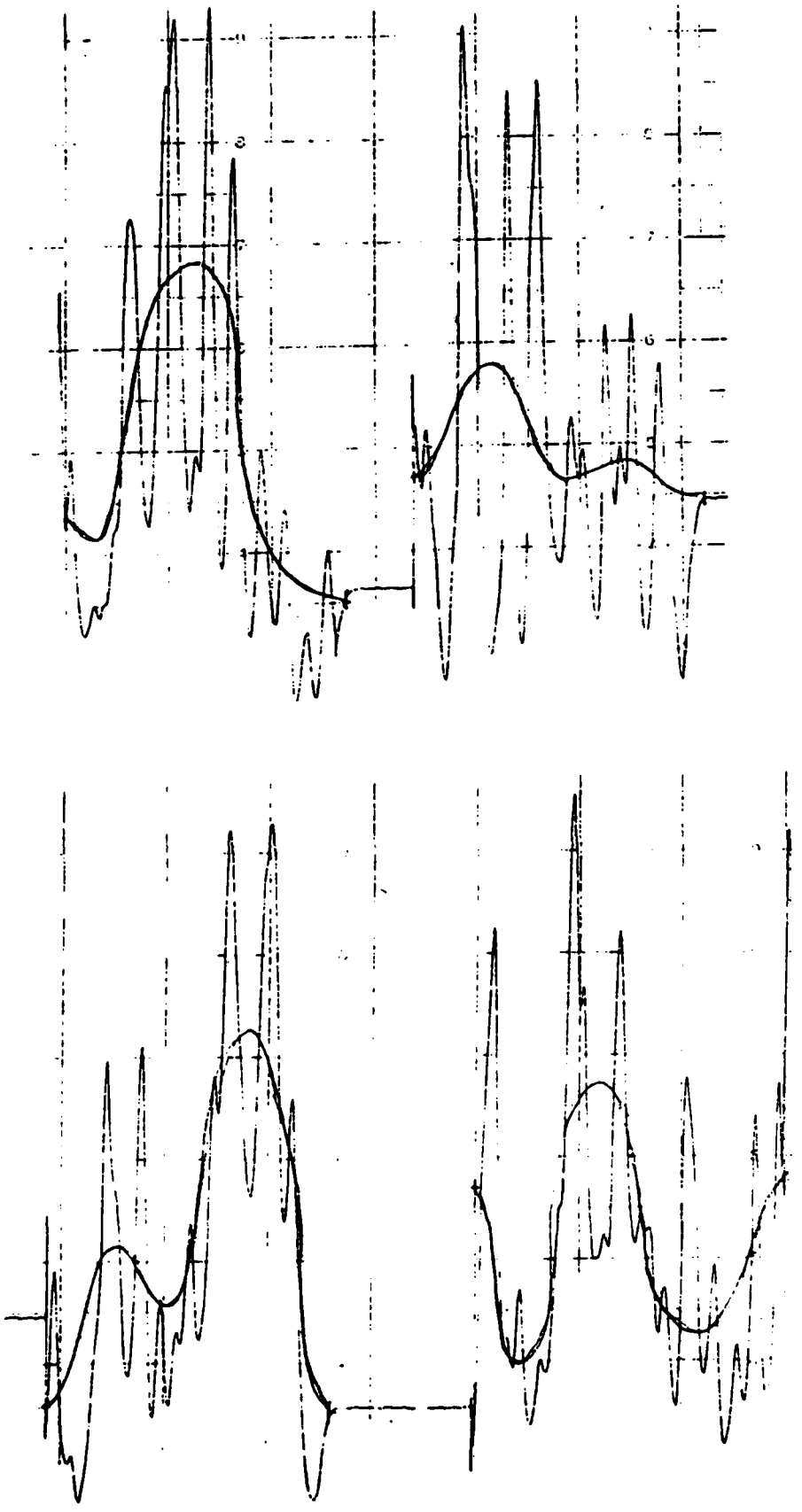

135 sec

Fig. 12c A series of densitometer traces of speckle patterns obtained after different periods of etching with bromine vapor

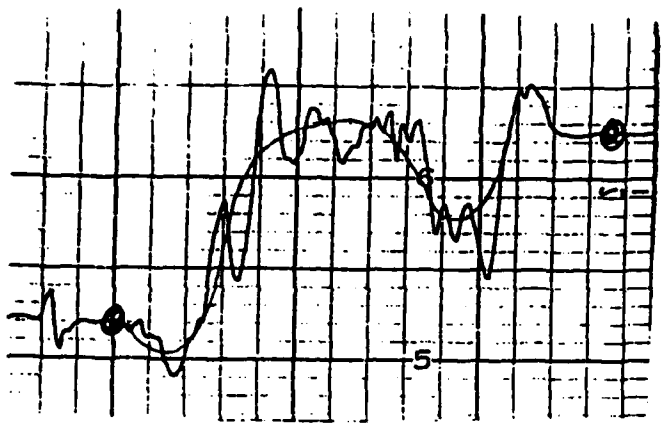

(a) CLA = 15 nm

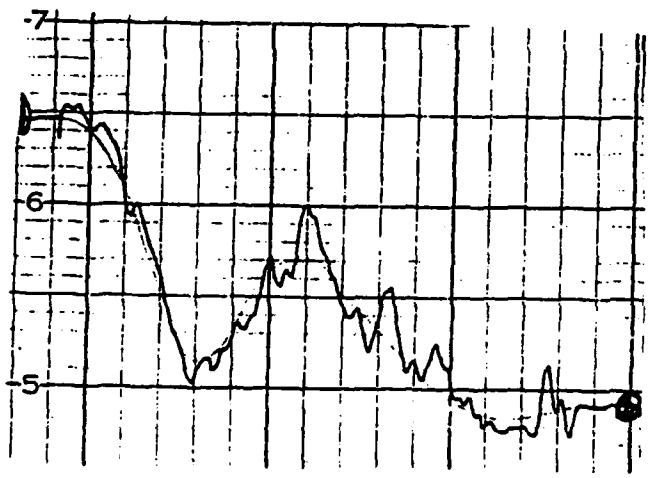

(b) CLA = 17 nm

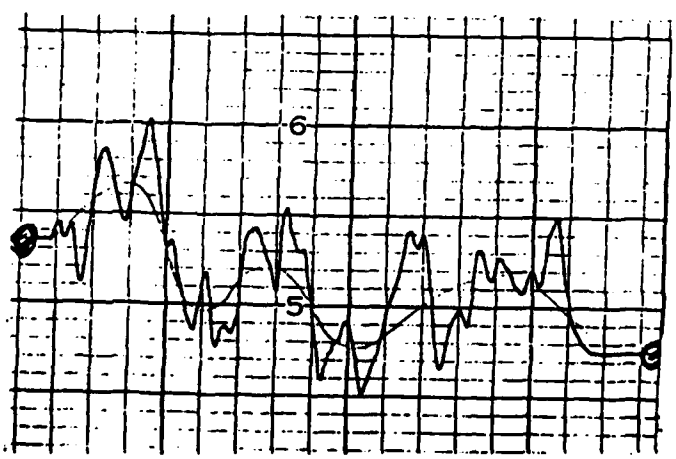

(c) CLA = 30 nm

Fig. 13 Densitometer traces of speckle patterns of M-50 steel specimens of roughness calibrated by a profilometer

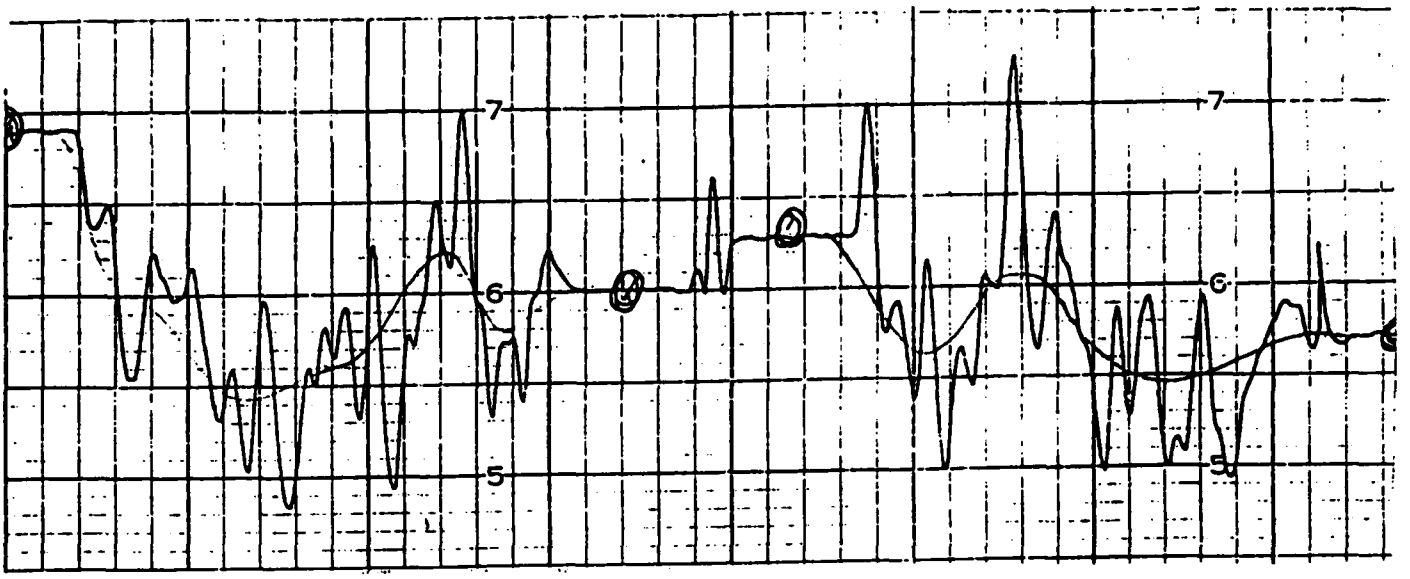

(d) CLA = 60 nm

Fig. 13 Densitometer traces of speckle patterns of M-50 steel specimens of roughness calibrated by a profilometer

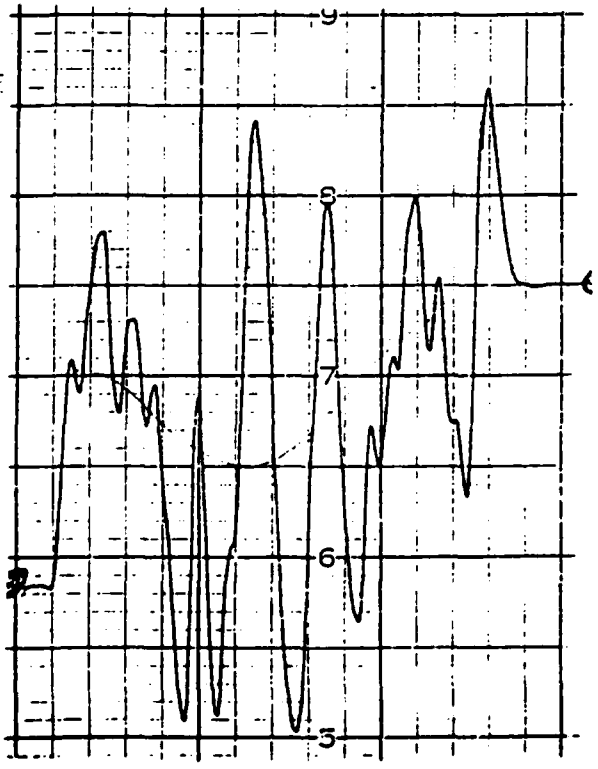

(e) CLA = 110nm

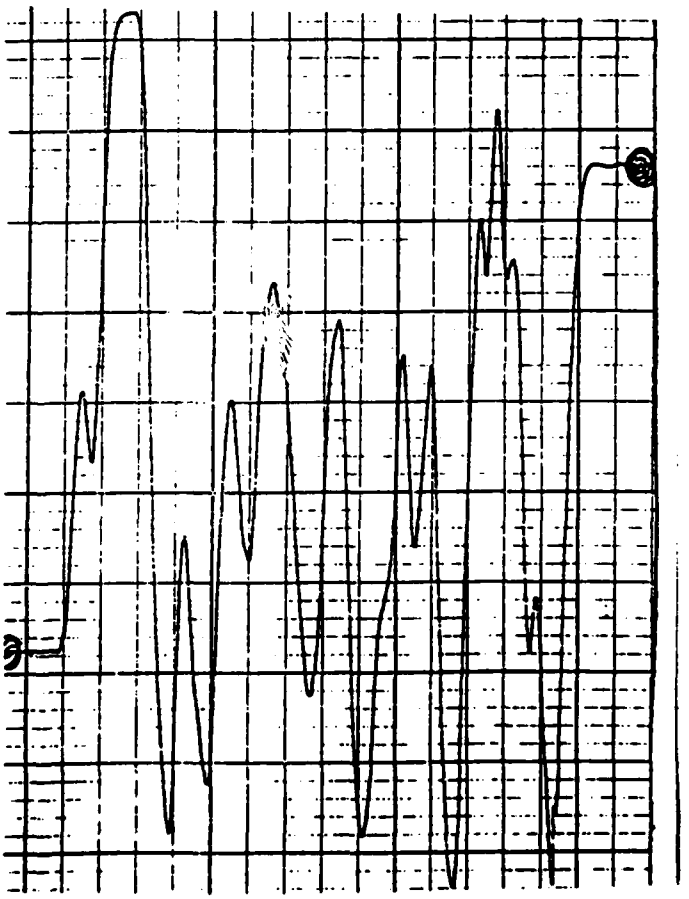

(f) CLA = 120 nm

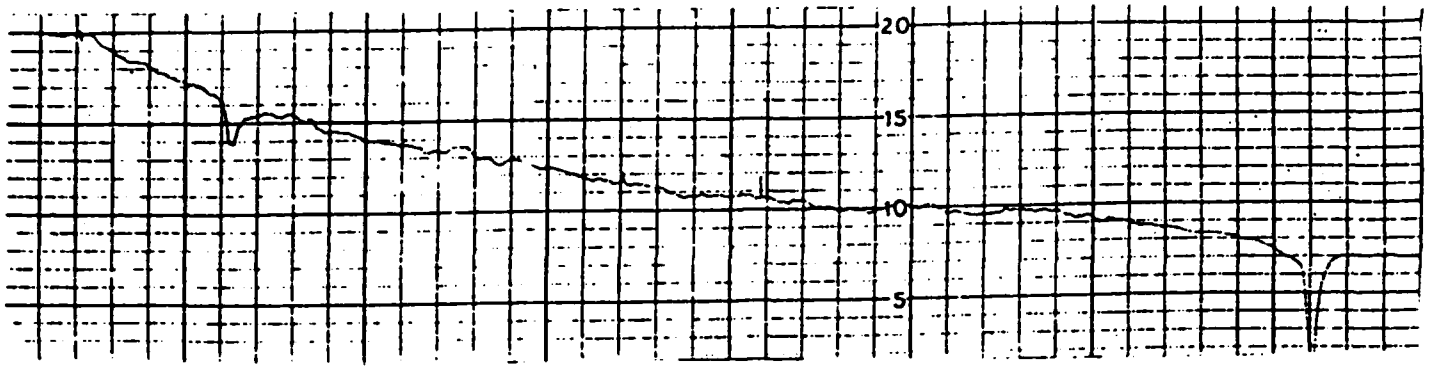

(a) CLA = 15 nm vertical magn 50,00
horizontal magn 20

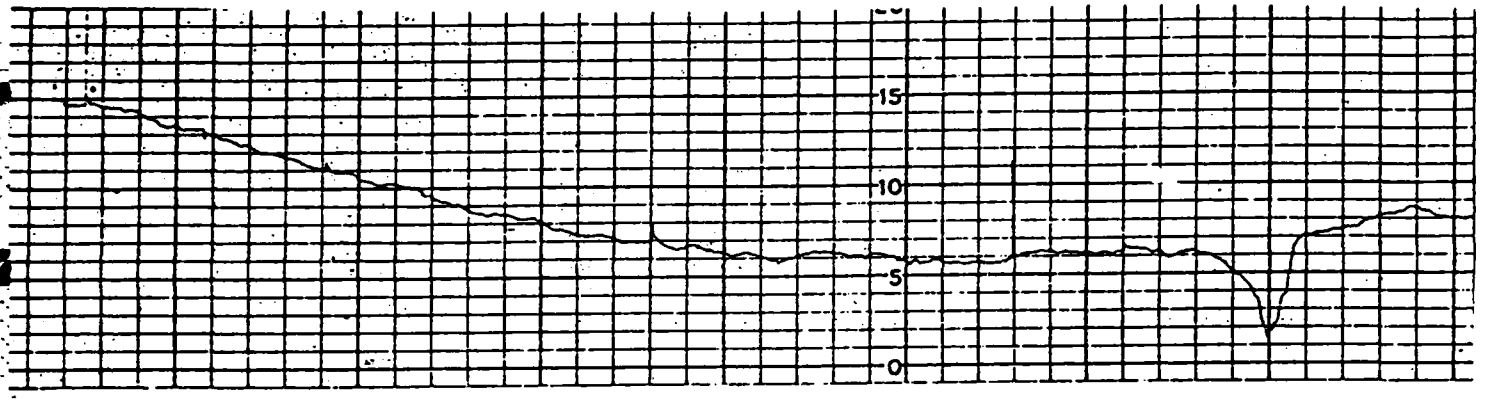

(b) CLA = 17 nm vertical magn 50,000
horizontal magn 20

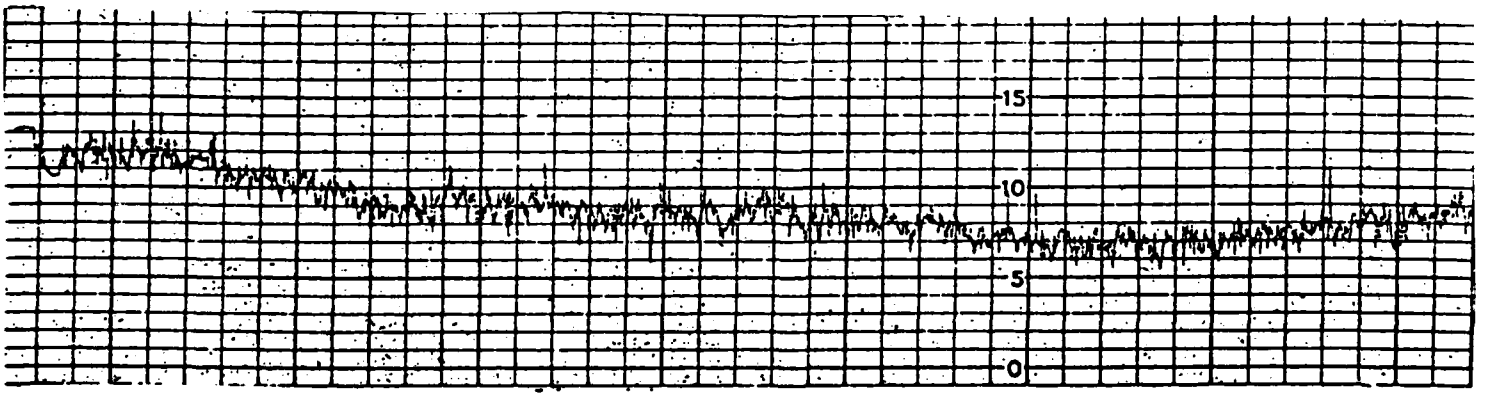

(c) CLA = 30 nm vertical magn 50,000
horizontal magn 20

Fig. 14 Some profilometer traces of specimens of Fig. 12

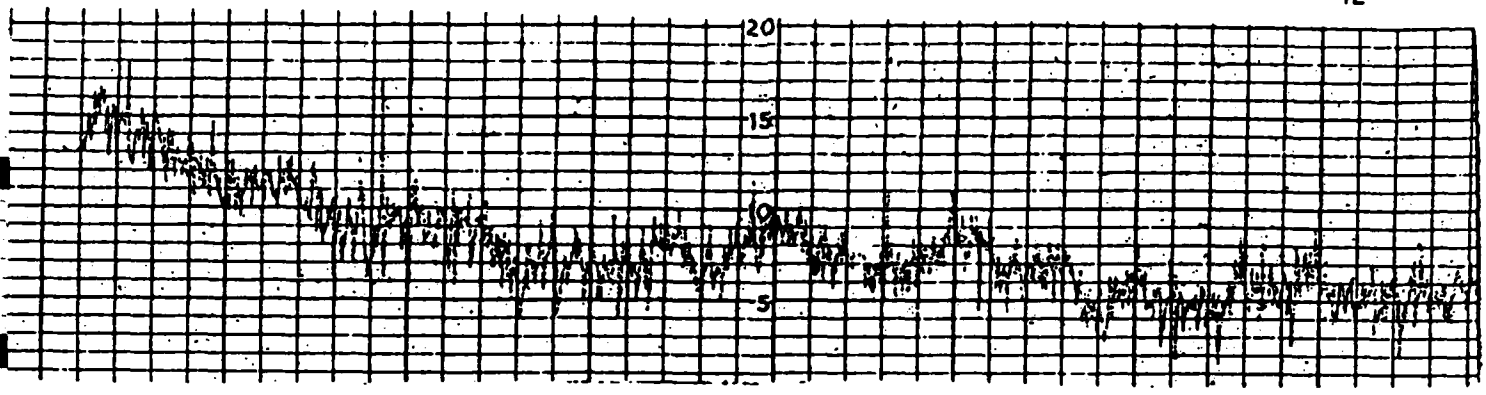

(d) CLA = 60 nm vertical magn 50,000
horizontal magn 20

(e) CLA = 110 nm vertical magn 20,000
horiztonal magn 20

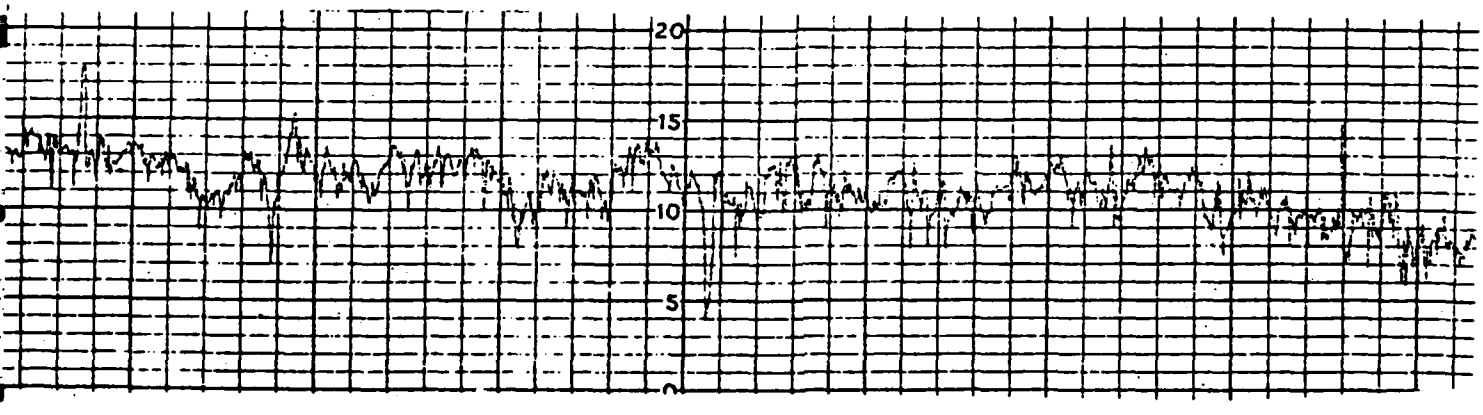

(f) CLA = 120 nm vertical magn 20,000
horizontal magn 20

Fig. 14 Some profilomter traces of specimens of Fig. 12

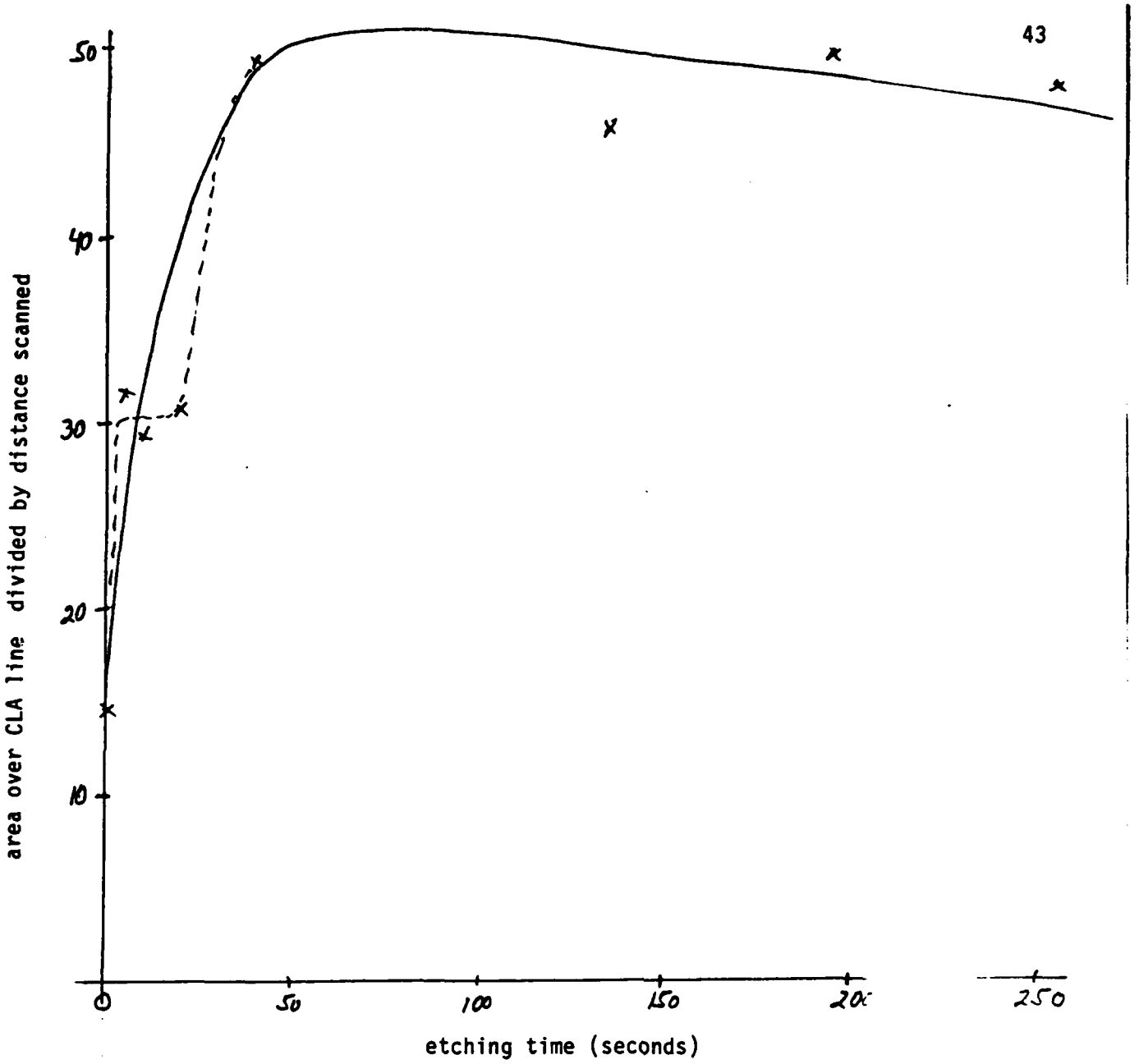

Fig. 15 Change of relative speckle contrast with etching time

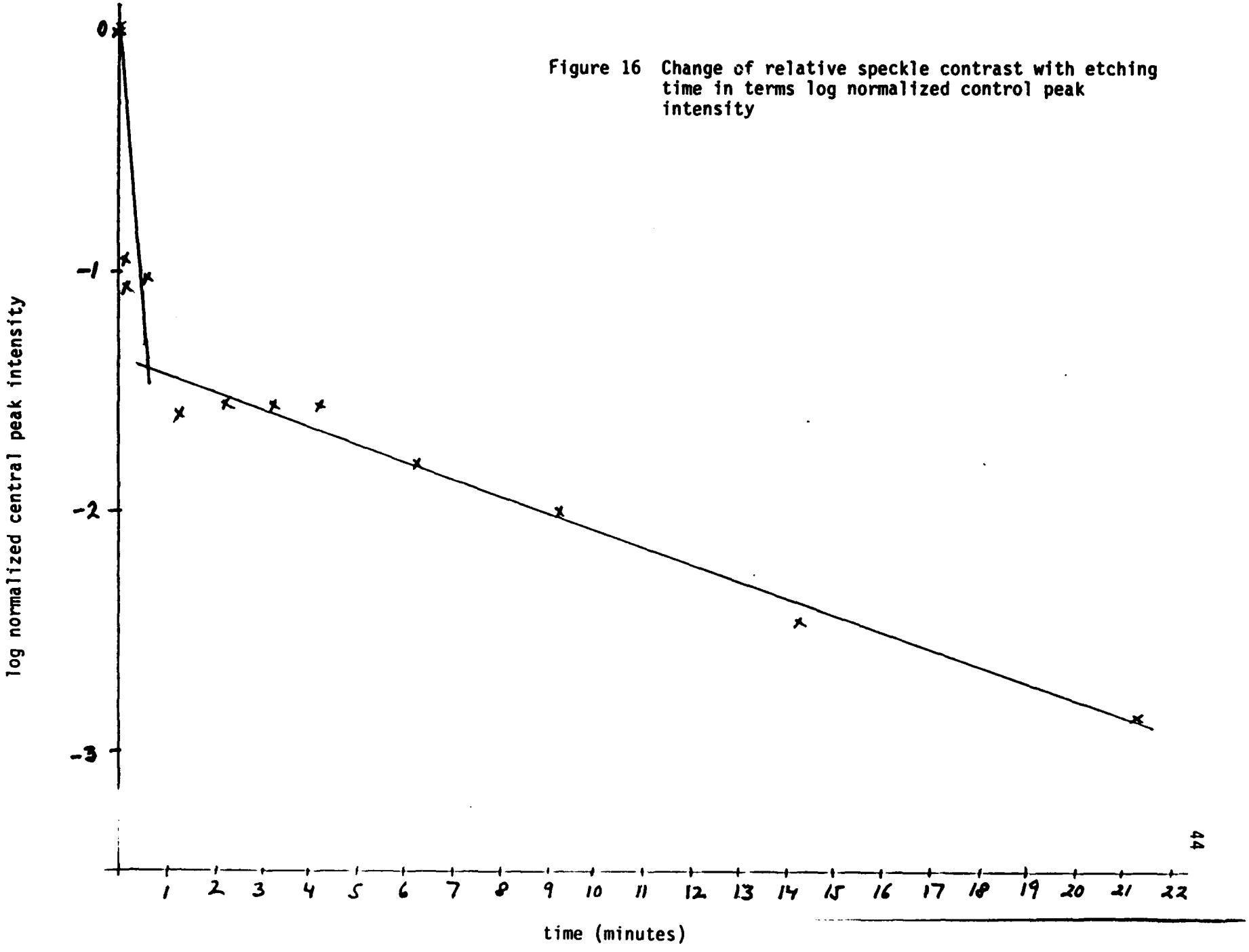

Figure 16 Change of relative speckle contrast with etching time in terms log normalized control peak intensity

APPENDIX I

APPENDIX I

General Description of Scanning Ellipsometer

We believe that our modifications have produced an instrument much superior to those of our predecessors and for this reason and because of a delay in its publication, the following description is rather detailed.

The light from a He/Ne laser (λ = 6328 Å) is linearly polarized by a polarizer--the polarizer angle can be changed by a motor-driven rotation stage attached to an encoder allowing position readout to ± 0.01 degree--and passes through a modulator. The modulator consists of a coil passing 500 Hz of alternating current. At the axis of the coil is a Faraday glass cylinder which rotates the plane of polarization of axially transmitted light by an angle θ, which is proportional to the cylinder length and the magnetic field, the proportionality constant being known as the Verdet constant. Then the light is reflected by the sample under investigation and is passed by a second polarizer, the analyzer, and by several lenses, which increase the optical resolution and is finally brought onto the detector surface (a diode detector or photomultiplier with built-in preamplifier.

The location of the modulator is somewhat arbitrary; it can be between the polarizer and the sample as shown in Fig. 2 or between the sample and the analyzer. The following description assumes the latter location for ease of understanding.

The linearly polarized light incident on the sample will, in general, become elliptically polarized on reflection. When the analyzer angle is set parallel to the major (minor) axis of the polarization ellipse there will be maximum (minimum) intensity on the detector. For other angles there will be an intermediate intensity. The figure below shows the intensity of the detector signal as a function of the detector signal as a function of analyzer angle schematically for a given polarizer angle. A_1, $A_3 = A_1 + \pi$, $A_5 = A_1 + 2\pi$ are angles parallel to the major axis of the ellipse and A_2, $A_4 = A_2 + \pi$, etc. are angles parallel to the minor axis of the ellipse. An alternating current through the modulator will rotate the ellipse back and forth with the modulation frequency by an angle given by $\theta_{max} = V \cdot \ell \cdot H_{max}$, where V is the Verdet constant and ℓ the length of the Faraday glass cylinder. Rotation of the ellipse by an angle θ has the same effect as rotating the analyzer by an angle $-\theta$. The effect of rotating the analyzer can readily be seen from the figure. If we have $A = A_3$ for θ=0, a modulation with a frequency ω produces an intensity varying with a frequency 2ω. This is true for all minima and maxima. If, however, we have $A = A'$ for $\theta = 0$, the detector signal intensity will vary with the same frequency as the modulating current. Thus the major and minor axis of the ellipse can be found by determining the analyzer angle A for which the 500 Hz component of the detector signal is zero.

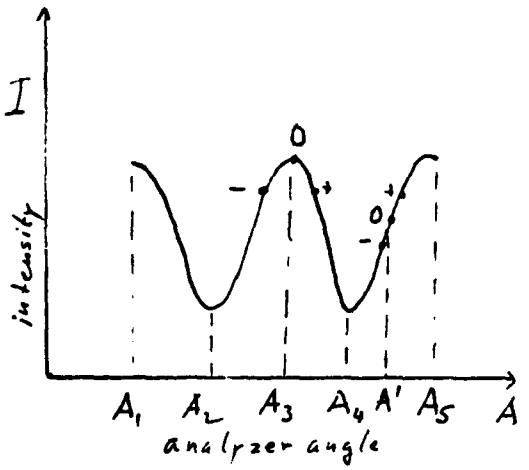

The detector signal is amplified by a preamplifier, an ac-coupled amplifier and then by an amplifier with automatic gain control; 500 Hz frequency is filtered out from the signal emerging from the last-named amplifier and the remaining signal with the "sample and hold" and the "sample and hold control" produces an error signal of sign such as to bring the analyzer back to the position for which the intensity is a minimum or a maximum. It will be noted that the 500 Hz frequency components are phase-shifted by π to the left and the right of the extremum.

The position of the polarizer and the analyzer are decoded and interfaced to a computer. The complete revolution of the polarizer gives us the analyzer angle A (for which the 500 Hz component is zero) as a function of the polarizer angle for $0 \leq P \leq 360°$.

The function A(P) also depends the ellipsometer parameters ψ and Δ.

Method of Calculation of Parameters

It was said above the the modulator could be located either downstream or upstream of the sample. The mathematical expressions are

$$\tan 2A = 2 \cos \Delta \frac{\tan \psi \tan P}{\tan^2 \psi - \tan^2 P}$$

for the former case and

$$\tan 2P = 2 \cos \Delta \frac{\tan \psi \tan A}{\tan^2 \psi - \tan^2 P}$$

where P is the polarizer angle (angle of the plane of polarization of the polarizer with respect to the plane of incidence) and A is the analyzer angle. Not surprisingly A and P change roles depending on the modulator location. These is an advantage of one location over the other in terms of sensitivity.

By continuously rotating the polarizer we also get corresponding analyzer angles, P_i^m and A_i^m. The decoders and counters give us very accurate changes of these angles. The main inaccuracy (tenths of degree) enters by assigning a definite absolute value to the first analyzer and polarizer angle. Because this error is constant, we assume that the true values for the polarizer and analyzer angle are given by

$$P_i = P_i^m + \Delta P$$

$$A_i = A_i^m + \Delta A.$$

There true values should fulfill the theoretically derived relation between A and P, so that

$$\tan 2(A_i^m + \Delta A) = 2 \cos \Delta \cdot \frac{\tan \psi \tan (P_i^m + \Delta P)}{\tan^2 \psi - \tan^2 P}$$

or

$$(A_i^m + \Delta A) = \frac{1}{2} \tan^{-1} \left(2 \cos\Delta \frac{\tan\psi \tan(P_i^m + \Delta P)}{\tan^2\psi - \tan^2 P} \right)$$

The unknown ΔA, ΔP, $\tan\psi$, $\cos\Delta$ are now determined by a least square fit. That means

$$E \equiv \sum_i \left[2(A_i^m + \Delta A) - \tan^{-1} \left(2 \cos\Delta \frac{\tan\psi \tan(P_i^m + \Delta P)}{\tan^2\psi - \tan^2 P} \right) \right]^2$$

should be a minimum with respect to ΔP, ΔA, $\tan\psi$, $\cos\Delta$. With $\alpha \equiv 2\cos\Delta$ and $\beta \equiv \tan\psi$

$$E = \sum \left[2(A_i^m + \Delta A) - \tan^{-1} \left(2 \frac{\beta \cdot \tan(P_i^m + \Delta P)}{\beta^2 - \tan^2(P_i^m + \Delta P)} \right) \right]^2$$

should be a minimum with respect to α, β, ΔP, ΔA. With the definitions for

$$F_i \text{ where } E = \sum (F_i)^2$$

$$g_i = \alpha \frac{\beta \tan(P_i^m + \Delta P)}{\beta^2 - \tan^2(P_i^m + \Delta P)} \quad \text{and} \quad d_i = \beta^2 - \tan^2(P_i + \Delta P)$$

we get four non-linear equations

$$\frac{\partial E}{\partial(\Delta A)} = \sum 2F_i \cdot 2 = 4 \sum F_i = 0 \tag{1}$$

$$\frac{\partial E}{\partial \alpha} = \sum 2F_i \left(-\frac{1}{1+g_i^2} \right) \cdot \frac{g_i}{\alpha} = 0 \tag{2}$$

$$\frac{\partial E}{\partial \beta} = \sum 2F_i \left(-\frac{1}{1+g_i^2} \right) \left(\frac{g_i}{\beta} - 2\frac{g_i}{\alpha_i} \right) = 0 \tag{3}$$

$$\frac{\partial E}{\partial(\Delta P)} = \sum 2F_i \left(-\frac{1}{1+g_i^2} \right) \cdot \frac{\alpha\beta}{d_i \cos^2(P + \Delta P)} \cdot \left[1 + 2\frac{g_i d_i}{\alpha\beta^2} \right] = 0 \tag{4}$$

If equation (2) is satisfied, the first part of equation (3) is automatically zero. We can also get rid of constant multipliers and finally get

$$\sum F_i = 0$$

$$\sum F_i \frac{g_i}{1+g_i^2} = 0$$

$$\sum \frac{F_i g_i}{(1+g_i^2) d_i} = 0$$

$$\sum \frac{F_i}{(1+g_i^2) d_i \cos^2(P_i^2 + \Delta P)} \left[1 + \frac{2 g_i^2 d_i}{\alpha^2 \beta^2} \right] = 0$$

This system of non-linear equations is solved by Newton's method for non-linear systems. We can write it as

$$\underline{F}(\underline{x}) = 0$$

where $\underline{x} = \begin{pmatrix} \Delta A \\ \alpha \\ \beta \\ \Delta P \end{pmatrix}$ where F_i are the four functions on the left side of the system of equations. $\underline{F}(\underline{x}) = 0$ will be true for the correct values of ΔA, α, β, ΔP.

If we start with some value $\underline{x}$ in the neighborhood of the correct solution the iteration

$$x^{(k)} = x^{(k-1)} - \underline{\underline{J}}^{-1}(\underline{x}^{(k-1)}) \underline{F}(\underline{x}^{(k-1)})$$

converges to the true solution.

$x^{(k)}$ is x after the k'th iteration

$\underline{\underline{J}}(\underline{x}^{(k-1)})$ = Jacobian matrix

$$= \begin{pmatrix} \frac{\partial F_1}{\partial \Delta A} & \frac{\partial F_1}{\partial \alpha} & \frac{\partial F_1}{\partial \beta} & \frac{\partial F_1}{\partial \Delta P} \\ \frac{\partial F_2}{\partial \Delta A} & - & - & - \\ \cdot & - & - & - \\ \cdot & - & - & - \end{pmatrix}$$

evaluated at $\underline{x} = \underline{x}^{(k-1)}$

$\underline{F}(\underline{x}^{(k-1)})$ is the left side of the system of equations for $\underline{x} = \underline{x}^{k-1}$, in general $\neq 0$.

The Jacobian matrix is found by differentiating E once more

$$\frac{\partial F_i}{\partial \Delta A} = \frac{\partial^2 E}{\partial^2 \Delta A} \qquad \frac{\partial F_i}{\partial \alpha} = \frac{\partial^2 E}{\partial \Delta A \partial \alpha} \qquad \text{etc.}$$

If an analytic expression for the Jacobian matrix can be found, $\underline{\underline{J}}$ and $\underline{F}$ can be calculated. To find

$\underline{\underline{J}}^{-1}\,\underline{F} = \underline{y}$ we have to solve the linear system

$\underline{\underline{J}}\underline{y} = \underline{F}$

After we know $\underline{y}$ we can calculate

$$\underline{x}^{(k)} = \underline{x}^{(k-1)} - \underline{y}$$

and repeat the above until $\underline{F}(\underline{x}^{k})$ is close enough to 0.

This calculation provides us with

ΔA, $\alpha = 2\cos\Delta$, $\beta = \tan\psi$, ΔP.

We therefore know $\pm\Delta$ (or Δ, $360-\Delta$) and ψ

Note: $\tan\psi > 0$ $\qquad [\tan\psi = \frac{\rho''}{\rho^{\perp}} > 0]$

$0 < \tan\psi < \infty$

$0 < \psi < 90°$

also $\Delta = \Delta_{\parallel} - \Delta_{\perp}$ is not restricted (except $0 < \Delta < 2\pi$). Because our experiment involves only cos Δ, we cannot determine Δ unambiguously. One measurement will supply two Δ's.

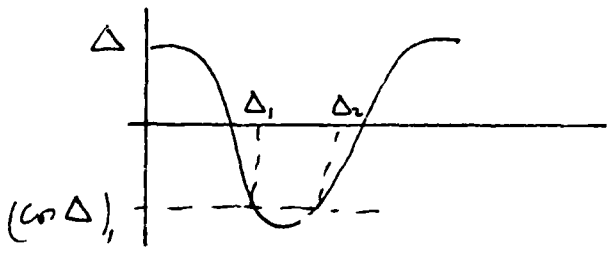

To determine Δ unambiguously would have to involve a measurement of sin Δ. We would have to determine whether the light is partly left or right-rotated in its polarization. Calculation shows that the fourth component of the Stokes vector after the modulator contains sin Δ.

The figure below shows how the analyzer angle A depends on P, Δ, and ψ. It will be noted that for increasing polarizer angle the analyzer angle decreases.

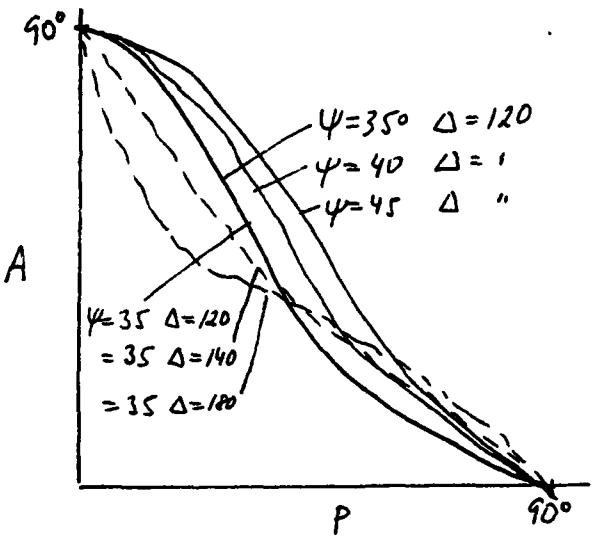

The analyzer angle A is 45° for $P = \psi$.

Increasing ψ leads to a larger A for the same P.

Increasing A leads to smaller A for $P < \psi$ and to larger A for $P > \psi$.

This follows from

$$A = \frac{1}{2}\tan^{-1}\left(2\cos\Delta\,\frac{\tan P\tan\psi}{\tan^2\psi-\tan^2 P}\right)$$

Note that P is periodic with period of 180°
A is periodic with period of 90°

$$A(P=0) = 0 \pm n\cdot 90° \text{ where } n = 0,\pm1,\pm2,....$$

$$A(P=90°) = 0 + n90°$$

$$A(180-P) = \frac{1}{2}\tan^{-1}\left(2\cos\Delta\,\frac{\tan(180-P)\tan\psi}{\tan^2\psi-\tan^2(180-P)}\right)$$

$$= -\frac{1}{2}\tan^{-1}\left(2\cos\Delta\,\frac{\tan P\,\tan\psi}{\tan^2\psi-\tan^2 P}\right) = -A(P) \pm n\cdot 90$$

since $\tan(180-p) = -\tan P$

Therefore it is sufficient to know the behavior of A(P) for $0 < P < 90°$.

APPENDIX II

Microscopic Contour Changes of Tribological Surfaces by Chemical and Mechanical Action

by

James L. Lauer and Simon S. Fung

VOLUME 26, 4, 430–436
ASLE TRANSACTIONS

Microscopic Contour Changes of Tribological Surfaces by Chemical and Mechanical Action

JAMES L. LAUER and SIMON S. FUNG
Rensselaer Polytechnic Institute
Troy, New York 12181

An electronic optical laser interferometer capable of resolving depth differences of as low as 30 Å and planar displacements of 6000 Å was constructed for the examination of surface profiles of bearing surfaces without physical contact. This instrument was used to determine topological chemical reactivity by applying a drop of dilute alcoholic hydrochloric acid and measuring the profile of the solid surface before and after application of this probe. It was found that scuffed bearing surfaces reacted much faster than virgin ones but that bearing surfaces exposed to lubricants containing an organic chloride reacted much more slowly. In a separate series of experiments, a number of stainless steel plates were heated in a nitrogen atmosphere to different temperatures and their reactivity examined later at ambient temperature. The change of surface contour as a result of the probe reaction was found to follow an Arrhenius-type relation with respect to heat treatment temperature. This result could have implications on the scuffing mechanism.

INTRODUCTION

When nonconforming solid surfaces separated by a lubricant are in relative motion under increasing loads, the bulk temperature gradually increases and the lubricant film thickness decreases. At some point, the surfaces will begin to interact mechanically. At first, the peaks of the highest asperities will be reduced and the surfaces will become smoother. This interaction is an essential part of normal "run-in." At higher loads, scoring occurs, manifested by grooves and ridges in the surface oriented in the sliding direction. At still higher loads, a sudden failure may occur, which is called "scuffing." The scoring and scuffing events are often coincident and many authors have been using these terms interchangeably.

Because scuffing is likely to be catastrophic and without warning, measures were designed to postpone it or avoid it. Since welding of the contacting surfaces has been considered an essential part of scuffing, these measures usually entail the formation of interposed layers. For example, the use of extreme pressure (EP) lubricant additives is thought to result in the formation of renewable coatings of metal sulfides, chlorides, or phosphates preventing the welding. A durable coating of the surfaces with thin, hard, inert layers could also avert scuffing for the same reason and could work even without a lubricant—an added advantage under severe conditions, when the lubricant is subject to thermal breakdown.

Although the mechanism of scuffing is not yet fully understood, a temperature criterion is commonly postulated. The best known is the "total temperature" of Block (*1*), which consists of the bulk temperature of the metal parts and the instantaneous surface temperature rise of the surface area of contact. Others correlated scuffing failure primarily with chemical activity which, of course, is itself strongly influenced by temperature [Goldman (*2*)]. Implicitly, the assumption has been made that chemical reaction would take place primarily above the characteristic ("total") temperature between metal and lubricant components. Could it be that portions of metal surfaces exposed to temperatures above the characteristic temperature are inherently more reactive at any temperature?

The availability of an optical interferometer capable of resolving depth differences as low as 30 Å and planar displacements of 6000 Å provided us with a tool for attempting an answer to this question. Since vacuum is not required, we could carry out probe microreactions on neat and scuffed areas and compare the resulting changes of surface profile. We could examine both titanium-nitride-coated and uncoated bearing balls before and after use in this way and compare the results with subsequent scanning electron photomicrographs. Dilute alcoholic hydrochloric acid served as our probe. Metal surfaces heated to known temperatures were examined for reference. The results point to changes caused by the heat treatment, which produced chemical reactivity changes even at ambient temperature and likely mechanisms for the absence of scuffing with titanium nitride-coated balls.

Presented as an American Society of Lubrication Engineers paper at the ASME/ASLE Lubrication Conference in Washington, D.C., October 5–7, 1982

APPARATUS

AC Interference Microscope

The first instrument of this kind was originally designed and built for the examination of optical surfaces and elements by Johnson, Leiner, and Moore (*3*) at the Institute of Optics of the University of Rochester. Professor Moore helped us build our instrument which differs from his only in minor details relating to our different applications.

Basically, the instrument is a Twyman-Green interferometer with alternating current electronics, which is capable of a phase resolution of one two-hundredth of the wavelength of the red He/Ne laser line (6328 Å). Surface profiles can thus be obtained to about ± 30 Å without physical contact. Figure 1 is a schematic drawing of the instrument's optics. Radiation from an He/Ne laser is split by a beamsplitter; part of the radiation continues to a flat mirror oscillated by a piezoceramic transducer and part is deflected to the sample surface by way of a microscope objective. The split beams are reflected back to the beamsplitter, recombined, expanded by a microscope objective, and ultimately transferred to a photoelectric detector. Two scanning mirrors can be turned in such a way as to make possible scans parallel to the x and y directions in the sample plane. Phase differences between the two beam paths generate fringes in the detector plane. As the sample surface is scanned, the phase difference between the interferometer beams is changed and the fringes are moved over the detector surface proportionally, as determined by the optics.

The sensitivity of the instrument derives from an ingenious electronic arrangement. The reference mirror is oscillated piezoelectrically at 20 kHz. Correspondingly, the fringe pattern at the detector surface is oscillated with the same frequency but the intensity of a fringe peak—or valley—is oscillated at twice the reference mirror frequency, or at 40 kHz. Intuitively, this arises from the fact that the peak or valley intensity or the corresponding photoelectric potential can change in one direction only—downward for the peak and upward for the valley—while the radiation intensity anywhere else can become stronger or weaker. It is thus possible to "lock-in" on a peak at the 40 kHz frequency. The mean potential (halfway between peak and valley) or d.c. potential will follow the locked-in fringe and become a measure of the phase change as the sample surface is scanned.

At the present stage of the instrument, scanning is done nonlinearly, by varying the angle of the recombined beam with respect to the optic axis of the microscope objective facing the sample. For small excursions of the scanning mirror, the departure of a scan from linearity is small. The surface profile of Fig. 2, obtained with an inexpensive reflection-type diffraction grating, is an example. The distance between the first and second peaks is about 10 percent greater than that between the second and third peaks. Correction to linearity is, of course, possible. The intensity of the peaks of Fig. 2 is seen to fall off toward the right. The reason is the lack of planarity of the objective lens when used off-axis. Beyond a distance of 2.5 μm from an arbitrary chosen position, the scanning optics are evidently out of the field of view. The intensity of the peak at 3.0 μm is much less than that of the other peaks. As the grating was blazed, the slope to the left of every peak is expected to be shorter and steeper than that of the slope to the right. The angles are also about correct. The reason for the gentleness of the peaks and valleys, where sharp corners are expected, is the horizontal resolution limit of the objective lens in conjunction with the interferometer optics. We are confident that a good part of these limitations will be removed by digital image analysis.

Distance calibration of the instrument is simple. In the horizontal plane, the distances of successive peaks of a reflection grating provide the required information (Fig. 2). Depth calibration is done very accurately by the phase jump in the detector plane. The separation between two successive interference fringes corresponds to a phase difference of 2π between the sample and reference beams. In air, because of the phase reversal on reflection by the sample surface, this separation of fringes corresponds to a change in depth of sample surface profile of half a wavelength of the laser light (6328 Å) or 3164 Å in our case. In terms of the electric recorder output potential, this geometrical change corresponds to 10 volts. Any voltage changes are directly proportional to the phase changes and, therefore, to the changes of depth and the conversion can be carried out in terms of the 316.4 Å/volt relation.

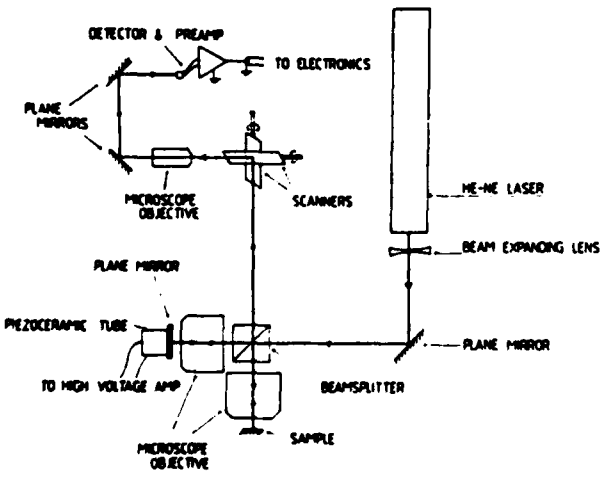

Fig. 1—Schematic drawing of interferometer

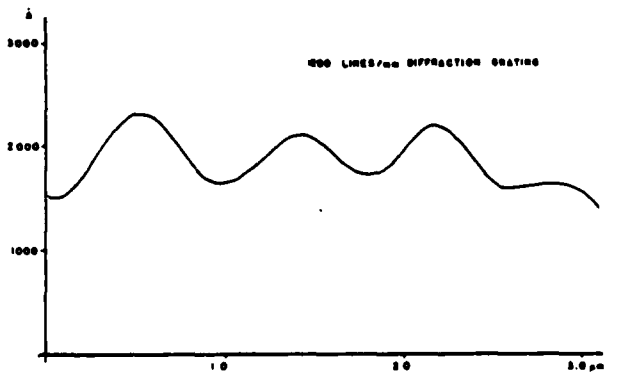

Fig. 2—Profile of a 12 line/mm diffraction grating

Ball/Plate Sliding Contact

The experimental setups used to obtain scuffing or scoring were the same we described in an earlier publication (*4*). They were ball/plate sliding EHD contacts in which a bearing ball of 2.25-inch diameter was turned by a horizontal shaft either on top of a diamond window (the plate), in the bottom of a cup containing the test fluid, or underneath a sapphire window (the plate). In either case, the ball was loaded from the top. The former setup was used primarily as part of our infrared analysis of the fluid under EHD conditions; the contact was always flooded. The latter setup would be used for EHD film thickness and traction measurements and would obtain the lubricant by a wetting and dragging mechanism. Here, too, conditions were such that starvation was excluded.

These contacts were operated for periods of about 100 hours under varying loads and speeds. Scuffing occurred only with uncoated steel balls.

MATERIALS

The bearing balls were of 2.25-inch diameter and made of 440 C stainless steel. Some of them were coated with titanium nitride by chemical vapor deposition (CVD method) to a uniform thickness of about 4 μm, as described by Hinterman and Boving (*5*). The smoothness of all the ball surfaces was about 0.01 μm initially (mean peak height), as determined with our optical profilometer. Since the lubricant film thickness in the EHD contact under the heaviest load and at the smallest continuously maintained shear rate was at least 0.5 μm as determined earlier (*4*), direct asperities interaction could only occur when the sliding speed was gradually reduced to zero.

The balls were run with polyphenyl ether fluid (5P4E) either pure or containing 1 percent by volume of 1,1,2-trichloroethane. Both of these fluids were also referred to in the same earlier publication (*4*).

Before use in the experiments discussed below, the balls were cleaned with acetone and mounted in a holder specially constructed for the interference microscope.

The stainless steel reference plates were of smoothness similar to that of the balls. They were made of polished No. 304 stainless steel and were 1" × 1" × 1/16" in size.

The probe solution was 0.04 M hydrochloric acid in absolute ethyl alcohol.

EXPERIMENTAL PROCEDURES

Heating of the Test Plates

The test plates were sandwiched in a holder between half-inch thick asbestos plates containing a three-quarter-inch-diameter hole in the center. Two pieces of a material melting or changing color at known temperatures were clamped onto top side of the sample, allowing temperature monitoring during heating. The two temperature indicators were selected in such a way that the maximum heating temperature was bracketed between them; in other words, heating would be stopped when either of them melted or changed color.

Heating was accomplished rapidly (at 220 K/s) with the hot gases just above the tip of an acetylene flame directed at the lower side of the plates. At the same time and for a considerable time thereafter, nitrogen gas was blown over the top side of the plate to reduce or prevent oxidation (cooling rate: 100 K/s). Oxidation could never be entirely prevented because vacuum was not used to remove absorbed gas. On the other hand, one of the purposes of this work was the simulation of realistic field conditions, in which oxide films are never absent.

Preparation of the Ball Samples

The balls were taken from the rigs after many hours of operation on polyphenyl ether with and without 1 percent of 1,1,2-trichloroethane. The steel balls without titanium nitride would have failed by scuffing.

The balls were cleaned with acetone, soaked in absolute alcohol overnight, rinsed, and placed in a vacuum desiccator to remove the absorbed alcohol. The principal purpose of applying the vacuum was to avoid the destruction of the filament in the scanning electron microscope.

Examinations of Ball Surfaces Run in Polyphenyl Ether with the Interferometric Microscope

Since the score or scuff marks on the balls were typically 100 μm in diameter, we found it useful to work with two different microscope objectives, 10X and 40X, the former enabling us to overlap the mark and the latter to look inside of it. Still higher magnification could have given us better lateral resolution but the short working distance would have

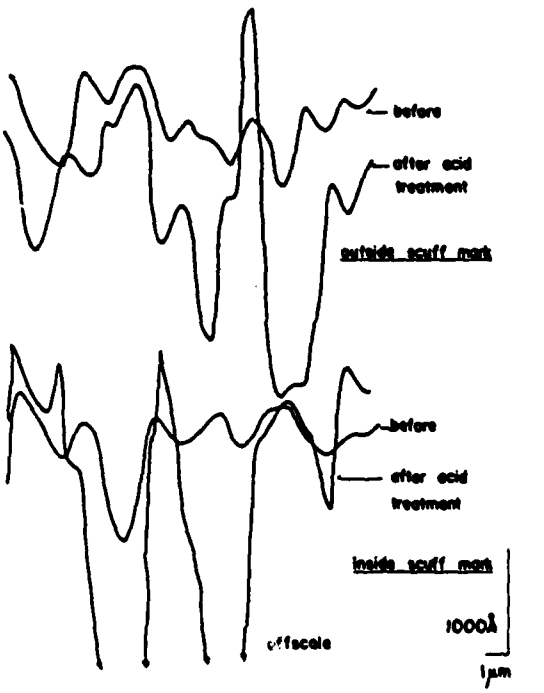

Fig. 3—Surface profiles of a stainless steel bearing ball scuffed in polyphenyl ether, before and after a test probe of 0.04 M alcoholic hydrochloric acid was applied. The top traces were taken outside the scuff mark and the bottom traces were taken inside the scuff mark. (In order to avoid overlap, the traces taken after the acid treatment were set off.)

made the application of the test fluid (0.04 M alcoholic hydrochloric acid) very difficult.

Figure 3 shows two of an area of such a used steel bearing ball, which includes parts within and without the scuff mark. A drop (0.05 ml) of test fluid was applied from a measuring syringe, care being taken not to move the ball-microscope alignment in any way. For this work, the ball was rigidly mounted on a holder, which itself was rigidly attached to the microscope frame, so that the entire system would vibrate as one unit. The drop would evaporate rapidly, and then another profile was recorded. As can be seen from Fig. 3, the changes outside the scuff mark were much smaller than the changes inside the scuff mark and, in either case, most of the profile was lowered by the test reaction.

In another instance, the difference of reaction inside and outside the scuff mark was even more drastic. Figure 4 presents a clear indication that changes of profiles can be both upwards and downwards. There can be no doubt that the changes produced by the test probe within the scuff mark were much greater.

Figure 5 represents the effects outside of the scuff mark of two successive probes on stainless steel bearing ball run to scuffing on polyphyenyl ether. The reactivity was much greater for the second treatment than for the first. The first treatment might have attacked the oxide layer, the second the metal itself.

Examinations of Ball Surfaces Run in Polyphenyl Ether Containing 1 percent of 1,1,2-trichloroethane (TCE) with the Interferometric Microscope

Figure 6 shows the profiles obtained with a bearing ball within and without the scuff mark, then the polyphenyl ether (5P4E) lubricant contained 1 percent of 1,1,2-trichloroethane (TCE). As can be seen, the differences of profile produced by the probe treatment were minimal in each case, although the changes within the track were a little bit more evident.

Examinations of Titanium-nitride-coated Bearing Ball Run in Polyphenyl Ether with or without 1,1,2-trichloroethane (TCE) with the Interferometric Microscope

In this case, scuffing did not occur. The profiles outside the barely visible score mark did not change at all on probe treatment, but, with TCE and within the score, continuous changes occurred. It turned out to be impossible to get reproducible profiles under these conditions. For these reasons, we assumed that cracks in the coating had occurred. The following section shows a confirmation of this hypothesis by photographs taken under the scanning electron microscope.

Scanning Electron Photomicrographs of Wear Surfaces

Perhaps the most interesting of these photos is Fig. 7, taken within and without the barely noticeable score mark of a TiN-coated ball. The light areas represent TiN coatings. The ladder-type structure within the score mark is very interesting and will be discussed later. The picture taken off the track shows the porosity of the TiN coating.

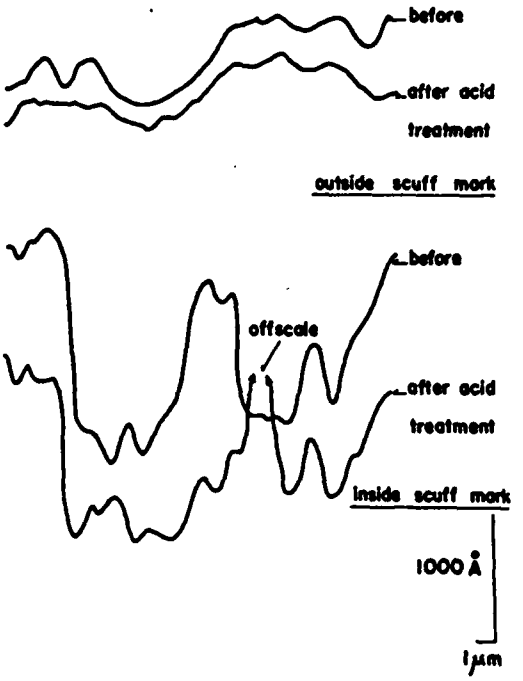

Fig. 4—Surface profiles of another stainless steel bearing ball scuffed in polyphenyl ether, before and after a test probe of 0.04 M alcoholic hydrochloric acid was applied. The top traces were taken inside the scuff mark. (In order to avoid overlap, the traces taken after the acid treatment were set off.)

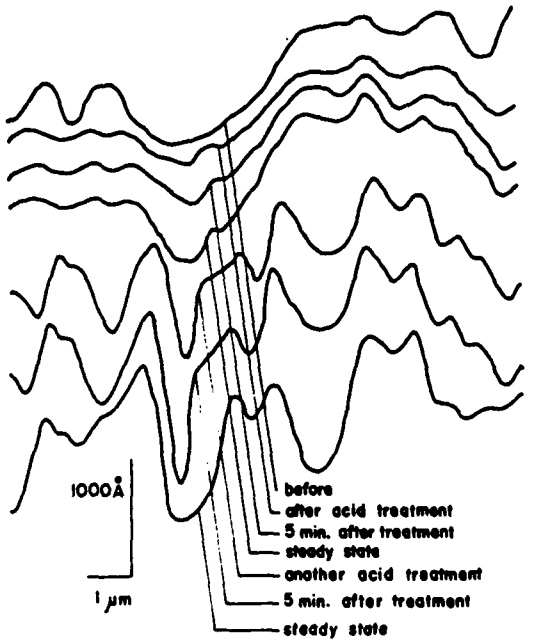

Fig. 5—Series of profiles of the bearing ball of Fig. 4 taken outside of the scuff mark. Two successive probe treatments were given. (Profiles were set off to avoid overlap.)

The electron photomicrographs of the bare ball after use with polyphenyl ether are also interesting. Without TCE, the wear track shows streaks and some of the characteristic scuff marks [Fig. 8(a)]. When TCE was present, however, round specks occur with high concentration in the track of

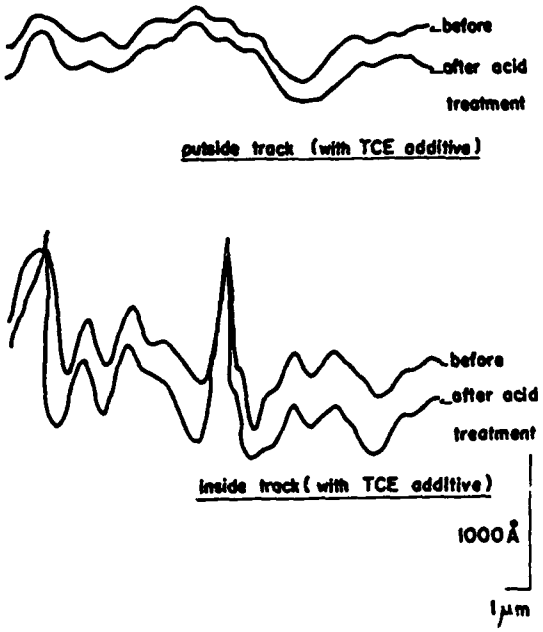

Fig. 6—Surface profiles of a different stainless steel bearing ball scuffed in polyphenyl ether containing 1 percent of 1,1,2-trichloroethane. The top traces were taken outside the scuff mark, whereas the bottom traces were taken inside the scuff mark. (The traces recorded after the acid treatment were set off to avoid overlap.)

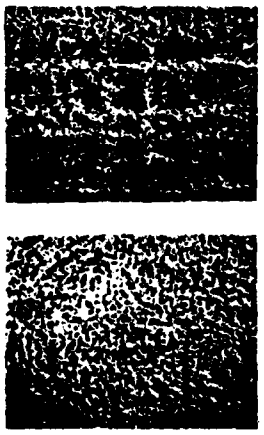

Fig. 7—SEM of TiN-coated ball taken (a) within the score mark, note ladder-like porous structure. (b) outside the score mark, note porous structure. The lubricant was polyphenylether (5P4E) with 1 percent of 1,1,2-trichloroethane.

highest wear [Fig. 8(b)]. Outside the wear track, these specks were essentially absent.

Profiles of Heated Plates Before and After Reaction with 0.04M Alcohol Hydrochloric Acid

To answer the question whether the heating above a "total" temperature would change the reactivity, we applied the same alcoholic hydrochloric acid probe we used for the scuffed balls to heated steel specimens. The probe was, of course, applied at room temperature. Figure 9 shows such profiles before and after treatment, when the plate was heated to 204°C and to 774°C. In the former case, the changes in contour were small; in the latter case, rather large.

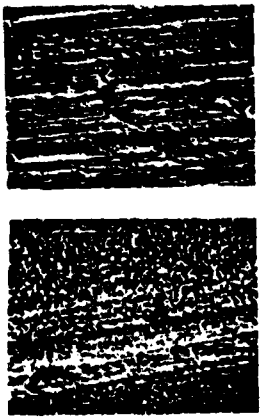

Fig. 8—SEM of 440C-steel ball run on (a) polyphenyl ether to scuffing. Note wear track with characteristic scuff marks, (b) polyphenyl ether containing 1 percent of 1,1,2-trichloroethane. Note the round specks.

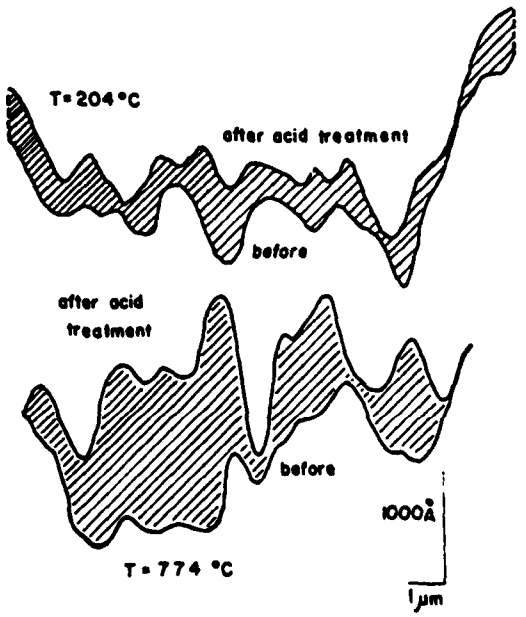

change in profile after acid treatment for heated specimen

Fig. 9—Change of surface profile after treatment with alcoholic hydrochloric acid of a stainless steel specimen heated to (a) 204°C, and (b) 774°C.

The heating was carried out as described previously. This "tempering" may have changed the microstructure of the steel and probably did so even though the metallurgically prescribed procedure was not followed. The resulting change of chemical reactivity is a point stressed in this paper.

Figure 10 is an Arrhenius-type plot of contour changes (the shaded areas of Fig. 9, for example) against temperature. The discrepancies from an average straight line, considering the relative crudeness of the method, are not great.

DISCUSSION

The results of our experiments can be summarized as follows:

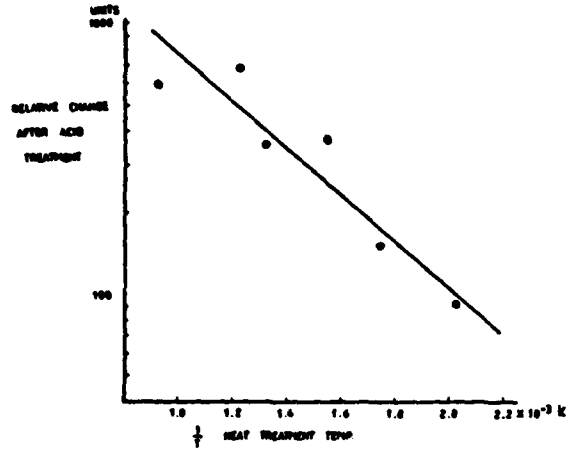

Fig. 10—Arrhenius-type plot of surface profile change of stainless steel specimens heated to different temperatures. Relative surface change after acid treatment of S.S. (304) specimens heated to different temp.

1. Scuffed steel bearing surfaces are more reactive toward alcoholic hydrochloride acid than virgin surfaces.
2. Scuffed bearing surfaces originally used on a lubricant containing a small concentration of an organic chloride are much less reactive toward alcoholic hydrochloric acid than surfaces that had become scuffed with the undiluted lubricant.
3. Titanium-nitride-coated steel bearing surfaces did not scuff under conditions where the uncoated surfaces did. They did show track marks, however. Furthermore the coating proved to be porous in general and exhibited a ladder-type structure on the track marks when run with polyphenyl ether containing 1 percent of 1,1,2-trichloroethane. When run without the chloride, the surface on the track marks was not changed but was just as porous as the virgin surfaces.
4. Uncoated steel bearing surfaces scuffed with polyphenyl ether lubricant containing 1,1,2-trichloroethane showed a high concentration of round specks in the track but only few such specks outside of it. No specks at all were shown when the chloride was absent. These specks are presumably metal chloride.
5. The reactivity of heated metal surfaces toward alcoholic hydrochloric acid at ambient temperature follows an Arrhenius-type relation with temperature. Point 5 would seem to indicate that a bearing surface heated at any one time to a high temperature, e.g. by direct contact, could become much more reactive and therefore prone to scuffing at a later time.

The Arrhenius plot of Fig. 10 would seem to be the result of a lasting change of the metal surface by its reheating or tempering. Perhaps the so-called "chemostress" coefficient defined by Ciftan and Saibel (*7*) plays a role. These authors have shown a change of chemical potential of an adsorbate with stress in the substrate. The chemical potential expresses the change of free energy with concentration of a chemical constituent and the free energy change ΔG for a reaction is related to the equilibrium constant K. Therefore, the ratio of a product of product concentrations to that of reactant concentrations, by the well-known thermodynamic relation

$$K = \exp(\Delta G/RT)$$

an Arrhenius relation between a product of reaction (e.g. surface profile change) and the absolute temperature can be derived by thermodynamic and continuum mechanics alone. However, the heterogeneity of the metal surface could be the basis of a kinetic explanation: The tempering changes the surface composition logarithmically with temperature because it is diffusion-controlled and the chemical reaction rate depends on the number of reaction sites thereby created. This argument would equally lead to an Arrhenius relation.

Both of these explanations could be valid simultaneously, but the latter seems to be more important on the basis of chemical and especially electrochemical experience. Their relative importance will be determined by repeating the experiments with pure solid surfaces.

It was important to note that titanium-coated balls barely scuffed under our conditions. Yet, when 1,1,2-trichloroethane was present in the lubricant, the rather remarkable ladder-type structure appeared. The crests at right angles to the direction of ball motion could have been formed in a manner similar to the well-known washboard effect on highway surfaces. In both cases, a liquid was able to creep below the surface as our measurements with the interference microscope indicated and which were confirmed by the scanning electron microscope. The same theory seems to be applicable in both cases. Work along these lines is in progress.

The reason for the increased metal surface reactivity as a result of heating to high temperatures could be a change of metal structure, α phase change, or a migration of impurities. Such phenomena are well-known to corrosion engineers (*6*).

ACKNOWLEDGMENT

This work was funded in part by grants from the Air Force Office of Scientific Research, Grant No. AFOSR-81-0005 and from the National Aeronautics and Space Administration, Grant No. NSG-3180-12-81.

We also with to thank (1) H. E. Hinterman and H. J. Boving of Laboratoire Suisse de Recherches Horlogeres for helping us obtain the TiN-coated Balls, (2) Wolfgang Holzhauer for the scanning electron photomicrographs and (3), above all, Duncan T. Moore of the Institute of Optics of the University of Rochester for his wonderful help with the interference microscope.

A useful discussion with William R. Jones, Jr. of NASA-Lewis in Cleveland, Ohio is gratefully acknowledged.

REFERENCES

(*1*) Blok, H., "The Postulate About the Constancy of Scoring Temperature," *Interdisciplinary Approach to the Lubrication of Concentrated Contacts*, NASA-SP-237, P. M. Ku, editor, July 15–17, 1969, pp 153–248.

(*2*) Goldman, I. B., "Corrosive Wear as a Failure Mode in Lubricated Gear Contacts" *Wear*, **14**, pp 431–444 (1969).

(*3*) Johnson, G. W., Leiner, D. C., and Moore, D. T., "Phase-Locked Interferometry," *Optical Eng.*, **18**, pp 46–52 (1979).

(4) Lauer, J. L., Keller, L. E., Choi, F. H., and King, V. W., "Alignment of Fluid Molecules in an EHD Contact," *ASLE Trans.*, 25, 3, pp 329–336 (1982).
(5) Hinterman, H. E. and Boving, H., "Wear-Resistant Thin Layers," *Die Technik* (1978), 7, pp 387–398, and further references given in this article.
(6) Uhlig, H. H., *Corrosion and Corrosion Control*, Second Edition, John Wiley & Sons, Inc., New York 1971, pp 131*f*.
(7) Ciftan, M. and Saibel, E., "The Chemostress Coefficient," *Solid State Communications*, 27, pp 435–437 (1978).

DISCUSSION

HEIHACHIRO OKABE (Member, ASLE)
Tokyo Institute of Technology
Tokyo, Japan

The authors have provided a very useful tool, especially in studying oil film behavior under EHD lubrication. The method shown in this paper would give us predictive techniques in a new framework of surface topography relating to contact initiation in EHD lubrication.

The discusser is interested in knowing the chemical reactivity change before the scuffing occurs.

Asperities on rubbing surfaces are actually under periodic heating. The authors suggest that we could obtain information of topographical and chemical changes of the surfaces in a process leading the rubbing surfaces to the scuffing. If the authors' method could detect such a change of the surface before scuffing occurs, it would be very useful for considering additive formulations bearable for long running operation.

Did the authors try to detect the reactivity change of the surface before the scuffing?

DISCUSSION

E. RABINOWICZ (Fellow, ASLE)
Massachusetts Institute of Technology
Cambridge, Massachusetts 02139

Papers describing a new technique are usually of considerable interest, and this one proves to be no exception. It is obviously of great value to have available a technique for studying small surface profile changes, but it is not clear to me whether with the new technique the surface being examined can be taken out of the microscope while its profile is being changed.

I have a number of specific comments.

a) Was the time interval between the scuffing tests and the acid treatment tests controlled? In studies we have carried out using exoelectron techniques, the reactivities of metal surfaces varied drastically with the time that had elapsed since these surfaces were produced.

b) To what do the authors attribute the growth of surfaces (Figs. 3 and 4) during acid treatment?

c) Typical Arrhenius-type processes have activation energies such that the rate of reaction doubles for every 10°C increase in temperature. In the Arrhenius plot of Fig. 10, the rate doubles for every 150°C increase in temperature, giving an improbably low activation energy value.

REFERENCE

(B1) March, P. A. and Rabinowicz, E., "Exoelectron Emission for the Study of Surface Fatigue Wear," *ASLE Trans.*, 20, pp 315–320 (1977).

AUTHORS' CLOSURE

An objective of our work has been to find a change in bearing surface reactivity *before* scuffing. Having found a large change after scuffing makes our success more likely. Our reason for starting the way we did was the destructive nature of the test; once a bearing surface has been removed from an operating bearing for testing, it cannot be put back again and it has been difficult to prepare exactly equal surfaces for tests of different lengths. However, this work is in progress both with our present reactivity test procedure and with others which are potentially nondestructive. Unfortunately, as our work has shown, no measure of surface contour is by itself sufficient to predict chemical reactivity. We hope these comments will have answered Professor Okabe's questions.

The destructive nature of our test may also provide a partial answer to Professor Rabinowicz's comment. We cannot, at this time, control the time between scuffing and our test procedure, since the bearing must be taken apart for our test. Our results from both the reported and other data lead us to believe that the time interval is essentially infinite with respect to reactivity change. Therefore, the differences in reactivity between scuffed and unscuffed parts of the bearing surface can be considered permanent.

The "growth" of the surfaces during acid treatment (Figs. 3 and 4) does not necessarily mean only the addition of volume. Since a new surface composition is likely to have optical properties different from the previous ones, the phase on reflection is now different. The surface profiles measured with our interference microscope are really phase profiles and not material profiles such as those measured by a stylus. A phase change can, therefore, look like "growth" even when none occurred. For this reason, we avoided stating an activation energy calculated from our data of Fig. 10. Since the optical constants of the new surface were unknown to us at the time, we were not concerned that the "apparent" activation energy we had calculated came out to be chemically nonsensical. We have been careful to refer to observed profile changes only without giving them a material meaning. However, we will soon be able to measure the phase changes independently by ellipsometry and obtain "proper" activation energies.

APPENDIX III

Emission FTIR Analyses of Thin Microscopic Patches of Jet Fuel Residues Deposited on Heated Metal Surfaces

by

James L. Lauer and Peter Vogel

Applications of Surface Science 18 (1984) 182–206
North-Holland, Amsterdam

EMISSION FTIR ANALYSES OF THIN MICROSCOPIC PATCHES OF JET FUEL RESIDUES DEPOSITED ON HEATED METAL SURFACES

James L. LAUER and Peter VOGEL

Department of Mechanical Engineering, Aeronautical Engineering and Mechanics, Rensselaer Polytechnic Institute, Troy, New York 12181, USA

Received 14 July 1983; accepted for publication 20 October 1983

Deposits laid down in patches on metal strips in a high pressure/high temperature fuel system simulator operated with aerated fuel at varying flow rates were analyzed by emission FTIR in terms of functional groups. Significant differences were found in the spectra and amounts of deposits derived from fuels to which small concentrations of oxygen-, nitrogen-, or sulfur-containning heterocyclics or metal naphthenates had been added. The spectra of deposits generated on strips by heating fuels and air in a closed container were very different from those of the flowing fluid deposits. One such closed-container dodecane deposit on silver gave a strong surface-enhanced Raman spectrum.

1. Introduction

Aircraft fuels containing oxygen often have a tendency to form hard, sticky, carbonaceous and generally insoluble deposits on contacting surfaces at elevated temperatures. Small concentrations of nonhydrocarbons, such as nitrogen- and sulfur-containing materials, often enhance the deposit-forming tendency. In aircraft gas turbine engines these deposits may clog critical passages in valves and nozzles and decrease heat transfer efficiency through heat exchanger surfaces. These problems may increase in newer engines due to the higher temperatures and longer residence times expected with higher compression ratios and staged fuel injection. Future fuels are likely to be richer in aromatics and nonhydrocarbons than present ones and therefore likely to aggravate the deposit problems even more.

Clearly there is a need for the testing of fuels for their deposit-forming tendencies. In the longer run, however, an understanding of the mechanisms leading to deposit formation must be developed so that future fuels and engines can be designed to minimize deposit problems. Most of the testing is done today with small flow systems allowing for fuel and surface heating and the injection of controlled amounts of air or oxygen into the flowing test fuel. These JFTOT systems (Jet Fuel Thermal Oxidation Testers) typically use 0.3 cm diameter stainless steel or aluminum tubes, about 15 cm long, for deposit

0378-5963/84/$03.00

collection on their outer surface. These tubes are located in the stream of test fuel and are heated by the passage of electric current. A thermocouple in the center of their hollow interior records an average temperature, but this method of heating practically insures a temperature gradient along the tube axis. Furthermore, the large curvature of the mantle surface on which fuel deposits are formed, is very inconvenient for most methods of nondestructive chemical analysis. A superior device for deposit collection was therefore constructed at NASA-Lewis, where the surfaces are flat and removable strips of metal (shims) and of relatively large size (about 2 cm^2), yet small enough compared to the overall flow system to ensure uniform surface temperature.

For the study reported here both these shim deposits and deposits formed in our own laboratory on similar shims in a small corrosion test bomb under stationary conditions were used. The fuels for this study were selected to be typical of actual ones. They were used either neat or containing small concentrations of simple molecules representative of typical nonhydrocarbon contaminants. Not unexpectedly the deposits formed under stationary conditions were different from those formed under flow because of the difference in precursor or intermediate species availability. However, the former deposits were found to be different also when shims of different metals were simultaneously used and thus provided a simple – and inexpensive – procedure for evaluating substrates. Deposit formation from liquid fuels depends very strongly on the nature of the solid boundary surfaces.

In view of the complexity of the process and the very small quantities of deposits formed in reasonable test times, say a few hours, it is not surprising that the standard deposit evaluating procedure today is still visual comparison of the deposit color with those on a standard color chart. A JFTOT "Tube Deposit Rater" (TDR) by which the reflected color is compared, has also been used. Unfortunately the "color number" so found does not provide much information of a chemical nature and therefore tells us little or nothing about the nature or mechanism of deposit formation. The procedure used in this study was Fourier infrared emission microspectrophotometry (FIEMS), which is extremely sensitive and very powerful for the solution of problems in molecular and crystalline structure. Preliminary studies of aircraft fuel deposits by FIEMS were reported previously [1] so that the apparatus and its capabilities need only a brief description. The results of the flow experiments showed that both the quantity and the nature of the deposits are altered with change of fuel composition and to some extent, change of nonhydrocarbon additive ("spike"). A strong influence of the substrate was shown in the bomb experiments.

In one instance, surface-enhanced Raman spectroscopy (SERS) was used to analyze a bomb deposit formed from dodecane on a silver surface. Because it is the first application of SERS to a "real" material, the very respectable spectrum is communicated here also.

2. Experimental

2.1. Apparatus and experimental conditions of deposit collection

Fig. 1 is a photograph of the Modified JFTOT Flat Sample Rig (MJFSR). For this work it is important to note that the test specimens (shims) had a rectangular area of 10 × 20 mm exposed to the flowing fuel. Since the deposit weights varied between 0.02 and 0.2 mg (fig. 9) and their density was estimated as close to unity (between polyolefins and phenolic resins), thicknesses of 1000 Å to 1 μm could be estimated. These values are similar to our previously estimated values of 1000 Å, which were arrived at by scanning electron microscopy (SEM) [1]. Since these weights were obtained by differential weighings and represent small differences between relatively large numbers, their accuracy is not high. The higher weights were usually observed when naphthenates had been added to the fuels. These materials are surfactants and caused deposits to be formed on both sides of the shims.

The conditions of the MJFSR runs were: test duration near 120 min and

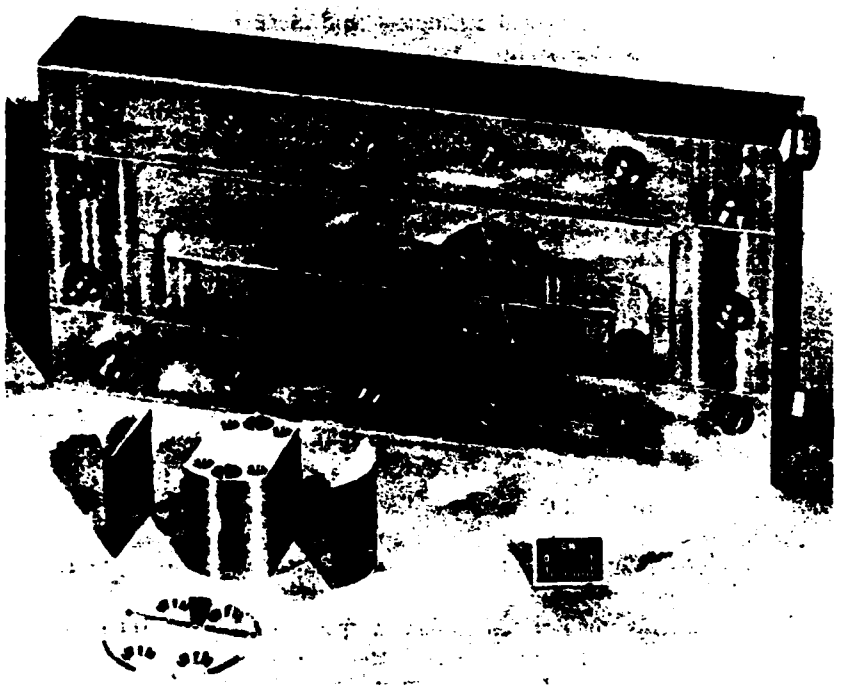

Fig. 1. NASA–Lewis deposit sample holder.

run temperature near 250°C. These values were deduced by interpolations and small extrapolations from peripheral measurements and were achieved and maintained to better than one percent (±1%).

Work is now in progress to determine deposit thicknesses by ellipsometry.

For the stationary experiments in our laboratory a standard 500 ml stainless steel corrosion bomb was used. It was provided with inert (silicone or Viton) gaskets, filled with 10 ml of hydrocarbon test fluid; several shims were inserted, and then heated to 250°C for 3 h. Therefore the hydrocarbon was in large excess over the oxygen and complete combustion was excluded, an analogy to the situation of the MJFSR where aerated fuels are used. The conditions of the bomb experiments insured that the metal strips (shims) suspended within the bomb were at uniform temperature throughout and at the same temperature as the fuel. Differences in amount and character of the material deposited on these strips must therefore be attributed exclusively to differences in the strip material and cannot be attributed to temperature gradients, for example.

The deposit samples obtained from the MJFSR were all collected on commercial stainless steel foil and the same foil was also employed in the bomb experiments. However, in the latter, strips of aluminum foil and silver foil were also used as deposit collectors. For the Raman experiment a microscope slide covered with a thin evaporated silver film ("island film") was momentarily dipped into the test fluid after the test. The bomb deposit samples were very much thinner than the MJFSR ones, for they were barely visible as a change of reflectivity. The roughness of the stainless steel foil was far greater (at least three times) than that of the aluminum and silver foils; the roughness of the aluminum foil was about 50% greater than that of the silver foil. These estimates are based on the graybody background intensities in infrared emission.

2.2. Test fuels

Three base fuels were used in the MJFSR: (1) Jet A, a representative jet fuel consisting of about 17% by volume of mononuclear aromatics, 0.1% of olefins, 2% of naphthalenes, and the balance of saturates; (2) ERBS, an experimental broadened-properties reference fuel, consisting of 35% of mononuclear aromatics, 0.3% of olefins, 7.5% of naphthalenes, and the balance of saturates; (3) dodecane, which is, of course, an essentially pure saturated hydrocarbon (aromatic and olefinic impurities: < 0.006 and 0.03% respectively). In addition, a few runs were made with a mixture of 80% dodecane and 20% tetralin. Tetralin is well known for its peroxide-forming tendencies and a preliminary study of its influence on the formation and composition of the deposits was thought to be worth including.

The "spikes" or additives were tested in the MJFSR in varying concentra-

tions. They were thiophene, furan, pyrrole and copper and iron naphthenates. For Jet A and ERBS the concentrations were: pyrrole 0.1 wt%, thiophene and furan 1.0 wt%, copper naphthenate 2 ppm and iron naphthenate 1 ppm. For dodecane all the amounts were twice the above. Thiophene and pyrrole were thought to be good initial representatives of nonhydrocarbon components in fuel. The naphthenates were used because it was thought that a portion of the metals present in fuels are in organometallic form. However, the naphthenates can behave like soaps and alter the flow pattern at boundary surfaces.

Only two hydrocarbon liquids were used in the bomb experiments, dodecane and toluene.

2.3. Spectroscopic analyses

Our preferred method of analysis was essentially the same Fourier emission microspectrophotometry we had used previously [1]. The schematic drawing of fig. 2 was taken from our previous publication. However, a number of improvements were made. Thus, for example, the chopper and the blackbody were relocated to a position between the heated sample and the lens. The old position below the lens, chosen for reasons of space and convenience, would

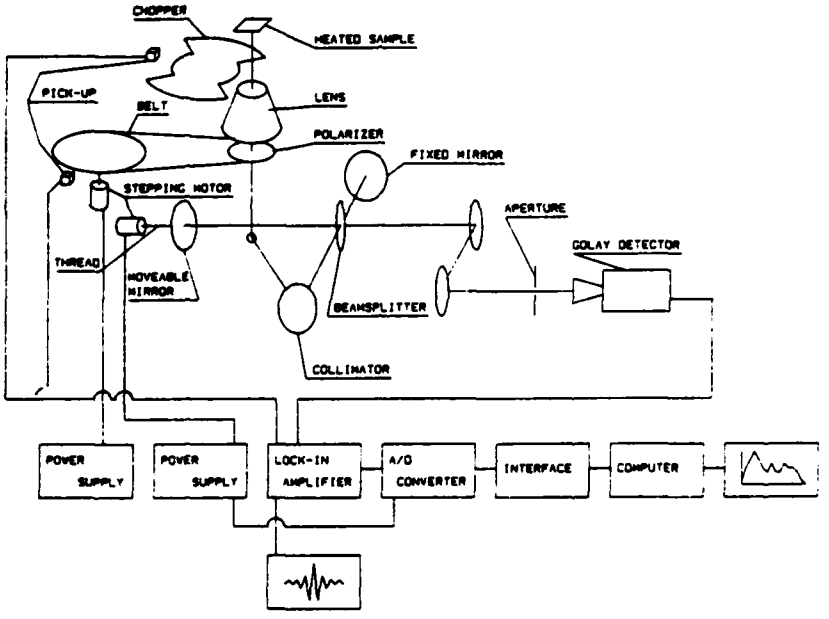

Fig. 2. Schematic drawing of Fourier emission microspectrophotometer.

lead to increased background radiation as the lens would heat up and itself become a source of radiation. This problem became particularly acute when the sample temperature was raised from 40 to 130°C to improve the signal/noise ratio of extremely thin deposits. The tuning fork chopper was replaced by a rotating wheel at 45° with the optical axis of the lens to introduce sample and blackbody radiation alternatingly into the spectrometer. The wheel was more stable and a better reflector than the tuning fork tines. However, perhaps the most important innovation of primary importance for the analysis of the extremely thin deposits produced in our bomb experiments was a heated sample holder that would allow the planes of the shims to be placed at a high angle with the optic axis. Doing that also required a lens of longer working distance than the one used previously. A large angle of emission is of great importance when very thin samples on metal surfaces are analyzed by infrared emission, for then the metal surfaces produce an intensity pattern that has its maximum at viewing angles of 70°–80° from the surface normal (Greenler [2]).

Introduction of a variable viewing angle thus added another element of complexity in our sample location system. It is not important to describe it in detail in this paper, but it should be mentioned that a region in a deposit sample can be reproducibly located by X, Y, Z and rotational adjustments in both a horizontal and a vertical plane to about ± 0.05 mm and 0.1° of angle. To make use of this precision, all the instrumentation is set on a optical table of high quality. Depending on the objective lens used the deposit area viewed can be varied from about 1 cm^2 to 100 μm^2, so that small spots of deposit can be analyzed.

In the work reported here polarization modulation was not used. The viewing angle was kept between 45° and 75°, with respect to the surface normal. The influence of viewing angle on a typical deposit spectrum is shown in fig. 3. At 0° very little structural detail appears above the background. At 45° strong bands at 1470, 1610, 1730 and 1780 cm^{-1} are very distinct. These bands can be assigned to the CH_2 scissoring mode, the asymmetrical stretch of carboxylic acid salts, and the C=O stretches of ketones and p-lactones, respectively. As pointed out by Greenler [2], the most intense emission bands from a material adsorbed in a thin layer on a metal surface are likely to be those originating from a transition dipole vector having a strong component vibrating perpendicularly to the surface.

Our slow-scanning Fourier spectrometer is ideally suited for the analysis of the very weak infrared emissions (small sample areas, sample temperature as low as 40°C with a room temperature detector and very thin samples on metal surfaces) [3], but practical considerations allow the averaging of only a few (three to four) spectra. In general, only the spectral region from 600 to 2000 cm^{-1} could be used because of the rapid radiation intensity fall-off at higher frequencies. Furthermore, it proved to be convenient to separate this spectral

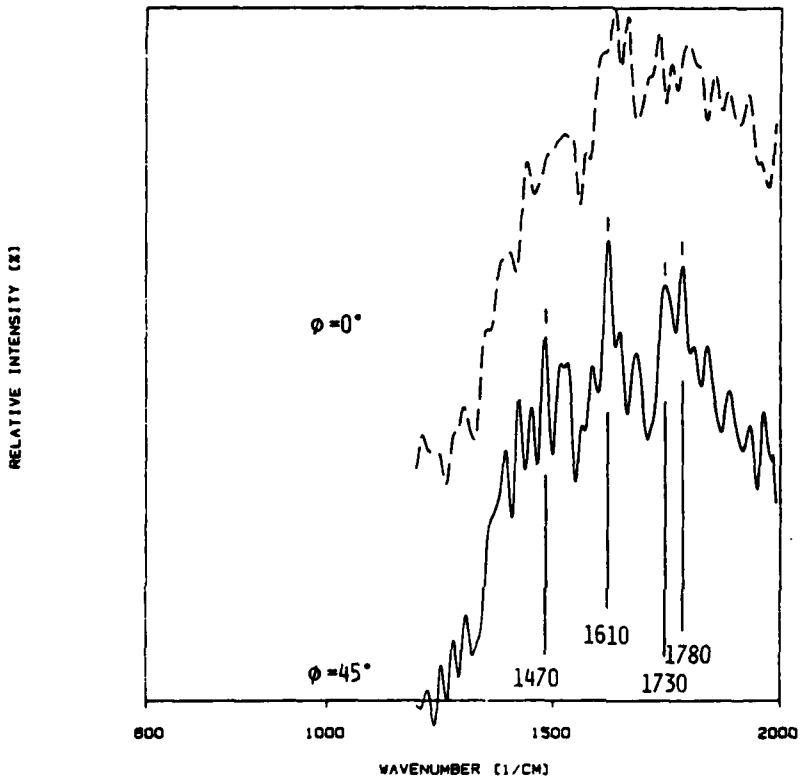

Fig. 3. Change of spectrum with observation angle.

region into three parts by optical filtering (600–1200, 1100–1400, and 1300–2000 cm^{-1}) to reduce the dynamic range. Not all ranges were run for all the spectra. The reciprocal resolution was ± 5 cm^{-1}. The last two ranges required complete removal of moisture and carbon dioxide from the spectrometer atmosphere.

The Raman spectra were obtained with a Spex spectrometer in the RPI Physics Department.

2.4. Calibration

Fig. 4 shows an emission spectrum of a 2.5 μm thick film of Mylar at 60°C. It is included here not only to show that all the absorption bands are clearly distinguishable as emission bands and that they appear at the same frequencies but also the three spectral ranges we use, which are separated by optical filters

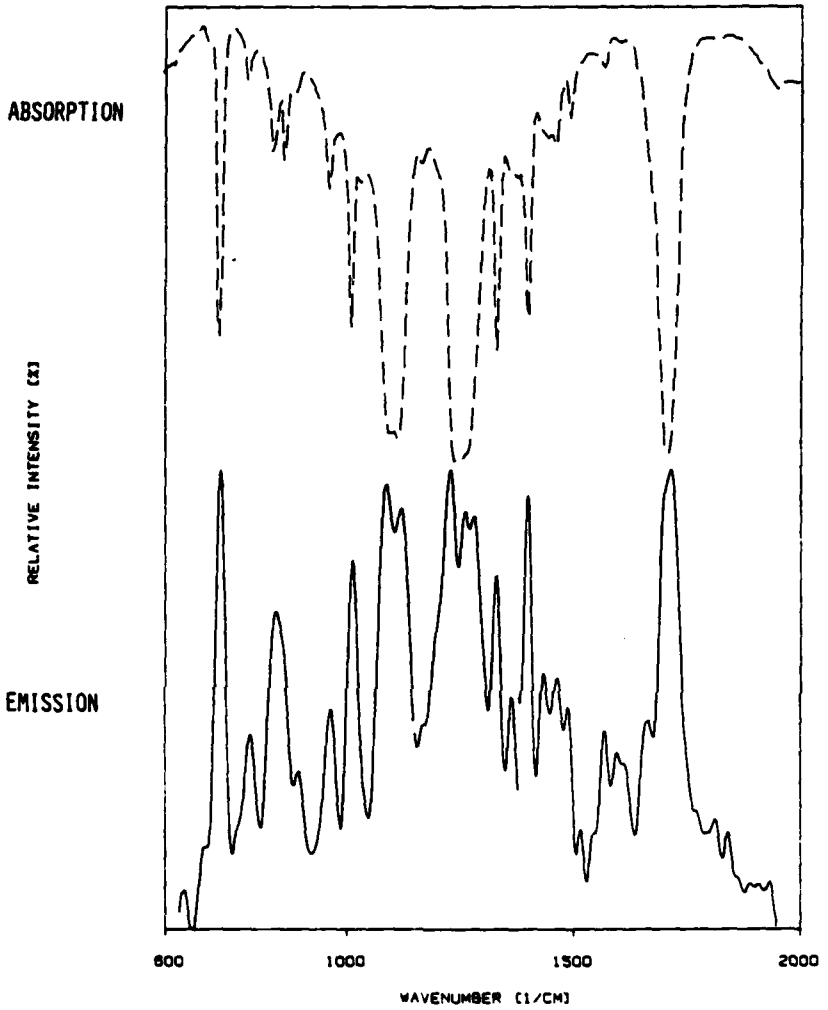

Fig. 4. Absorption and emission spectrum of Mylar.

of sharp cutoffs. That the spectrum was not ratioed to the blackbody, is one reason that the relative intensities of the various bands are not those observed in absorption. Another reason for the intensity differences is the effect of the substrate and polarization.

The Mylar spectra are single spectra, not averages of many spectra as has become common practice in Fourier infrared spectroscopy.

3. Results and discussion

3.1. Bomb experiments

3.1.1. Infrared emission

Figs. 5 and 6 contain three infrared emissions each of deposits from dodecane and toluene, which were collected simultaneously on stainless steel, aluminum and silver strips. Thickness data are lacking, but visual comparison

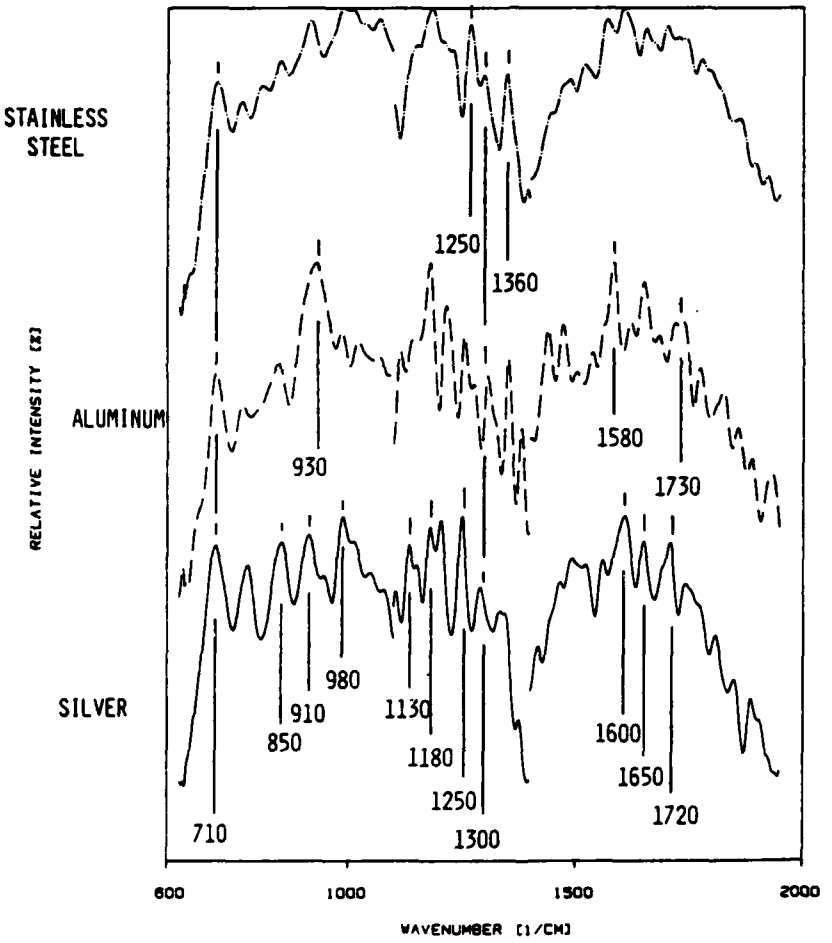

Fig. 5. Emission spectra of dodecane deposits collected on three different metals in a corrosion bomb.

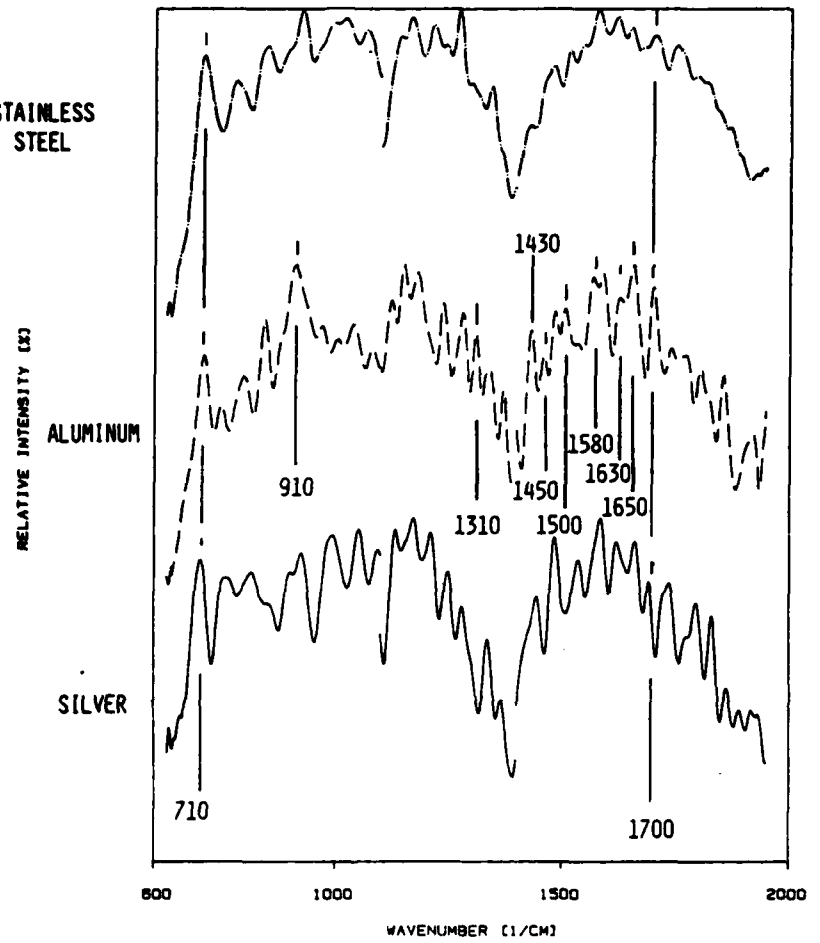

Fig. 6. Emission spectra of toluene deposits collected on three different metals in a corrosion bomb.

with deposits on tubes, whose thickness was estimated by scanning electron microscopy, would seem to indicate that these strip deposits were less than 100 Å thick. The spectra of these figures were all normalized and displaced vertically in the order of background intensity, stainless steel furnishing the highest background, no doubt because it is the poorest reflector and had the roughest surface. It should also be pointed out that all these spectra were separately obtained in three separate wavenumber regions although the com-

posite spectra of figs. 5 and 6 appear to be continuous. Casual comparison of the spectra shows that the contrast is highest for the aluminum deposits and lowest for the stainless steel deposits, the silver deposit spectra occupying an intermediate position. The order of the spectral contrasts parallels that of the reflectivity of the substrate in the infrared (in the infrared aluminum is a somewhat better reflector than silver).

The strongest and most outstanding emission band in the spectra of the aluminum deposits formed from both dodecane and toluene is peaking at 930 cm^{-1} for the former and at 910 cm^{-1} for the latter. A weaker band in this spectral range is also present in all the other spectra. For this reason and because of the wavenumber difference it is unlikely that this band is merely the aluminum oxide phonon described by Mertens [4]. The chances are that it is both due to this phonon and the OH...O out-of-plane hydrogen deformation of the carboxyl dimer. This assignment is confirmed by a strong band at 1300–1310 cm^{-1}, which is present in all the dodecane deposit spectra but only in the toluene deposit spectrum from aluminum. This band is considered to be caused by the C–O stretch of the carboxyl. Another carboxyl dimer band, the C=O stretch expected to be located between 1680 and 1740 cm^{-1} is strongly present in both of the aluminum deposit spectra. The aluminum deposit spectra also contain a strong band at 1580 cm^{-1} and a weaker one at 1430 cm^{-1}, which are usually assigned to the asymmetric and symmetric stretching modes of carboxylic acid salts, as well as a strong band at 1650 cm^{-1}, which can be assigned to C=C (olefin) stretch. The presence of a carboxylic acid in the aluminum deposits from dodecane is also indirectly confirmed by the series of nearly equispaced bands between 1200 and 1320 cm^{-1}, which represent the harmonics of the CH_2 wagging mode; these bands are usually particularly intense in paraffinic carboxylic acids and salts. On the other hand, the toluene deposits on aluminum show characteristic bands near 1580 and 1630 cm^{-1}, at 710 cm^{-1} and around 1450 and 1500 cm^{-1}, which can be assigned to the phenyl group. A band near 710 cm^{-1} in all the dodecane deposits is likely to be the CH_2 rock. A band near 1730 cm^{-1} for the dodecane deposits and near 1700 cm^{-1} for the toluene deposits must be assigned to carbonyl.

There is much less evidence for carboxylic acids and little if any, for salts in the silver deposits and essentially none for either in the stainless steel deposits. In the latter the most identifiable bands, i.e., 1260 and 1350 cm^{-1} for dodecane are CH_2 and CH_3 deformations. The silver deposit spectra, however, do show carbonyl bands as well.

The spectra of the bomb deposits can therefore be summarized as follows: On aluminum the hydrocarbons were partly oxidized all the way to carboxylic acids and salts, and partly to aldehydes and ketones, on silver also partly to carboxylic acids and to aldehydes and ketones and on stainless steel probably mostly to hydrocarbon polymers. The latter spectra show little evidence of the presence of carbonyl groups.

How do these spectra compare with the MJFSR spectra? A good example is shown in fig. 7.

Dodecane deposits on stainless steel are compared for the two situations. If at all present the 1260 and 1350 cm^{-1} bands of the bomb experiments are essentially absent for MJFSR. However, the MJFSR spectrum does show possible evidence for C = O bands at 1700, 1730 cm^{-1} and a strong band at 840 cm^{-1} may be indicative of olefin epoxidation. Olefins are also very likely evidenced by bands near 1600 cm^{-1}. It would appear therefore that oxidation went further in MJFSR than in our bomb.

Unfortunately our emission spectra regions do not extend beyond 2000 cm^{-1} because the available energy is too low beyond that frequency. Others encountered the same limitation (Suëtaka [5]).

3.1.2. Surface enhanced Raman (SERS) spectrum

The Raman spectrum of fig. 8, obtained by momentarily dipping a silver-coated microscope slide into the partly oxidized dodecane after the bomb test,

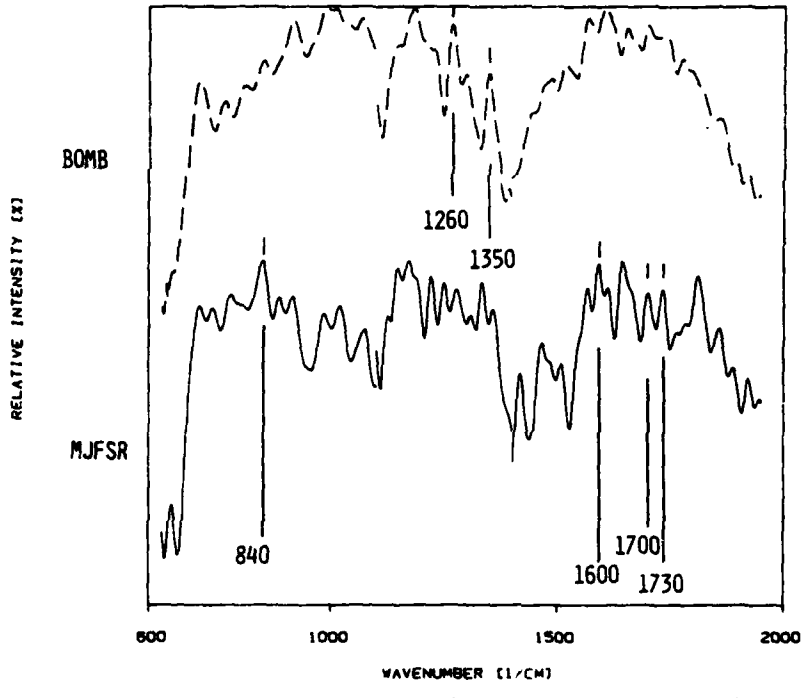

Fig. 7. Comparison of spectra from dodecane deposits collected on stainless steel in the MJFSR and the stainless steel bomb.

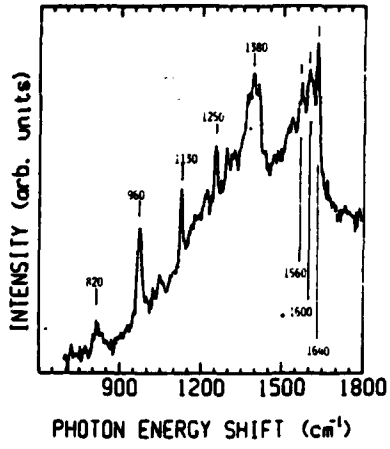

Fig. 8. Raman spectrum of a dodecane deposit collected on silver in a stainless steel bomb.

was surprising for its quality. The deposit was barely visible as a minute reflectivity change and was probably no more than a few molecular layers thick. It shows strong bands at 820, 960, 1130, 1250, 1380, 1560, 1600 and at 1640 (strong) cm^{-1}. The principal infrared emission bands in the dodecane deposit on silver (fig. 5) are at 850, 910, 980, 1130, 1180, 1260, 1600, 1650 (weak) and 1730 cm^{-1}. Perhaps the most outstanding difference between these spectra is the clear absence of a Raman band at 1700 cm^{-1} and the presence of broad and strong Raman bands but weak infrared bands grouped near 1400 and 1640 cm^{-1}. Since the carboxylic acid dimer is centroxymmetric, the asymmetric carbonyl stretch would be expected to fall at 1700 cm^{-1} and be infrared-active only and the symmetric stretch to fall at 1640 cm^{-1} and be Raman-active only. An infrared band near 1600 cm^{-1} and a Raman band near 1400 cm^{-1} are similarly expected for the coupled oscillators in carboxylic acid salts. Other bands in both the infrared and Raman spectra can be assigned to olefins and alkanes as shown in table 1, which summarizes the data.

There is a great deal of recent literature on different selection rules for SERS and for ordinary Raman spectroscopy [6]. Some authors consider chemisorption a prerequisite for SERS. Our data would still be consistent with the assignments made, but no conclusions should be made on the basis of relative band intensities.

3.2. Lewis thermal stability (MJFSR) spectra

3.2.1. Overview

Fig. 9 is a comparison of the deposit weight on the standard 2 cm^2 stainless steel surface and the "greatest unnormalized amplitude" (GUA) of our in-

Table 1
Infrared emission and Raman bands of dodecane deposits from bomb experiments

Infrared emission				Raman	
Aluminum (cm^{-1})	Substrate assignment	Silver (cm^{-1})	Substrate assignment	Silver (cm^{-1})	Substrate assignment
710	CH_2 rock	710	CH_2 rock		
840	Epoxy	780	CH_2 deformation	820	Secondary alcohol
930	Carboxyl	850	Epoxy	960	C–C stretches (alkanes)
1180	CH_2 wag (alkanes)	910	CH_2 wag of C = C	1130	C–C stretches (alkanes)
1210	CH_2 wag (alkanes)	980	CH_2 wag of C = C	1250	Epoxy
1250	CH_2 wag (alkanes)	1130	CH_2 wag (alkanes)	1380	Carboxylate salt
1310	CH_2 wag (alkanes)	1180	CH_2 wag (alkanes)	1560	Coupled C = C stretches
1350	CH_2 wag (alkanes)	1200	CH_2 wag (alkanes)	1600	(1540–1620) of polymers
1380	CH_2 wag (alkanes)	1250	CH_2 wag (alkanes)	1640	Symmetric C = C (alkyl) stretch and carboxylic acid dimer
1430	Carboxylate salt	1290	CH_2 wag (alkanes)		
1470	CH_3 deformation	1490	CH_3 deformation		
1580	Carboxyl (salt)	1600	Carboxyl (salt)		
1650	Olefin C = C stretch	1650	Olefin C = C stretch		
1720	Carbonyl	1700	Ketone or ester carbonyl		
1740	Carbonyl				

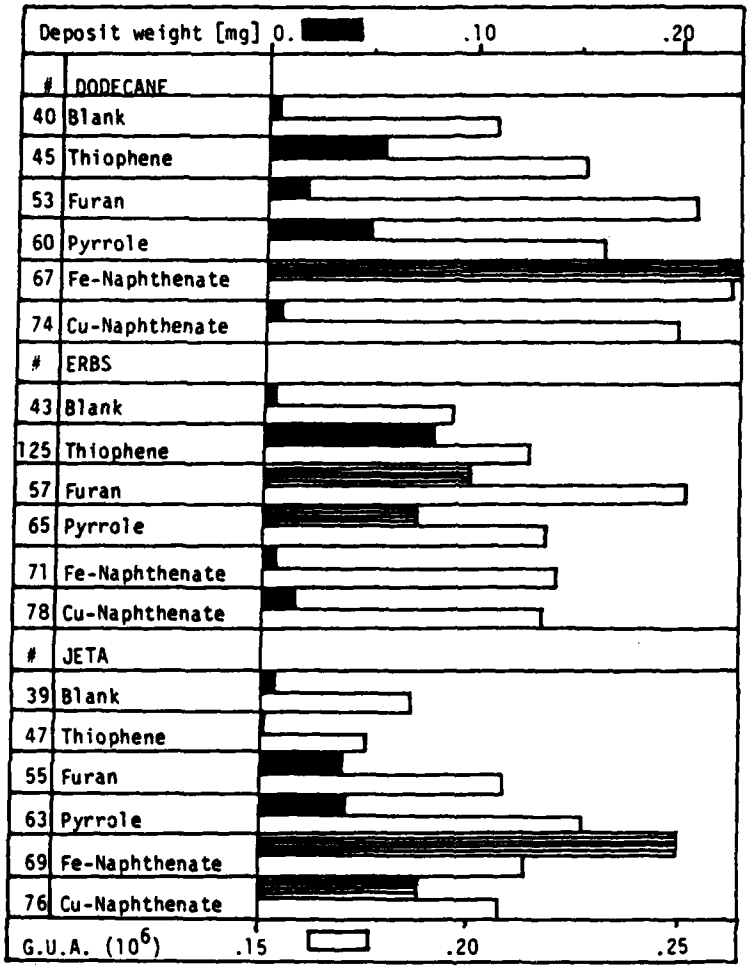

Fig. 9. Comparison of MJFSR deposit weights and infrared emission intensity (GUA). The bars containing the horizontal lines represent weights of deposits formed on both sides of the collecting strip.

frared emission spectra in the 650–1250 cm^{-1} wavenumber region. This region includes essentially only bands representing C–C or C–H vibrational modes and the overall intensity in this region would be expected to be related only to carbonaceous, i.e., not oxidized, material. Some of the bars for the deposit weights contain question marks to indicate that the measurements are probably

invalid; material crept under the sample shim. It is clear that the spikes (i.e., the additives) increased deposit weights considerably, especially thiophene, furan, and pyrrole, but the naphthenates had only little influence, presumably because of their lower concentrations, if the bad data are excluded. The GUA's

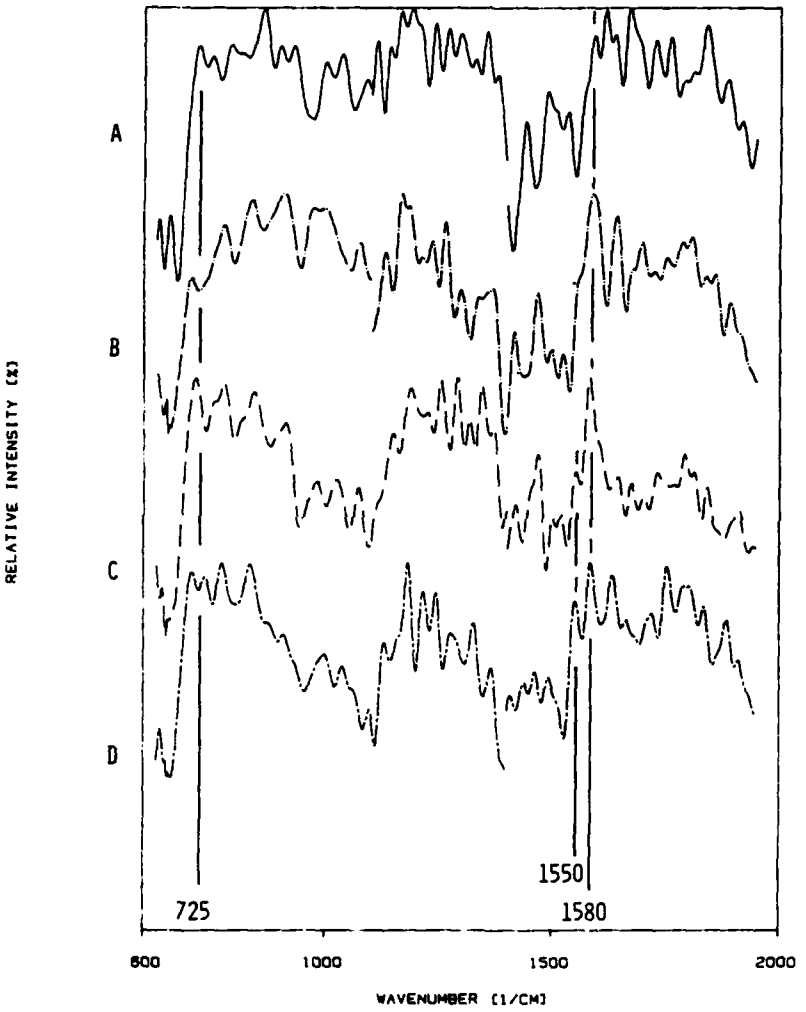

Fig. 10. Emission spectra of dodecane deposit on MJFSR stainless steel shims: (A) neat fuel; (B) with copper naphthenate; (C) with iron naphthenate; (D) with furan.

parallel the deposit weights in a general way, e.g., the GUA for the blanks (i.e., deposits from the neat fuel) are relatively low, but they are not proportional to them. The ratio of GUA to weight is high for the blanks and the deposits from

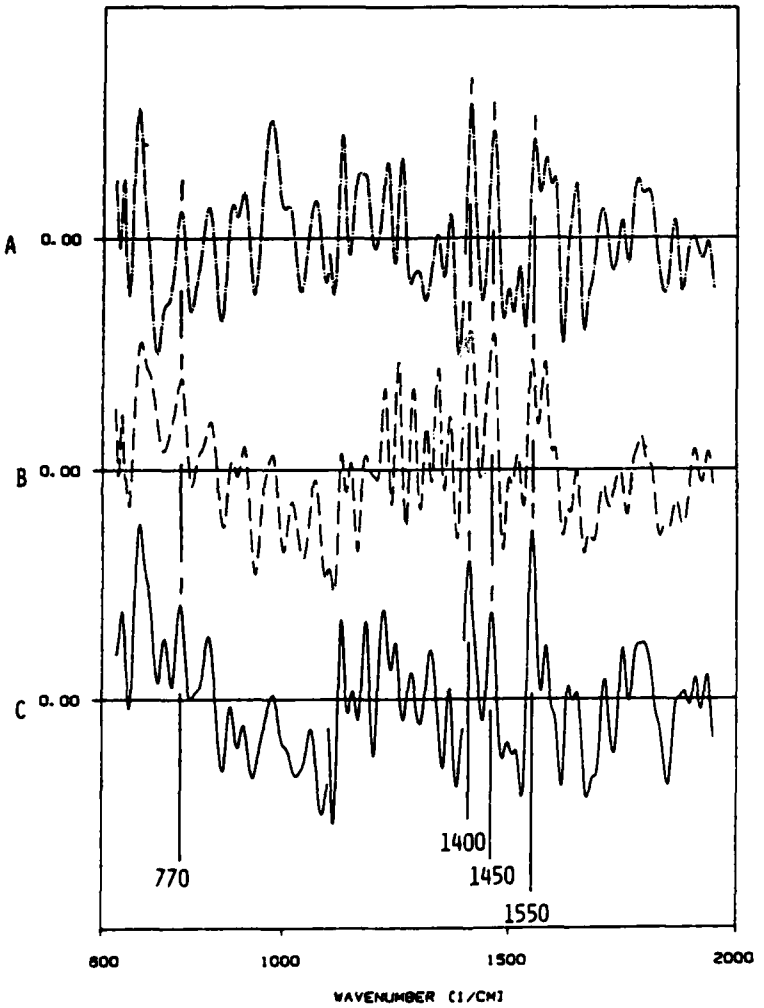

Fig. 11. Difference spectra of MJFSR deposits from dodecane with additives and those of the straight fuel: (A) with copper naphthenate minus neat; (B) with iron naphthenate minus neat; (C) with furan minus neat.

the naphthenate spikes, but is much lower for the other spikes. If the lengths of the bars for the GUA's are added for a given fuel, then dodecane comes out first, ERBS fuel second and JETA third, but if the same is done for the deposit weights, ERBS fuel is first and JETA and dodecane about the same. What these comparisons show is the different nature of the deposits, thick deposits do not necessarily give intense spectral bands. The aromatic fuels contain less hydrogen per unit mass than the paraffinic and also give rise to aromatic deposits whose infrared emission bands are therefore weaker in the C–H

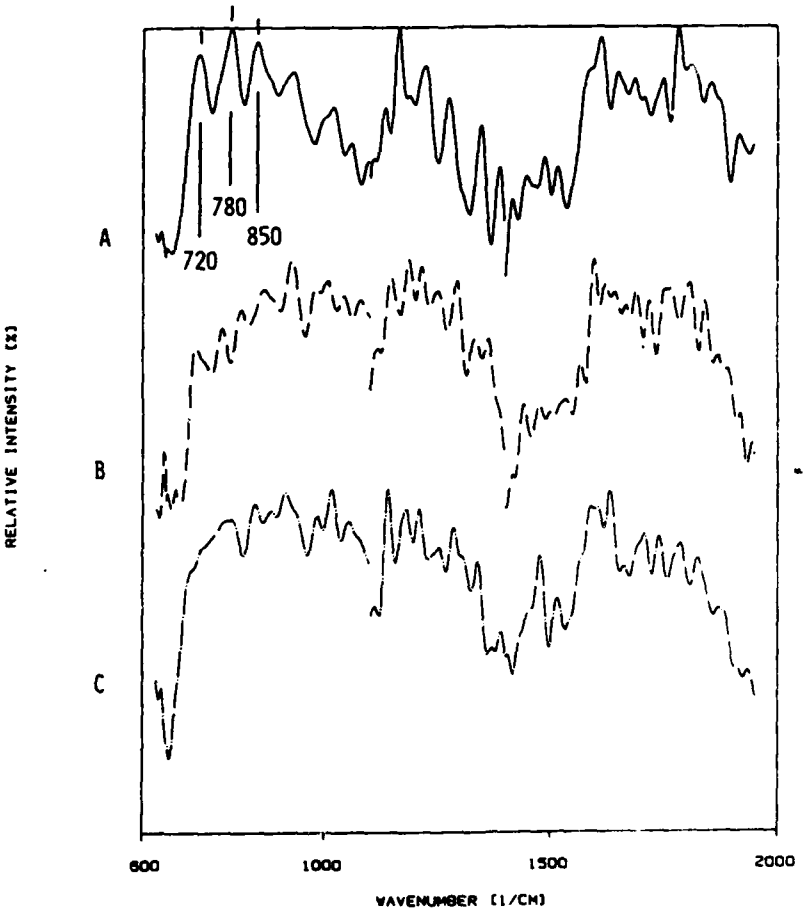

Fig. 12. Emission spectra of Jet A fuel deposits on MJFSR stainless steel shims: (A) neat fuel; (B) with copper naphthenate; (C) with iron napthenate.

region. Visual inspection of the deposit layers on the shims shows the difference in their nature by slightly different colors.

3.2.2. Dodecane spectra

Fig. 10 shows 600–2000 cm^{-1} emission spectra of dodecane deposits formed at MJFSR on stainless steel shims. These spectra are included to show the complexity and the effect of the additives. Perhaps the single most important difference to be noticed in these spectra is the enhancement of a

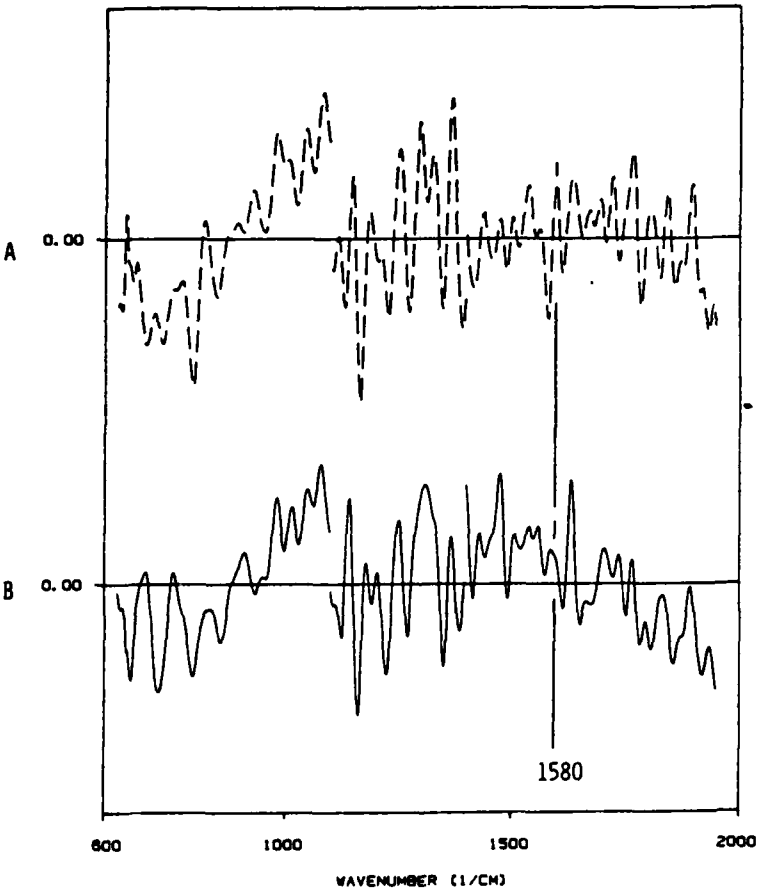

Fig. 13. Difference spectra of MJFSR deposits from Jet A fuel with additives and those of the straight fuel: (A) with copper naphthenate minus neat; (B) with iron naphthenate minus neat.

band at 1580 cm^{-1} relative to its neighbors by the additives furan and the naphthenates. With the copper naphthenate spike this band is already the strongest in the spectrum, but with iron naphthenate this band is the outstanding feature in the 1400–2000 cm^{-1} spectral region.

As mentioned earlier, the 1580 cm^{-1} band was assigned to carboxyl salts. Therefore, the naphthenates, in particular, would seem to concentrate in the deposits.

To show the effect of the spikes more clearly the difference spectra of fig. 11

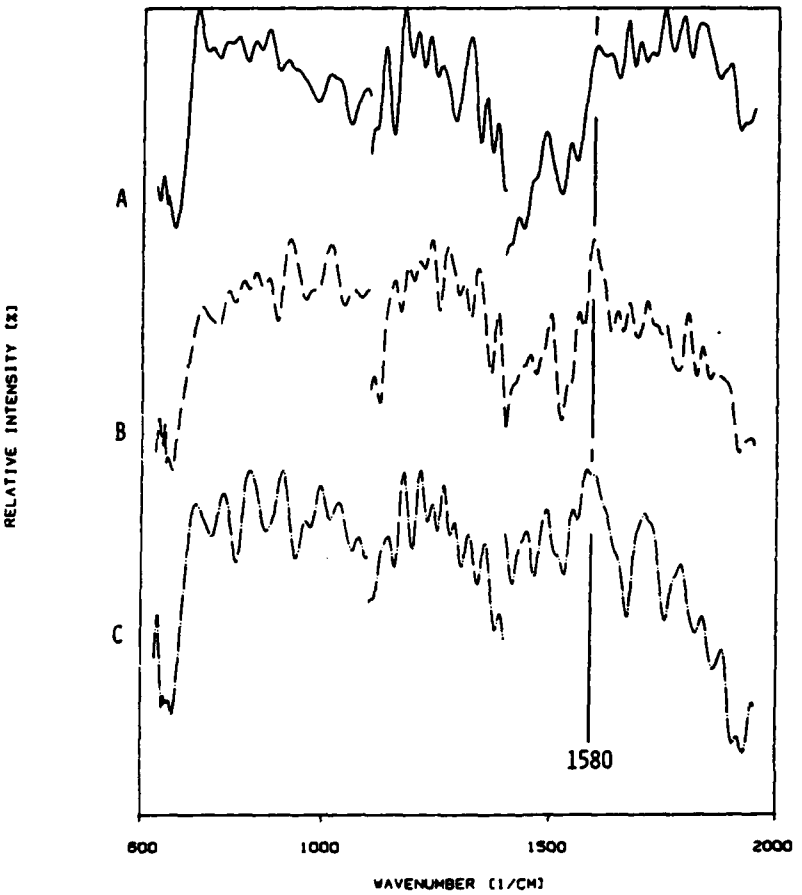

Fig. 14. Emission spectra of ERBS fuel deposit on MJFSR stainless steel shims: (A) neat; (B) with copper naphthenate; (C) with iron naphthenate.

were plotted by computer. These spectra take into account that different spectra have different overall intensities. In all cases the deposit spectrum derived from pure dodecane was subtracted from the spectra derived from dodecane containing the spikes. Contributions of the spike are pointing up, subtractions down. It will be noticed that all the additives enhance bands near 770, 1400, 1450 and 1550 cm^{-1}. Iron naphthenate and furan resolve the 1550 cm^{-1} band from its 1580 cm^{-1} neighbor. These bands occur in the additives. Thus the spectra show an increased concentration of additive material in the deposits.

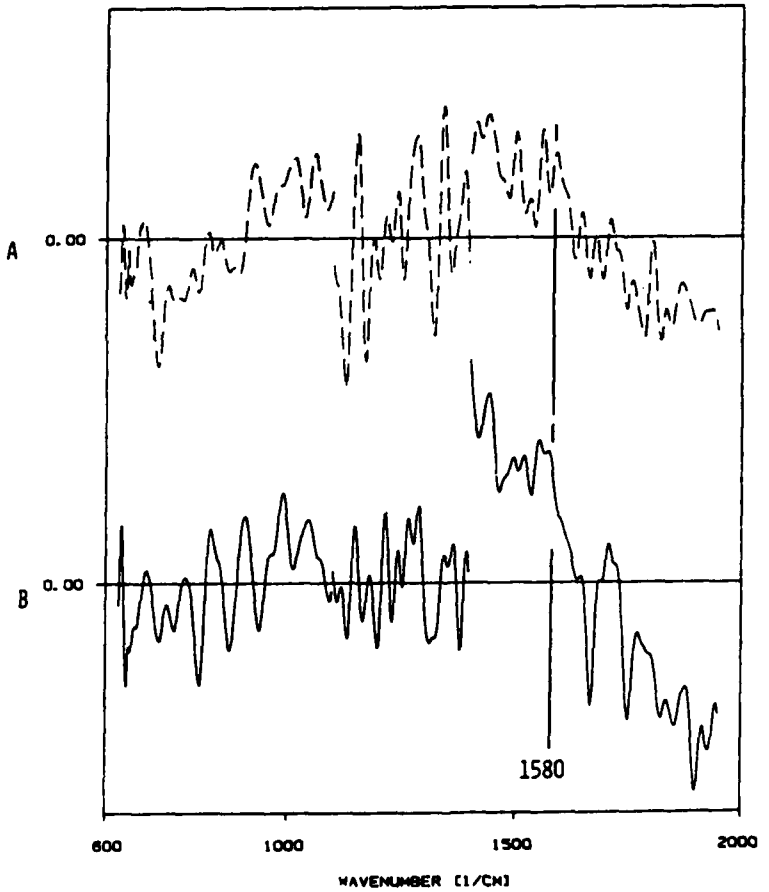

Fig. 15. Difference spectra of MJFSR deposits from ERBS fuel with additives and those of the straight fuel: (A) with copper naphthenate minus neat; (B) with iron naphthenate minus neat

The first two small emission bands on the left right after the steep initial rise of the background (caused by the optical filter) should also be compared in the spectra of fig. 10. These bands, located at 720 and 730 cm^{-1} represent the "amorphous" and "crystalline" components of the CH_2 rocking mode of paraffinic chains. In the liquid phase only the 720 cm^{-1} component is present. The "crystalline" mode arises from interactions between neighboring chains. Clearly the naphthenates enhanced the 720 cm^{-1} band but virtually wiped out the other component. Tetralin did the same. These bands may therefore be related to the relative stickiness of the deposits.

3.2.3. Jet A and ERBS spectra

In figs. 12 and 13, 600–2000 cm^{-1} emission spectra and their differences for Jet A are shown. When the "blank" is compared with the deposits from the spiked fuels, it will be noticed that the 720, 780, 850 cm^{-1} triplet corresponding to aromatic substitution is reduced in relative importance by the naph-

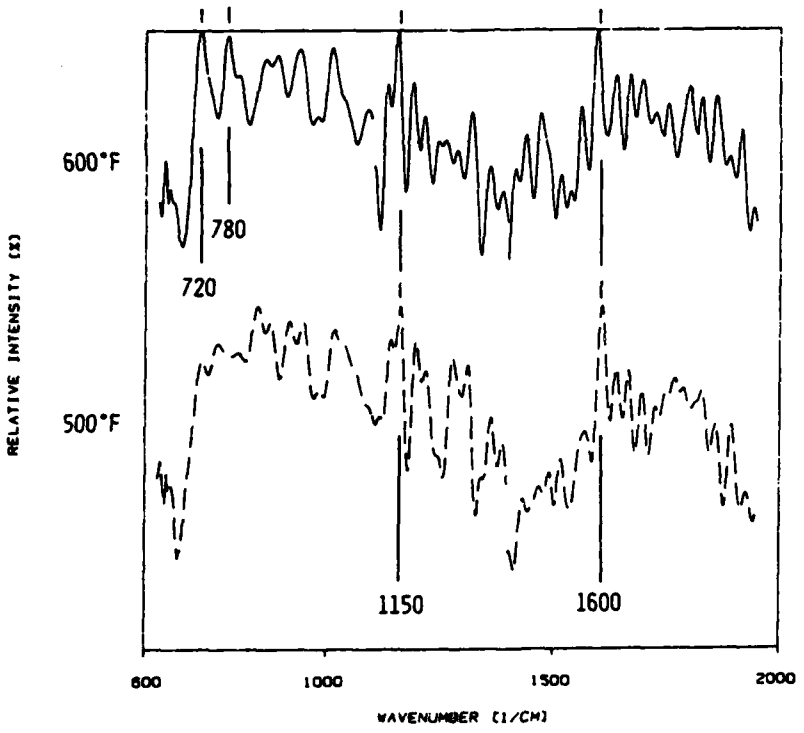

Fig. 16. Emission spectra of an ERBS fuel deposit collected at 500 and 600°F.

thenates (it should be remembered that these are normalized spectra) while the 1580 cm^{-1} carboxyl salt band is relatively enhanced. Again the conclusion is that these spikes concentrate on the surface.

The conclusions drawn from the ERBS emission spectra of figs. 14 and 15 are similar. The spikes enhance the 1580 cm^{-1} carboxyl salt band, showing their increased concentration there.

3.2.4. Effect of deposition temperature on the spectrum of an ERBS deposit

Fig. 16 shows an ERBS deposit spectrum obtained at 500°F and one at 600°F in the MJFSR. The strong aromatic bands at 1600 (naphthalene)and 1150 (*m*-substitution) cm^{-1} are similar in both spectra. However, the higher temperature deposit also show strong bands at 720 and 780 cm^{-1} which, if they belong to the same species, are characteristic of vicinal trisubstituted benzenes (fused polyphenyls?). An enhancement of these materials would be expected in the deposit, but confirmation of this result will be required.

4. Conclusion

If the reader has got the impression of enormous complexity, he has got the correct impression. Even a relatively simple, pure hydrocarbon such as dodecane give rise to various polymeric and oxidized reaction products in its deposits and the distribution of these products depends on the nature of the collecting surface as well. The basic mechanism of liquid phase oxidation, viz. formation of alkyl hydroperoxides by the reaction of alkylperoxy radicals with hydrogen atom donors, which can be the hydrocarbon itself, has been well established [7]. In some instances peroxides are formed instead of hydroperoxides. The decomposition of these peroxides then leads to unsaturates, aldehydes, ketones and acids with the strong possibility of chain reaction stimulations leading to polymers. The metal substrate can influence the deposit reaction, such as salt formation with carboxylic acid group. Our bomb experiments showed that an aluminum surface favors carboxylic acid formation, in other words more oxidation, and oxidative properties of aluminum oxide have been reported [8]. Since all the substrates in the bomb experiments were at constant temperature, their influence on deposit composition could be distinguished.

The MJFSR deposits were more highly oxidized, e.g., had more carboxyl groups, than the stationary bomb deposits, presumably because (i) more oxygen was available (it was continuously injected into the stream) and (ii) oxidized intermediates could be carried by convection as well as by diffusion. Hence the different compositions can be easily accounted for.

The Raman spectra (SERS) came out surprisingly well and were very helpful in the interpretation of infrared deposit spectral data. However, the

procedure is clearly not routine and seems to work only with silver substrates, which are not realistic.

Much more realistic is the effect of the additives or spikes. Furan, thiophene and pyrrole are all very "aromatic" in their chemical behavior. They all promote deposit formation; pyrroles, e.g., were found to react strongly with peroxides to form polymeric sediments [9], but the detailed mechanism is unknown. Tetralin also reacts with peroxy radicals, even with its own hydroperoxy radical by serving as a hydrogen atom donor, to form hydroperoxides [10]. The soluble copper and iron naphthenates are oxidation catalysts as well as micelle-formers like soaps. Dissolved copper in lubricating oils was found to be a good chain-initiation catalyst, dissolved iron a good chain-branching catalyst. Micelle formation of dissolved copper has been considered the reason for the maximum oxidation rate observed with increased concentration. Thus the naphthenates would also promote carboxylic acid formation from fuel and these acids would chemisorb on metal surfaces.

As was shown by one example, temperature can have a profound influence on surface deposits; higher temperatures increase the oxidation rate.

Thus fuel composition, temperature, the nature of the boundary surfaces and small amounts of nonhydrocarbons can be of great importance with regard to fuel stabilisty and wall deposits. Oxidation is the prime chemical cause. And the spectroscopic procedures of infrared emission and Raman (SERS) spectroscopy can assist in differentiating between good and bad actors and in establishing mechanisms.

Acknowledgements

This work was funded by NASA Lewis Grant NAG 3-203. Some support was also given by ARO Grant No. DAAG 2483K0058 and by AFOSR Grant No. AFOSR-81-005. We are very thankful to our sponsors.

The "flow-fuel" deposits were provided us by Dr. Gary Seng of NASA-Lewis, who ran the simulator. This work and his comments and encouragements throughout this project are most gratefully acknowledged.

The assistance of Professor T.E. Furtak and his students in obtaining the Raman spectra is acknowledged.

References

[1] J.L. Lauer and L.E. Keller, Appl. Surface Sci. 15 (1983) 50.
[2] R.G. Greenler, Surface Sci. 69 (1977) 647.
[3] P.R. Griffith, Chemical Infrared Fourier Transform Spectroscopy (Wiley, New York, 1975) pp. 311–317.

[4] F.P. Mertens, Surface Sci. 71 (1978) 161.
[5] K. Wagatsume, K. Monma and W. Suëtaka, Appl. Surface Sci. 7 (1981) 281.
[6] R.K. Chang and T.E. Furtak, Surface-Enhanced Raman Scattering (Plenum, New York, 1982).
[7] E.R. Bell, J.H. Raley, F.R. Rust, F.H. Seubold and W.E. Vaughan, Disc. Faraday Soc. 10 (1951) 242.
[8] I.D. Chapman and M.L. Hair, in: Proc. 3rd Intern. Congr. on Catalysis (North-Holland, Amsterdam, 1965) p. 1091.
[9] A.A. Oswald and F. Noel, J. Chem. Eng. Data 6 (1961) 294.
[10] G. Hartman and F. Seibert, Helv. Chim. Acta 15 (1932) 1390.

APPENDIX IV

Topological Reaction Rate Measurements Related to Scuffing

by

James L. Lauer, Simon S. Fung
and
William R. Jones, Jr.

PREPRINT NO. 83-LC-2B-1
ASLE PREPRINT

Topological Reaction Rate Measurements Related to Scuffing

JAMES L. LAUER (Member, ASLE) and SIMON S. FUNG
Rensselaer Polytechnic Institute
Troy, New York 12181
and
WILLIAM R. JONES, JR. (Member, ASLE)
NASA-Lewis Research Center, MS 23-2
Cleveland, Ohio 44135

The contact area of the plate of a ball/plate (both consisting of hardened M-50 steel) sliding elastohydrodynamic contact run on trimethylolpropane triheptanoate with or without tricresylphosphate (TCP) additive was optically profiled periodically with a phase-locked interference microscope (PLIM), both before and after exposure to alcoholic hydrochloric acid. As scuffing was approached, the change of profile within the contact region changed much more rapidly by the acid probe and assumed a constant high value after scuffing. A new nonetching metallurgical phase was found in the scuff mark, which was apparently responsible for the high reactivity. Soaking the metal surfaces in the lubricant before running affected the subsequent reactivity.

The microscopic profile changes (sensitivity ± 30 Å in depth) involved primarily the small asperities of radius < 3 μm, while the larger ones were unaffected. Soaking the steel in TCP smoothed the fine structure of the surface profile, but increased *the reactivity toward hydrochloric acid before sliding was started. This behavior parallels chemical changes of TCP-exposed surfaces observed previously.*

It would appear that this type of examination could be used for screening of potentially scuff-resistant materials.

INTRODUCTION

Scuffing or scoring of stainless-steel bearing surfaces was found to increase the chemical reactivity at room temperature (*1*). A phase-locked interference microscope (PLIM) was used to show on a microscale that the same exposure to dilute alcoholic hydrochloric acid produced much greater contour changes within than without the score track. On the conjecture that a maximum temperature reached during scuffing or scoring was responsible for the reactivity difference, a series of stainless-steel plates were briefly heated to increasing temperatures and their reactivities toward alcoholic hydrochloric acid measured at room temperature. Indeed, the reactivity was higher the higher the preheat temperature. Based on this result, it was assumed that the scuffing reaction depended on a critical preheat temperature but that, in contrast to the implications of the total contact temperature concept of Blok (*2*) and others, scuffing does not have to occur right at that temperature. Presumably, a metallurgical change would occur on heating of the metal surfaces which could eventually affect a large enough contact region to promote the fast chemical changes associated with scuffing. Alternatively, or in addition, a chemical change could take place on the surface, such as a transformation of oxides or of other surface compounds (*8*).

In this paper, we report on series of experiments in which a lubricated ball/plate (both of hardened M-50 steel) sliding contact was run long enough under appropriate operating conditions until scuffing occurred. However, the plate was removed at known intervals before scuffing and the reactivity of the contact region towards diluted hydrochloric acid was determined at room temperature.

Our present measurements were made both with an additive-free base oil and with the same oil containing a tricresyl phosphate (TCP) antiwear additive. Soaking the bearing surfaces prior to contact operation was also investigated, originally to pursue some of the observations reported by Shafrin (*4*) some time ago. Using Auger spectrophotometry, Shafrin had found that exposure to TCP initially formed a phosphide on a steel surface but that this phosphide changed to a phosphate on prolonged exposure. This change in the nature of the surface would be expected to affect bearing lubrication.

MATERIALS

Lubricant

The lubricant used in this work was the base oil of a research lubricant prepared by NASA and designated as G-MIL-99. The fully formulated lubricant was designed to represent those manufactured under MIL-L-23699 specification.

Specifically, the base stock of G-MIL-99 is pure trime-

Presented as an American Society of Lubrication Engineers paper at the ASLE/ASME Lubrication Conference in Hartford, Connecticut, October 18–20, 1983

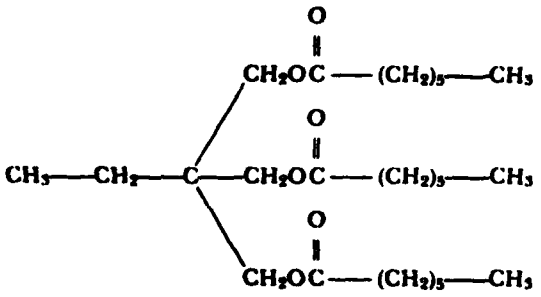

Its principal physical properties are:

Viscosity, cSt at 98.9°C	3.5
at 37.8°C	15.2
Pour point, °C	−67.8
Specific gravity, 25°C	0.963

Shell 4-Ball Wear Test

Force Newton	Scar Diameter mm, at 54°C 600 rpm, 1 hour
9.8	0.21
98	0.43
392	0.57

M-50 is a 4 percent Cr, 4 percent Mo, 1 percent C, martensitic steel. The heat treatment procedure was the following:

Preheat	816°C
Harden	1110°C
Quench (in molton salt)	552°C
Air Cool	Room Temperature
Temper* (2 hours)	538°C
Air Cool	Room Temperature
Temper (2 hours)	538°C
Air Cool	Room Temperature
Three more tempers at	524°C

*Tempering should be started as soon as room temperature is reached to avoid cracking

Our samples were heat treated by a local heat-treating company. The hardness of the steel after the heat treatment was 62–63 (Rockwell C).

Our samples (20.6-mm diameter balls and 22-mm × 11-mm × 7-mm plates) were ground before the heat treatment. After heat treatment, a grayish finish appeared on the surface. The plates were then mounted in epoxy plastic and all the specimens were lapped by machine. They were polished successively with 240-, 400-, and 600-grade sandpaper under water, then with 9-micrometer diamond-imbedded paper without water, and then with 0.3-micrometer aluminum oxide under water, until practically a mirror finish was reached. Under the metallurgical microscope (nital etching) the structures typical of tempered martensite were apparent (Fig. 1). Some chunks of carbide (white areas) can be seen.

Fig. 1—Photomicrograph of M-50 steel as used. The surface was etched with nital. Magnification 1600X.

The steel maker also supplied us with the following physical properties for this steel:

specific gravity	8.0
specific heat, J/kgK	418.6
thermal conductivity, watt/cm°C	
at 100°C	0.37
300°C	0.35
500°C	0.34

APPARATUS

AC Phase-Locked Interference Microscope (PLIM)

This instrument is the same as that used in our previous investigation (*1*), but with certain improvements. Only the improvements deserve detailed attention here. A major improvement was the addition of an argon ion laser which makes it possible to use a number of different wavelengths as surface probes. If the surface scanned is metallic, such as gold, or coated by a transparent oxide, such as aluminum oxide (Fig. 2), the profiles are the same for different wavelengths. However, with steels usually covered by an light-absorbing oxide coating, the profiles appear to be different (Fig. 3). Since the oxide layers are known to be extremely thin, the same metal surface is always the source of sample reflection. The differences are, therefore, ascribed to phase changes on reflection, which are wavelength-dependent. When a wavelength is partially absorbed by the oxide e.g. blue light by a red oxide, the phase change is dependent on the thickness of the oxide layer and significantly different from that produced by the pure metal. Therefore, the "apparent depth profile" scanned by this wavelength is different from that scanned by a wavelength which is not absorbed. From this difference, the thickness of the oxide

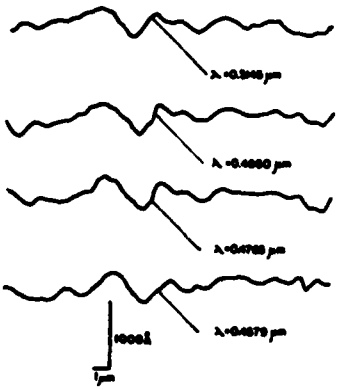

Fig. 2—Optical profiles of an aluminum plate obtained with different wavelengths of an argon ion laser.

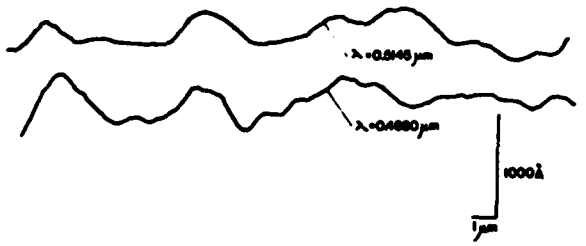

Fig. 3—M-50 plate profile before tests. Profile difference with wavelengths are noted.

layer can be calculated provided its optical parameters are known. (We are now in the process of constructing an ellipsometer attachment to the PLIM to determine these parameters). In our reactivity studies, real profiles and apparent profiles are mixed since only profile changes are observed. For this reason, care must be taken not to imply that the observed profile changes are always true surface contour changes.

Distance calibration of the instrument is very simple. In the horizontal plane, a reticule, such as those standard with optical microscopes, can be used. The horizontal magnification is essentially determined by the magnification of the objective. The larger the magnification and, therefore, in general, the numerical aperture (NA), the smaller the field of view and, also, the higher the resolution of sharp surface contours. Clearly, a steep asperity of less than two micrometers base diameter cannot be resolved if the effective resolution of the objective is less than that. Unfortunately, the higher the magnification of the objective lens, the shorter also its working distance. Depth calibration is done very accurately by the phase jump in the detector plane. The separation between two successive interference fringes corresponds to a phase difference of 2π between the sample and reference beams. If there is no oxide or other dielectric layer on the sample surface, there is phase reversal at the sample surface and this separation of fringes corresponds to a change in depth of sample surface profile of half a wavelength of the laser light (e.g. 3164 Å for the He/Ne laser). This geometric change was made equal to 10V of recorder output potential.

A major improvement of the PLIM has been the substitution of two 40x, long-working-distance (18-mm) objectives for the old standard 40x objectives (4-mm working distance). The new objectives are Cassegrainian reflectors and should, according to established theory (*3*), be unsuitable for this work because a small portion of the paraxial beam is cut off. Contrary to theory and previous experience with other Cassegrainian reflecting objectives, they work beautifully; however, presumably because (a) the two objectives, i.e. one in the sample and one in the reference beam, are precisely matched and (b) the blocked center portion is very small compared to the two-inch diameter Cassegrainian collecting mirror. The long working distance makes it possible to obtain profiles of surfaces through windows.

RESULTS

Effect on Surface Profile of Surface Treatment with the Lubricant Containing 4.5 Percent of Tricresyl Phosphate

Figure 3 shows the profile of the original M-50 plate surface as it was obtained with two different argon ion laser wavelengths. The surface was very smooth but the profiles show some differences with wavelength, which we attribute to patches of an oxide layer, for our experiments were carried out in the ambient atmosphere. For this reason, the surfaces were very likely covered by adsorbed oxygen as well. The presence of adsorbed oxygen on M-50 steel in air was also inferred by Faut and Wheeler (*8*) from their experiments on the friction of TCP.

After contacting the same surface under the microscope with the TCP-containing lubricant for five minutes, the profiles (Fig. 4) at the same two wavelengths became smoothed. (Note that all our optical profiles were obtained on dry surfaces—after exposure to lubricant, the surface was rinsed with much alcohol and allowed to dry.) The smoothing is especially noticeable at 4880 Å.

After soaking in the TCP-containing lubricant for four days at ambient temperatures, the profiles (Fig. 5 taken at 4880 Å) became even smoother. We then applied a drop of 0.01 M hydrochloric acid in alcohol for about ten seconds and washed it off (our probe reaction). The small asperities were attacked and removed (base radii of 1–2 μm) but the large ones were unaffected. The "steady-state" situation was obtained after allowing the surface to rest for some time. It would appear that chemical reaction continued even after all the chloride was washed off. It could be more chloride formation, but it could also be oxidation subsequent to chloride formation. After another acid probe treatment, one of the original small peaks had become a valley. However, the large features of the profile remained.

To compare the TCP-treated surfaces with untreated surfaces, the series of profiles of Fig. 6 were obtained. Clearly, the changes after acid treatment are very small and even the acid of ten-times the original strength did not change the profile very much. On careful examination of these profiles, a certain long-range periodicity of asperities is noticeable. The corresponding "wavelength" could correspond to an average grain size (Fig. 1). Interestingly enough,

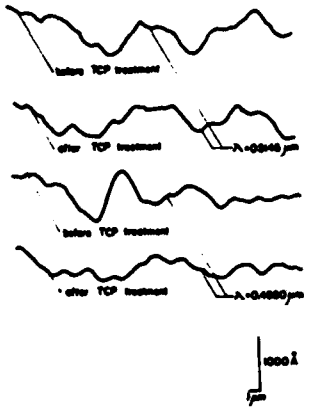

Fig. 4—M-50 plate profile after soaking for five minutes in tricresyl phosphate.

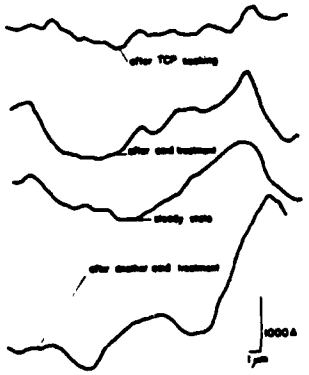

Fig. 5—M-50 plate profile after soaking for four days in tricresyl phosphate.

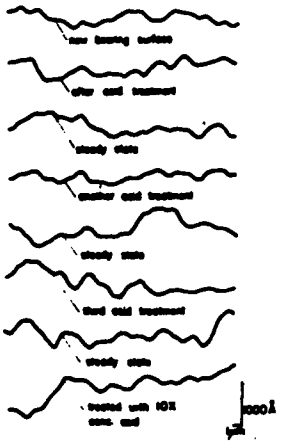

Fig. 6—Series of reactivity-test profiles at 5145 Å of the untreated M-50 plate.

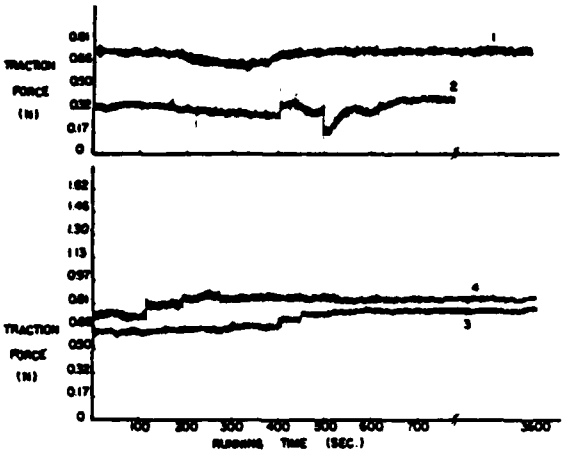

Fig. 7—Traction versus time of ball/plate contact operation. These are recorder traces of independent experiments. Traces 1 and 2 refer to base oil with tricresylphosphate (TCP) additive, the former with three hours of prior soaking at ambient temperature, the latter without soaking. Traces 3 and 4 are the corresponding traces for the base oil without TCP. The inversion of the numbers of the two pairs and the upward step at 400 seconds of all traces but 4 should be noted.

therefore, the TCP-treated steel surface was *much more reactive* toward our probe (certainly for small asperities) than the untreated steel surface.

Reactivity of M-50 Surfaces as a Function of Running Time Toward Scuffing

The ball/plate sliding contact described in one of our earlier publications (*5*) was modified to accommodate a 20.6-mm-diameter ball and a steel plate instead of a sapphire window. Both ball and plate were of the same hardened M-50 steel described earlier. The lubricant was fed into the contact region (on top of the ball) by means of a peristaltic pump. Traction, or at least a proportionate quantity, was monitored with a strain gauge. Loading took place from the top to an average Hertzian pressure of 20 kbar (Hertzian radius ~ 75 μm).

Figure 7 shows plots of traction versus operating time under these conditions. The top two curves correspond to the base oil containing the TCP and the bottom curves to the base oil alone. Both sets of plots also compare the effect of soaking the M-50 surface for three hours in the lubricant at ambient temperature. In the case of the base oil, prior soaking merely extended the time to scuffing from 120 seconds to 400 seconds, if scuffing is identified by the first steep rise of traction (subsequent examination of the wear track was consistent with this identification). The traction was somewhat reduced by the prior soaking, but not very much. In the case of the TCP-containing oil, prior soaking brought the traction to about the maximum value of the base oil; however, the traction was almost halved when soaking was eliminated. On the other hand, without soaking, the traction was very erratic over the course of the experiment, exhibiting steep rises as well as drops. It was difficult to obtain reproducible running times toward scuffing in that case.

Comparison of the traction curves of Fig. 7 shows a sharp increase near 400 seconds for all cases except the base oil without soaking. As this increase apparently corresponds to scuffing, it would seem that TCP, in general, does not delay scuffing.

Figure 8 shows a series of profiles within the wear track of the plate contact before and after acid treatment for zero,

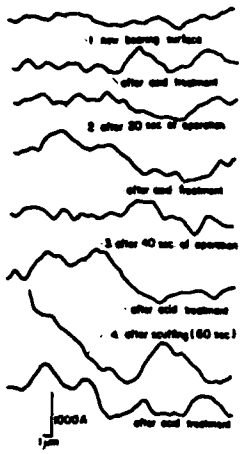

Fig. 8—Surface profiles within the wear track of M-50 plate as scuffing conditions were approached. The wavelength was 4880 Å and the temperature was ambient.

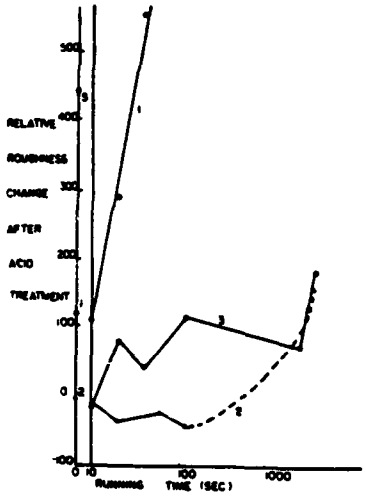

Fig. 9—Effect of acid probe on contact region roughness as scuffing conditions were approached. Roughness is defined as the area under the trace of the surface profile, which is bounded by the horizontal line representing the "center line average." Curves 1, 2, and 3 represent base oil without TCP or prior soaking, base oil without TCP but with prior soaking, and base oil with TCP and prior soaking for three hours at ambient temperature.

20 seconds, 40 seconds, and 60 seconds of running time (after scuffing in this particular experiment. The time to scuffing did not always reproduce.) It is clear that the reactivity of the plate contact changed continuously with running time and became particularly large after scuffing. For example, the asperity of the next-to-the-last profile (after scuffing) became a valley on acid treatment.

The profiles of Fig. 8 were obtained with the base oil lubricant without soaking prior to running. When the profiles before acid treatment are examined as a function of running time, a slight increase of roughness can be seen up to the scuffing transition, which is accompanied by a large increase of roughness. In general, the acid probe produced a profile of changed roughness, the increase nearly corresponding to the running time.

In order to evaluate the profile changes produced by the acid probe reaction and thus get a measure of the surface reactivity toward alcoholic hydrochloric acid, the standard center line average method was used. That is, a center line parallel to the horizontal axis was drawn in such a way that areas bounded by the profile and the center line were equal above and below that line and these areas were used as the reactivity measure sought.

In other words, the change of roughness so defined is a function of the action of the acid with respect to the surface. Figure 9 shows plots of these roughness changes produced by the acid probe as a function of operating time for three of the conditions of Fig. 8. Without soaking and with only the base oil used, the reactivity is seen to increase very rapidly corresponding to the early scuffing noted in Fig. 7. With soaking, the reactivities prior to scuffing are greater when TCP is present, but the sharp increase of surface reactivity subsequent to scuffing occurs at nearly the same time for both the TCP-containing oil and the base oil near 400 seconds of operating. 400 seconds was also the time at which traction sharply increased in these cases (Fig. 7). As a matter of fact, for the base lubricant, the profiles became smoothed (or hardly changed) as a result of the acid probe prior to scuffing.

Figure 9 also shows the very high reactivity toward the acid probe of the TCP-soaked surface before any traction at all. It is higher than any reactivity noted after running.

To confirm that the reaction within the scuff mark was much greater than without, a profile was obtained at the edge of the scar before and after acid treatment (Fig. 10). The scar was "filled in" after acid treatment. There was very little change outside the mark.

In order to investigate the nature of the material in the scuff mark further, the plate was barely polished and etched with nital. Figure 11 shows that material within the mark did not etch. The half-circular appearance of the mark would seem to indicate that the normal to the plate made a slight angle with the direction of the load. When the plate was polished a little bit more, the unetched material disappeared, even though some of the grooves still remained.

CONCLUSIONS

It would seem that a metallurgical change is produced on scuffing and even earlier—though to a much smaller extent. This change is long-lasting and responsible for rapid

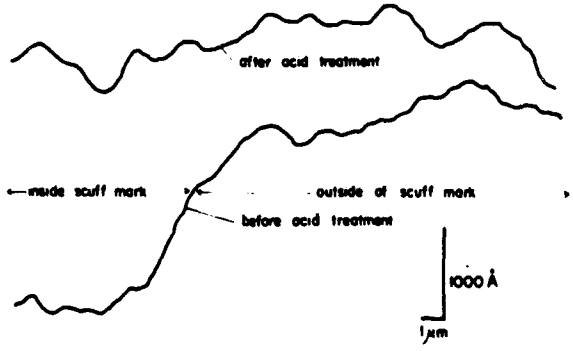

Fig. 10—Profile near edge of scuff mark

AD-A148 480 STRUCTURE OF SOLIDS SURFACES IN WEAR SITUATIONS(U) 2/2
RENSSELAER POLYTECHNIC INST TROY N Y DEPT OF MECHANICAL
ENGINEERING J L LAUER 17 OCT 84 AFOSR-TR-84-0970
UNCLASSIFIED AFOSR-81-0005 F/G 11/8 NL

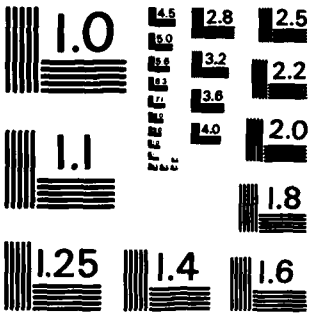

MICROCOPY RESOLUTION TEST CHART
NATIONAL BUREAU OF STANDARDS-1963-A

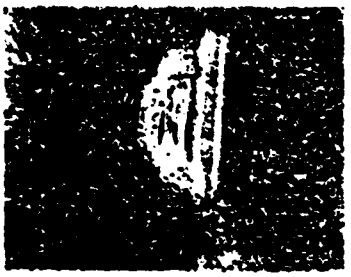

Fig. 11—Photomicrograph of scuff mark after nital etching

changes of profile on treatment with dilute alcoholic hydrochloric acid. It should be emphasized again that our measurements are carried out on a microscopic scale. The more macroscopic (microscopic in a plane, but *not* depth-sensitive) metallurgical etching tests showed the presence of a thin layer of a different, and apparently inactive, non-etching phase. It would appear that the new phase of Fig. 11, which is resistant to etching, is the same or similar to that reported by Rogers (*7*) for diesel piston rings.

At this time, no positive identification of the reactive phase has been made. Metallurgists identified some highly corrosive material when tempered martensite was heated to about 400°C and associated it with exceedingly small granular masses. Our calculations based on Archard's procedure show that we could certainly have exceeded this temperature in our ball/plate setup. These small grains set up electrochemical cells and their conglomerates can produce relatively high potentials. Perhaps these grains are so small that etching at the grain boundaries is not noticeable. This same high reactivity can then lead to scuffing with the appropriate lubricants.

The behavior of the TCP-containing lubricants and presumably TCP-coated surfaces resulting from it is somewhat different. Indeed, steel surfaces scuffed are also more reactive than the steel surfaces just soaked. In fact, the original M-50 surface is almost inert toward the probe but after exposure to TCP it becomes exceedingly reactive. A possible explanation is a surface layer of phosphide or phosphate as shown by Shafrin (*4*), which changes rapidly during wear. The work of Faut and Wheeler (*8*), showing that TCP-coated surfaces of M-50 steel exhibit less friction when heated beyond a characteristic transition temperature of 218°C, in their case, is consistent with our observations, viz. downward shifts in traction for the TCP-containing lubricants which were never observed in the absence of TCP and a particularly large reactivity for the TCP-soaked but not rubbed steel. Their results were also explained in terms of chemically different surface layers. Work now in progress in our laboratory is aimed at the chemical analysis of these layers.

It would appear that steel surfaces approaching or after scuffing, having been exposed to *high* temperatures, are also much more reactive at *ambient* temperature, at least toward diluted hydrochloric acid.

Conversely then, such a probe reaction can be very useful to determine scuffing tendencies for different solid materials and lubricants.

ACKNOWLEDGMENT

This work was funded by grants from the Air Force Office of Scientific Research, Grant No. AFOSR-81-0005 and from the National Aeronautics and Space Administration, Grant No. NSG-3180-12-81.

We also wish to thank Lavern D. Wedeven of NASA-Lewis Research Center, Cleveland, Ohio, for his help in obtaining the materials used in this research and for many helpful discussions. Eric Bamberger of the General Electric Company, Cincinnati, Ohio, supplied us with the information for the heat treatment of the steel.

REFERENCES

(*1*) Lauer, J. L. and Fung, S. S., "Microscopic Contour Changes of Tribological Surfaces by Chemical and Mechanical Action," ASME Paper No. 82-LC-3B-3. To be published in *ASME Trans.*

(*2*) Blok, H., "The Postulate about the Constancy of Scoring Temperature," *Interdisciplinary Approach to the Lubrication of Concentrated Contacts*, NASA SP-237, P. M. Ku, editor, July 15–17 (1969) pp 153–248.

(*3*) Smith, W. J., *Modern Optical Engineering*, New York, McGraw-Hill Book Company, (1966).

(*4*) Shafrin, E. G. and Murday, J. S., "Auger Compositional Analysis of Ball Bearing Steels Reacted with Tricresyl Phosphate," *ASLE Trans.*, **21**, 4, pp 329–336 (1978).

(*5*) Lauer, J. L., Keller, L. E., Choi, F. H., and King, V. W., "Alignment of Fluid Molecules in an EHD Contact," *ASLE Trans.*, **25**, 3, pp 329–336 (1982).

(*6*) Lauer, J. L., "Study of Dynamic Emission Spectra from Lubricant Films in an Elastohydrodynamic Contact Using Fourier Transform Spectroscopy," NASA CR-15 94 18, 120 pp., August 28, 1978. Available from the National Technical Information Science, Springfield, VA 22161.

(*7*) Rogers, Mal. D., "Metallographic Characterization of Transformation Phases on Scuffed Cast-Iron Diesel Engine Components," *Tribology*, **2**, 2, pp 123–7 (1969).

(*8*) Faut, O. D. and Wheeler, D. R., "On the Mechanism of Lubrication by Tricresylphosphate (TCP)—The Coefficient of Friction as a Function of Temperature for TCP on M-50 Steel," *ASLE Trans.*, **26**, 3, pp 344–350 (1983).

APPENDIX V

Optical and Other Properties Changes of M-50 Bearing Steel Surfaces for Different Lubricants and Additives Prior to Scuffing

by

James L. Lauer, Norbert Marxer
and
William R. Jones, Jr.

PREPRINT NO. 84-LC-2A-3
ASLE PREPRINT

Optical and Other Properties Changes of M-50 Bearing Steel Surfaces for Different Lubricants and Additives Prior to Scuffing©

JAMES L. LAUER (Member, ASLE) and NORBERT MARXER
Rensselaer Polytechnic Institute
Troy, New York 12181
and WILLIAM R. JONES, JR. (Member, ASLE)
NASA-Lewis Research Center
Cleveland, Ohio 44135

An ester lubricant base oil containing one or more standard additives to protect against wear, corrosion, and oxidation was used in an experimental ball/plate elastohydrodynamic contact under load and speed conditions such as to induce scuffing failure in short times. Both the ball and the plate were of identically treated M-50 steel. After various periods of operating time, the wear track on the plate was examined (a) with an interference microscope of ± 30 Å depth resolution and (b) sometimes also with a scanning ellipsometer, and (c) a scanning Auger spectrometer. The optically deduced surface profiles varied with wavelength, indicating the presence of surface coatings, which were confirmed by the other instrumentations. As scuffing was approached, a thin (~100 Å) oxide layer and a carbide layer formed in the wear track, in particular, when tricresylphosphate antiwear additive was present in the lubricant. The rates of the formation of these layers and their reactivity toward dilute alcoholic HCl depended strongly on the lubricant and additives. Based on these results, suggestions for improved formulations and a test method for bearing reliability could be proposed.

INTRODUCTION

In earlier work (*1*), (*2*) with an optical profilometer, we showed that preceding scuffing failure the wear track of M-50 alloy steel bearings operated under elastohydrodynamic or mixed lubrication became more reactive toward hydrochloric acid. Microscopic changes of the optical surface profile were used as measures of reactivity. The presence or absence of tricresylphosphate additive in the lubricating oil would have considerable influence on the profiles of the bearing surfaces even before exposure to the hydrochloric acid probe. Furthermore, our studies showed that TCP in a lubricant would reduce bearing traction significantly after soaking. In a related study, Faut and Wheeler (*3*) showed that the friction of TCP-lubricated M-50 bearings would be reduced by 30–50 percent when the contact temperature exceeded a critical value in the neighborhood of 218°C, the exact temperature depending on environmental conditions, notably the presence of oxygen and moisture. Such a decrease of friction by chemically active additives which exhibit poor lubricant action at low temperatures was explained much earlier by Bowden and Tabor (*4*) by a chemical reaction leading to the formation of a protective film. However, neither they nor other workers conclusively identified the nature of the film generated by TCP or other lubricants and compared the surface with that outside of the wear track. The changes in profile we found could be explained only in terms of a difference of chemical composition on the surface. Indeed, the appearance of the wear track after short failure-free bearing operation is often more likely a manifestation of a chemical change on the surface than of mechanical wear.

In the present study, we extended the previous measurements to additives other than TCP and to more operating conditions and developed more sophisticated techniques for the chemical and physical analysis of the surfaces along the wear track. A more conclusive identification of the new metallurgical phase found in the wear track, which was tentatively considered a carbide, was another objective. A high spatial resolution was required since the phase occurred in small patches. In addition to an improved version of the phase-locked interference microscope (PLIM) of our earlier work, an electronic ellipsometer and an Auger electron spectrometer specially adapted for this work were found to be particularly useful.

MATERIALS

Lubricants

In order to examine the effect of different additives separately and together, the same base stock was used with different additives in the same concentrations as in the fully formulated lubricant package. The latter was designed to represent the MIL-L-23699 standard. All lubricants were prepared for us by NASA.

Presented as an American Society of Lubrication Engineers paper at the ASLE/ASME Lubrication Conference in San Diego, California, October 22–24, 1984

The base stock was the same pure synthesized material, trimethylol propane triheptanoate (TMPTH), used in our earlier study and described in its paper (*2*). The lubricants were, in addition to the base stock, solutions in the base stock of

1. 0.0209 percent by weight of benzotriazole (BTZ), a corrosion inhibitor
2. 1.036 percent by weight of dioctyldiphenylamine (DODPA), an antioxidant
3. 1.036 percent by weight of phenyl-alpha-naphthylamine (PANA), also an antioxidant
4. 2.55 percent by weight of the antiwear additive tricresylphosphate (TCP)
5. all the above additives in the same concentrations together, forming the fully formulated oil, generic MIL-L-23699 (G-MIL-99)

Probe Solution

The probe solution was 0.04-M hydrochloric acid in ethanol.

Bearing Metal

Both components of the experimental ball/plate contact were made of the same alloy steel (M-50) and heat-treated the same way according to the manufacturer's specifications by a local heat-treatment company. The (martensitic) steel had the following composition: 0.80 percent carbon, 4.10 percent chromium, 1.00 percent vanadium, and 4.25 percent molybdenum. Its hardness after heat treatment was 62–63 (Rockwell C).

The samples were 20.6-mm-diameter balls and 10 × 12 × 3 mm plates, the plate dimensions determined by the inlet system of the scanning Auger spectrometer.

APPARATUS AND EXPERIMENTAL CONDITIONS

Ball/Plate Sliding Contact

In this rig, an M-50 bearing ball of 20.6 mm diameter could be rotated by a horizontal shaft supported by two bearings and driven by an electric motor. The ball was loaded from above by an M-50 plate supported by linear bearings on a horizontal loading platform in such a way that the friction force developed in the contact could be determined from the strain generated in a leaf spring connecting the plate with the loading platform. For this purpose, a strain gauge was mounted on the leaf spring and electrically activated in the standard way. The load could be varied by hanging weights on the loading platform. The lubricants were injected into the contact from a reservoir at ambient temperature by a peristaltic pump. No attempt was made to deaerate the lubricants or to control the atmosphere of the contact region.

The maximum Hertzian pressure was 0.1 GPa in all the experiments reported here. The ball speed was 220 revolutions per minute, corresponding to 0.2 m/s linear speed. The duration of every run was 30 minutes at which time the traction force had reached a near-steady value.

No attempt was made to control the contact temperature or to measure it. However, an estimate of the maximum surface temperature rise based on Winer's calculations (*5*) indicated that the temperature could have exceeded 220°C, the critical temperature for TCP/surface reaction according to Faut and Wheeler (*3*).

AC Phase-Locked Interference Microscope (PLIM)

The instrument used in this investigation was essentially the same as the one used previously (*1*), (*2*). It was, however, improved by a superior photodetector and miscellaneous changes of circuitry. Thus, the quality of the reference mirror and vibrational stability are now the major limitations to higher accuracy. At this time, ± 30 Å in depth and 0.5 μm along the surface plane are the limitations.

It was mentioned earlier that surface porfiles measured by the PLIM (or any other optical profile meter) are different from those measured with a stylus profile meter. Since an understanding of this difference is important, a careful analysis of the phenomenon was made. The following brief description should convey the essentials.

Comparison of Optical and Physical Surface Profiles

It will be recalled that any interferometer such as the PLIM compares a reference path length to an unknown length by means of a light beam (laser beam). In our case, the distances from the beamsplitter to the vibrating reference mirror and to the surface to be profiled are compared. If the distances are equal or differ by half a wavelength (i.e. a full wavelength of optical path), a bright fringe will be focussed on the detector; if the distances are not equal, a servoloop of the PLIM will apply a voltage to a piezoelectric crystal to move a mirror to make the distances equal and this voltage will be plotted and read in terms of a profile change. However, phases are compared by the laser beam, not real distances, for the position of the fringes depend only on phases. Phases are changed on passage through a medium as well as on reflection. Figure 1 gives a schematic drawing of the laser interferometer, showing the two beams being compared. If a slab of a transparent material, e.g. glass, is introduced into one of the beams, the instrument will record a change even though the surface-to-beamsplitter distance was not changed.

Figure 2 shows the actual situation near the surface to be profiled. The lens fulfills several functions: it focuses the laser beam on a small area, thus giving us spatial resolution and greater brightness, it limits the range of the angle of incidence and it limits the range of the angle of reflection that can return radiation to the PLIM and be detected. Thus, angles of incidence and reflection are limited to ± 30°. Figure 2 also shows a thin surface layer assumed to be uniform here for simplicity.

A more realistic surface layer is shown in Fig. 3 in the form of a wedge. The substrate is assumed to be iron, having a complex index of refraction $n_s = 1.5 - 1.6i$. The wedge is assumed to be an iron oxide for which the different indices of refraction shown in the figure have been used in the computation and of 0.1 μm maximum thickness. These values are realistic for bearing surfaces. The top drawing in this figure represents the physical profile of the wedge. The next plot is the optical path difference without taking the

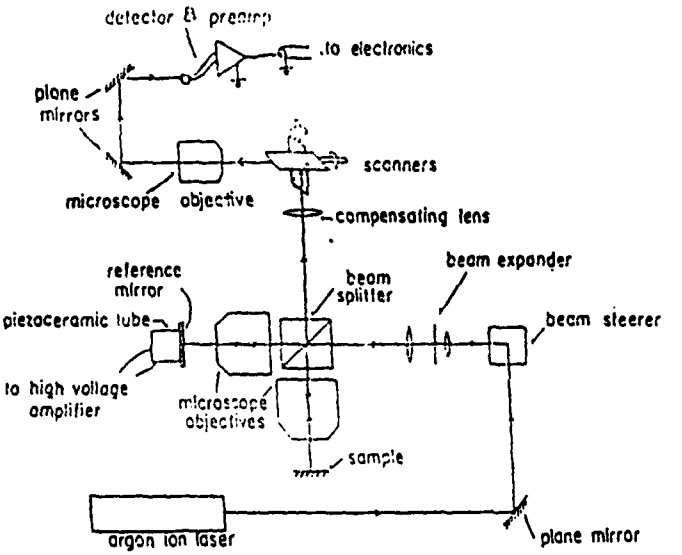

Fig. 1—Schematic drawing of laser interferometer

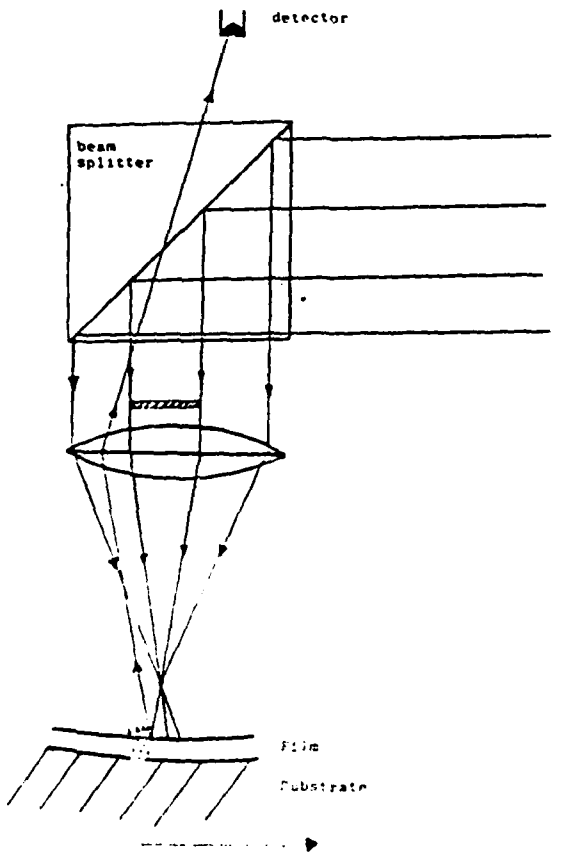

Fig. 2—Close up of light path near sample surface

phase change on reflection into account. The following plots are those that would be actually recorded; they include both the optical path difference and the phase change on reflection. Clearly, the recorded profiles were quite different from the actual physical profile. Different wavelengths will affect the phase profiles because the complex index of refraction (optical constants) changes with wavelength. The state of polarization of the laser light can also affect the profile.

Our analysis has shown that the thickness of the oxide layer and its optical constants are important factors responsible for the difference between physical and optical profiles. Oxide layers as thin as 0.03 μm or 300 Å can have drastic effects.

Is it possible to deduce the true physical profile from optical profiles? The answer is a qualified "yes," if optical profiles have been obtained for different angles of incidence at different wavelengths and perhaps also for different polarizations. In other words, the optical constants (complex indices of refraction) of both film and substrate must be determined from the profile differences. If they are known otherwise, say from ellipsometer data, then the calculations become much simpler. In any case, differences between optical profiles at different wavelengths or between optical and physical profiles are proof of the presence of surface films.

Faraday-Modulated Electronic Recording Scanning Ellipsometer (ESE)

A technique appropriate for the measurement of the thin surface films we found generated in wear tracks of elastohydrodynamic contacts is ellipsometry. It was necessary to make the ellipsometer spatially scanning and to improve its sensitivity sufficiently to allow identification of the surface materials. Auger electron spectroscopy (AES), which we also used, can also identify surface materials. The justifications for having an ellipsometer are not difficult to state: (a) ESE is faster and easier to use than AES since it does not require a vacuum; for the same reason it may also be more realistic, (b) ESE can supplement AES since it depends on molecular compositions, while AES basically will detect only atomic species, and (c) ESE can be used directly to measure film thickness, while film thickness measurements by AES require ion milling, i.e. sputtering with argon ions. On the other hand, ellipsometry is an indirect and less sensitive

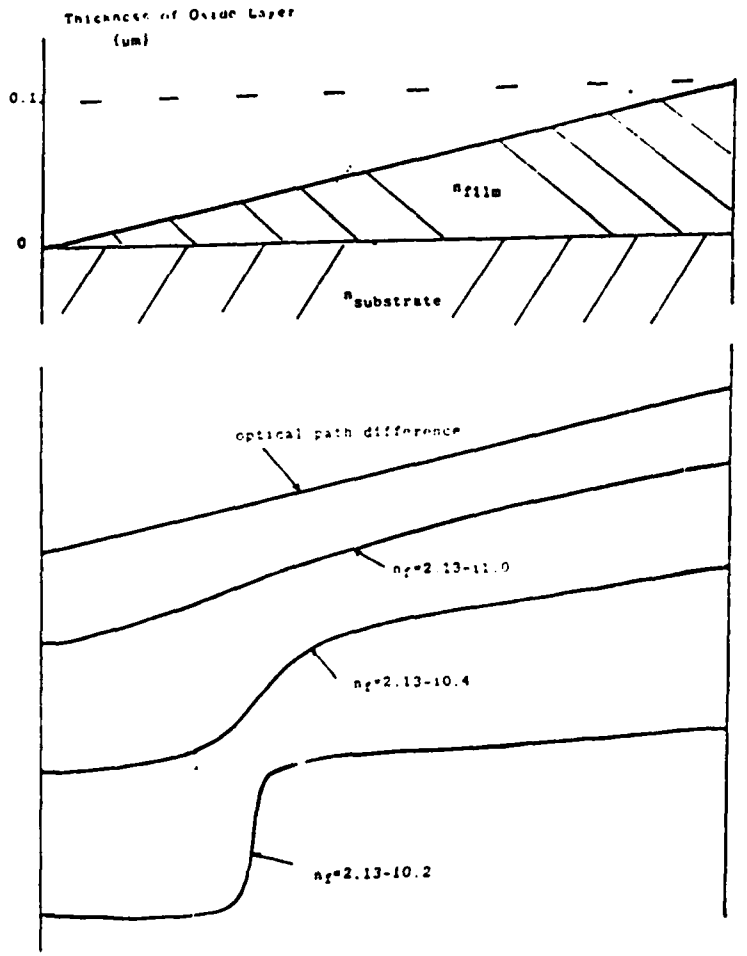

Fig. 3—Comparison of optical and physical profiles. The wedge-shaped iron oxide layer shown at the top can be transformed into the seep step at the bottom by variations of the absorption index.

method of analysis than AES. Clearly, it is advantageous to combine ESE with AES and this was done in this investigation.

Since ellipsometry for the study of bearing surface texture was very well described by Vorburger and Ludema (6) and since an extensive article on our ESE will be published elsewhere, only a brief description of our apparatus will be given here. A schematic diagram of the Faraday-modulated ellipsometer is shown in Fig. 4. This is the ellipsometer originally designed by Monin and Boutry (7), which was modified first by Sullo and Moore at the University of Rochester (8) and now by us. Radiation from the laser source *S* is polarized by the polarizer *P*, whose azimuth of vibration with respect to the plane of incidence is θ. On reflection from the sample surface *M*, the plane-polarized radiation has become elliptically polarized. The angle of the semimajor axis of the ellipse and the plane of incidence is γ. *FM* is a Faraday modulator consisting of a solenoidal coil with a Faraday glass cylinder at its axis. The magnetic field generated by the coil causes the azimuth of polarized radiation of the light traveling along the axis of the cylinder to be changed proportionally to the magnitude of the magnetic field and to the length of the cylinder, the proportionality constant being called the Verdet constant. This phenomenon is known as the Faraday effect. The coil is driven by a 500-Hz oscillator, causing the magnetic field to vary with that frequency. By the Faraday effect, the inclination angle of the polarization ellipse with respect to the plane of incidence is also varied with the same frequency. Monin and Boutry used transmission through a cylinder of water to modulate the elliptically polarized radiation instead of Faraday glass (ytterbium-doped glass). The Faraday glass, having a much larger Verdet coefficient, produces an order of magnitude greater oscillation amplitudes and, therefore, stronger signals, allowing the ellipsometric analyses of sample areas as small as 100 μm diameter or less. The radiation from the Faraday modulator is passed through the polarization analyzer *A* of azimuth β and is finally detected by the photocell or photomultiplier *PM*.

Faraday glass was used by Sullo (8). Our instrument uses two separate Faraday modulators in series instead of the one shown in Fig. 4. The first modulator contains a 10-cm-long, 0.6-cm-diameter Faraday glass cylinder (three times as long as Sullo's) and the second a Faraday glass cylinder of 3-cm length. The current in the first coil is modulated with a 500-Hz frequency, but the current in the second coil is direct current. If the analyzer angle β is equal to the true azimuth γ, the radiation detected at the 500-Hz frequency

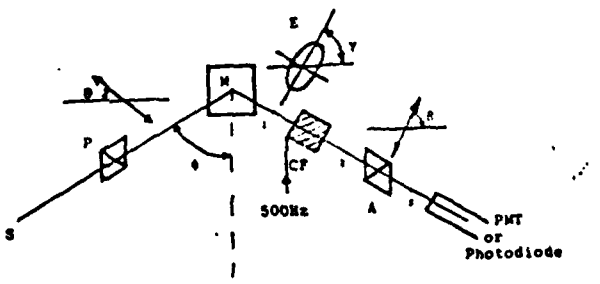

Fig. 4—Schematic drawing of ellipsometer [see discussion in the text; from Ref. (6)].

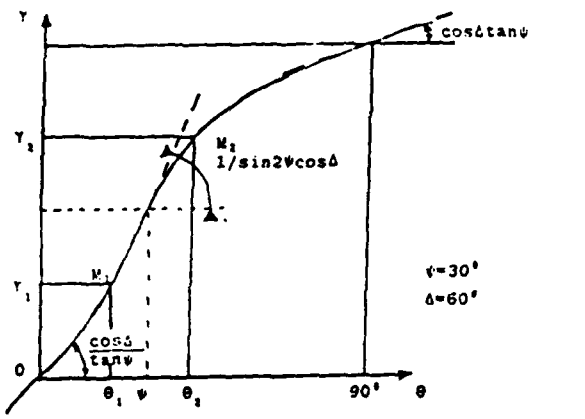

Fig. 5—Determination of the ellipsometer parameters [see discussion in the text; from Ref. (6)].

by phase-sensitive electronic detection is zero and the electronic system is "locked." At the same time, the amplitude of the first harmonic (1000 Hz) is monitored to make sure it is nonzero. If, however, the amplitude detected at 500 Hz is nonzero, an error signal is used to add to the DC bias of the second Faraday coil. This adds a DC rotation to the polarization azimuth emerging from the Faraday cells and is equivalent to rotating the analyzer. The direction of the biasing depends on which side of the null the analyzer is at. While the DC bias could be applied to the same coil as the AC, as was done in the Sullo version, having two independent AC and DC coils provides for much greater experimental flexibility and thereby extends the range of the instrument.

Scanning of a sample surface is done by moving the sample M parallel to its plane while recording the corresponding change in DC bias. Thus, only the change in azimuth ($\Delta\gamma$) is plotted (the greater portion is set by the analyzer angle β) and the instrument is sensitive to extremely small changes. This, of course, is the main value of electronic detection and scanning.

Thus, the method of measurement consists essentially of directing a beam of linearly polarized light at oblique incidence onto the film-covered surface, the thickness and refractive index of the film being determined by analysis of the reflected elliptically polarized beam. The analysis of this elliptical vibration can be carried out in a number of ways, the most commonly adopted one involving the measurement of the parameters Δ and ψ; Δ represents the phase difference between the reflected p and s components vibrating parallel and perpendicular to the plane of incidence, respectively, while tan ψ is the ratio of the reflected amplitudes r_p/r_s. The calculation of Δ and ψ can be done numerically or graphically as shown in Fig. 5. Sets of θ and γ are determined for locations on the sample surface by a number of scans at different angles of polarization and plots such as the one of Fig. 5 are drawn for every location. The slopes of the γ vs θ curve at $\gamma = 0$, 45, and 90° then provide the values of Δ and ψ. Once Δ and ψ are known, the index of refraction n and the film thickness t can be calculated, but since n is complex, consisting of two variables, more than two measurements are needed, e.g. at more angles of incidence, (not just at 45°), different wavelengths, etc. The computations can become quite extensive, but are easily performed on a small laboratory computer.

RESULTS

Tractions and Surface Roughness. Effect of the Acid Probe

Figure 6 shows traction curves for the different lubricants after the ball and plates were soaked in them for three hours at ambient temperature. These curves are all comparable except for the two antioxidants DODPA and PANA (low final traction) and for the fully formulated oil (high final traction). However, without prior soaking, the traction with TCP was much lower. The operating conditions were such that scoring or scuffing would occur very soon for the fully formuated oil, thereby allowing us to maximize the differences with respect to scoring or scuffing for the additives. From these results, differences between the bearing surfaces for the antioxidants and the TCP without soaking and the other additives could be inferred. To check this idea, the surface roughnesses of Table 1 were determined from the optical profiles. The same data were plotted in Fig. 7. These roughnesses were obtained as follows: A center line was positioned through the optical profile over a distance L in such a way that the sum of the areas under the profile curve above L was equal to the sum of the areas below L. Then roughness was the sum of the areas bounded by L and the profile divided by L times the vertical magnification. The antioxidants DODPA and PANA show the least change over the measured time period within the error limits. DODPA and PANA are also the only lubricants giving a significant reduction of roughness in the initial phase of operation when the acid probe was applied (Fig. 8). Since these measurements were made in separate experiments, the consistency of the traction, roughness, and acid probe data must be significant. Another interesting observation is the sharp increase in relative roughness change after acid treatment for both BTZ and TCP (Fig. 8) in the final stage of the ball plate run, while the roughness change remained about constant during most of the run.

A closer examination of Fig. 7 reveals some interesting correlations. Since the vertical scale is arbitrary and the curves were displaced by arbitrary amounts to avoid confusion, only trends are significant. The fully formulated oil (G-MIL-99) and the two amine additives PANA and DODPA

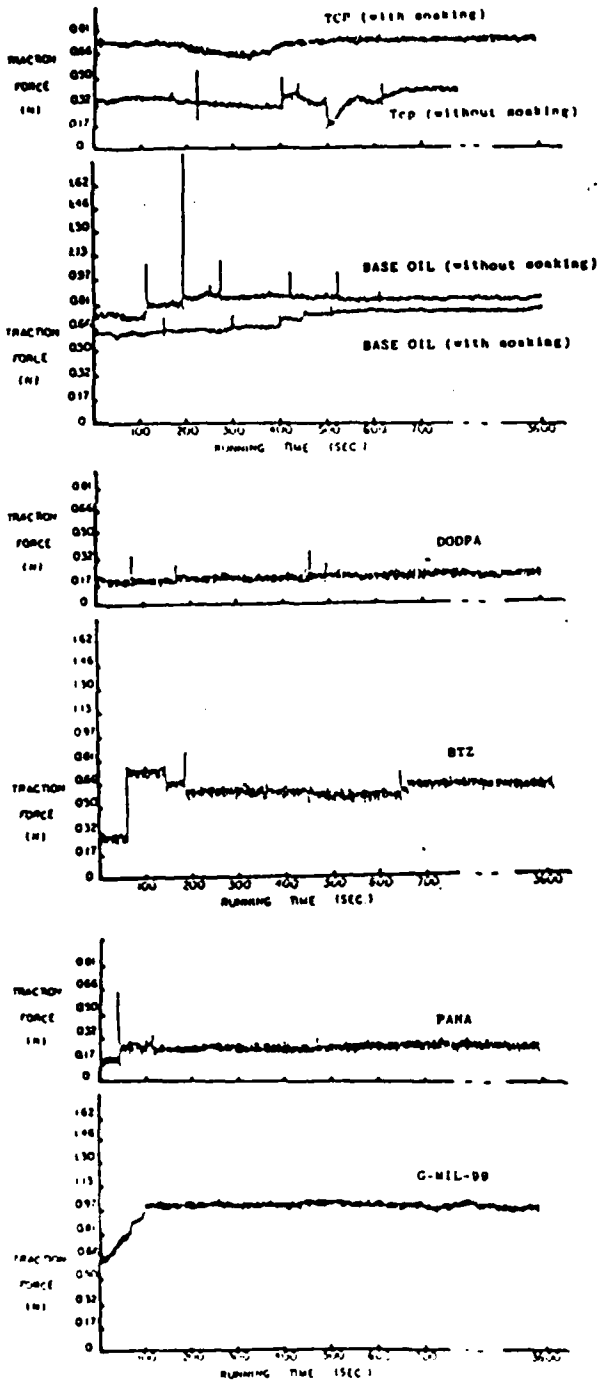

Fig. 8—Traction traces for different lubricants. The coordinates are identical for all the plots.

gave rise to roughness peaks at about 20 seconds. The fully formulated oil, the base oil and BTZ, the anticorrosion additive, had roughness peaks at about 80 seconds. Only TCP shows a descending slope beyond 100 seconds. These differences might be related to the formation of different surface oxides.

If the additive acted by producing a surface film already on soaking, then one might as well just use the base oil without the additive during bearing operation. This procedure was followed in the experiments that produced the curves of Fig. 9. Here all the surfaces were soaked for three hours in the respective lubricants, cleaned and dried, and then immediately used in the traction test with clean base oil. The results are very similar for all lubricants with the notable exception of TCP, which had a very much lower traction. BTZ was the next lowest, but the significance of its shift with respect to the others could be questioned. However, BTZ and TCP showed similarity before as was pointed out previously (data of Fig. 8). The antioxidants DODPA and PANA and the fully compounded oil had the highest traction force at the end of the experiment.

It will be noted that the curves of Fig. 9 all slope up while those of Fig. 8 are mostly flat. The slope is especially high for TCP. This behavior could be ascribed to the removal or change of a surface film or to a change in the surface metallurgy. Just soaking in the additive is practically inadequate.

Ellipsometry of Wear Tracks

In Fig. 10, the changes of azimuth with distance across the wear track were plotted. The sample (ball/plate) was soaked in the TCP lubricant for three hours and then run in the ball/plate experiment. Clearly, the nature of the surface is different inside the wear track. The change is not caused by a change of reflecting angle for the reflected laser beam is very restricted by apertures. When the angles and corresponding azimuths were changed in order to compute the film thickness and the optical constants, the former came out to be about 60 Å at the maximum and the latter corresponded roughly to Fe_2O_3 by comparison with the data of Leberknight and Lustman (9). The identification is tentative and not unique for lack of reference data, which will be obtained later.

Similar but much weaker changes were found over the wear tracks of the other lubricants containing different additives. The preferential production of a thin oxide layer on wear tracks would seem to be general, but is strongest for those produced in the presence of TCP.

It should be pointed out that the collection of data such as those of Fig. 10 presents problems different from those encountered when ellipsometry is used with dielectric substrates (10). Most ellipsometric work today refers to dielectrics and semiconductors. The most important difference is reflectivity—high for metals and low for dielectrics and semiconductors. Furthermore, metals have a complex index of refraction (two optical constants), dielectrics only a real index of refraction.

Auger Electron Spectrograms

Since Buckley (11) presented an excellent review of the technique as it applies to tribology, only the results will be given here.

The plates were analyzed after the ball experiments with every lubricant. Three areas were selected, two within the wear track and one outside of it for reference. After the ball experiment, the specimens were washed with lots of alcohol and allowed to dry and not handled or treated prior to their introduction into the Auger spectrometer. As a control, a polished M-50 plate not used in a ball/plate ex-

TABLE I*—AVERAGE ROUGHNESS OF M-50 BEARING SURFACE AFTER VARIOUS PERIODS OF OPERATING TIME WITH BASE OIL AND BASE OIL CONTAINING VARIOUS ADDITIVES (WITH SOAKING)

	0 s	10 s	20 s	40 s	1 min	2 min	1 h
Base oil	245 ± 62	317 ± 72	420 ± 80	418 ± 69	687 ± 148	589 ± 90	645 ± 110
TCP	264 ± 72	246 ± 48	291 ± 88	482 ± 42	460 ± 83	432 ± 56	401 ± 130
DODPA	360 ± 80	306 ± 66	412 ± 52	314 ± 35	308 ± 49	283 ± 26	427 ± 76
PANA	443 ± 74	322 ± 86	459 ± 129	314 ± 43	281 ± 95	349 ± 49	403 ± 67
BTZ	406 ± 150	341 ± 55	271 ± 27	435 ± 62	513 ± 105	318 ± 40	519 ± 126
G-MIL-99	436 ± 35	419 ± 96	598 ± 130	355 ± 152	551 ± 125	296 ± 185	661 ± 227

*The average roughness was measured by the centerline average method and the profiles were obtained at 4880 Å wavelength. These data have been plotted in Fig. 7.

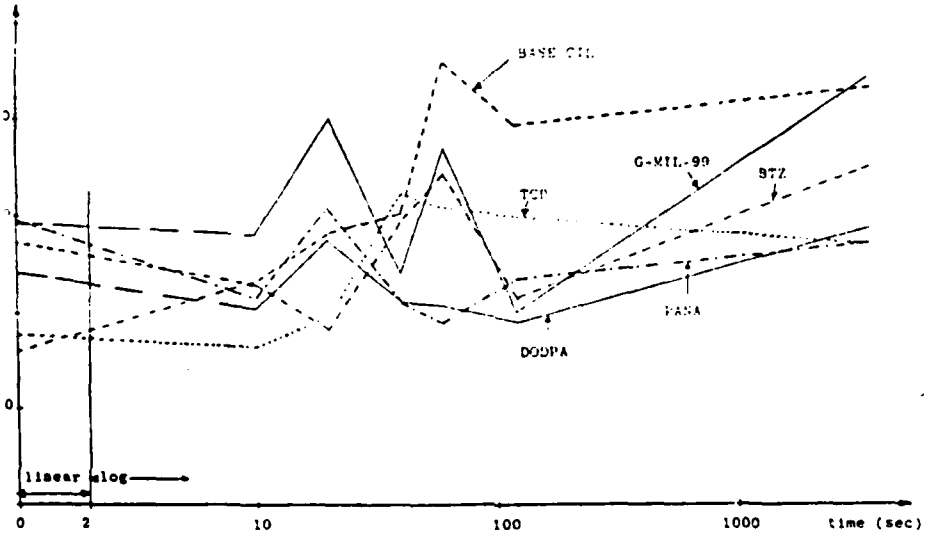

Fig. 7—Roughness changes with operating time of bearing contact. The units of the ordinate are arbitrary, but equal for all the lubricants. The curves for the different lubricants are displaced vertically to reduce confusion. Roughness is defined as the area on the optical profile plot, which is bounded by the center line and the curves above and below for an arbitrary distance.

periment was included in the set of Auger analyses.

Figure 11 shows an Auger spectrum for a TCP run within the wear scar prior to any treatment within the spectrometer. The principal peaks have been assigned to the elements C, O, Cl, Cr, and Fe. Since C, O, and often Cl are likely outer surface contaminations, a routine of ion milling was adopted. Sputtering was performed with argon ions in such a way that about 10 Å were removed per minute.

After six minutes of ion bombardment, the spectrum of Fig. 12 was obtained. Now most of the C and O, but not all, were removed and the iron peaks were relatively stronger. The Cl, evidently an impurity, disappeared. At the off-scar position and with the same amount of ion bombardment, the strengths of the C and O peaks were weaker relative to those of the iron peaks. The Mo and Cr peaks were about of the same strength off-scar and on-scar.

All the other lubricants and the reference gave about the same spectra in the as-received condition. However, after six minutes of ion bombardment, all the spectra from outside the wear scar as well as from the reference plate were essentially free of O and C while those from inside the wear scar, notably those from TCP and perhaps also from BTZ had a higher O and C content.

In order to show the effect of ion bombardment on elemental composition, the plots of Fig. 13 were drawn for a position within the wear scar. They present the ratios of the O and C peaks to one of the Fe peaks as a function of time. A sharp change of slope after two-to-four minutes probably signifies the removal of a surface layer. The following observations can be made:

1. All the C-ratios reached a low plateau value after two minutes of ion bombardment (or less). The highest plateau values corresponded to TCP; next was BTZ.
2. All the C-ratios showed only one change of slope with time of ion bombardment.
3. All the O-ratios except that of the reference, showed two changes of slope, at two and at four minutes. After six minutes of ion bombardment TCP, the fully formulated lubricant (GMIL) and BTZ had the highest O-ratio, the reference very difinitely the lowest. Thus there are two O-containing films.
4. The shapes of the O-ratio plots for TCP and GMIL were similar.

From these observations the following deductions would seem to be reasonable:

1. The high C-ratios and O-ratios in the outermost sur-

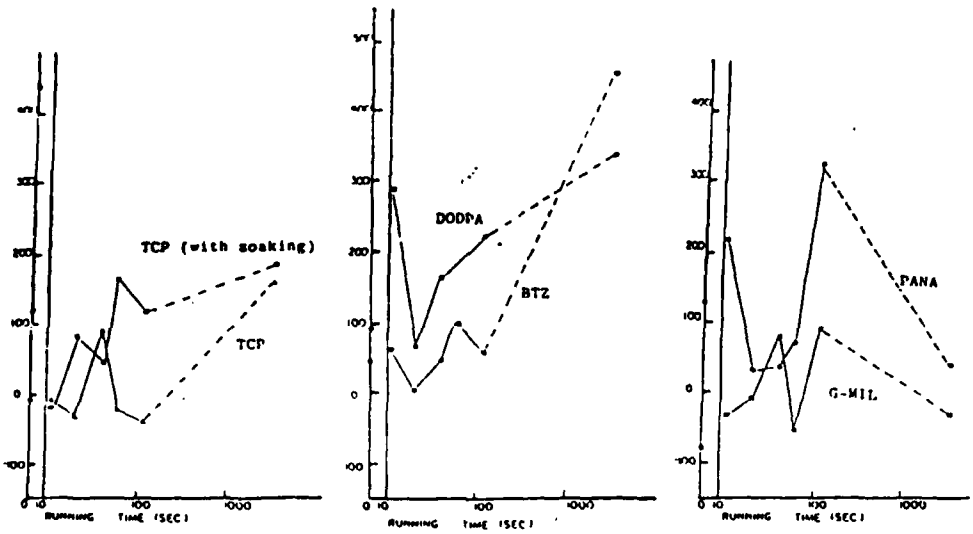

Fig. 8—Effect of acid probe on contact region roughness. (Roughness was measured by the centerline average method and the profiles were obtained at 4880 Å wavelength). The relative roughness change is defined as the difference between the roughness before and after acid treatment when roughness itself is defined as the area on the optical profile plot, which is bounded by the center line and the curves above or below for an arbitrary distance.

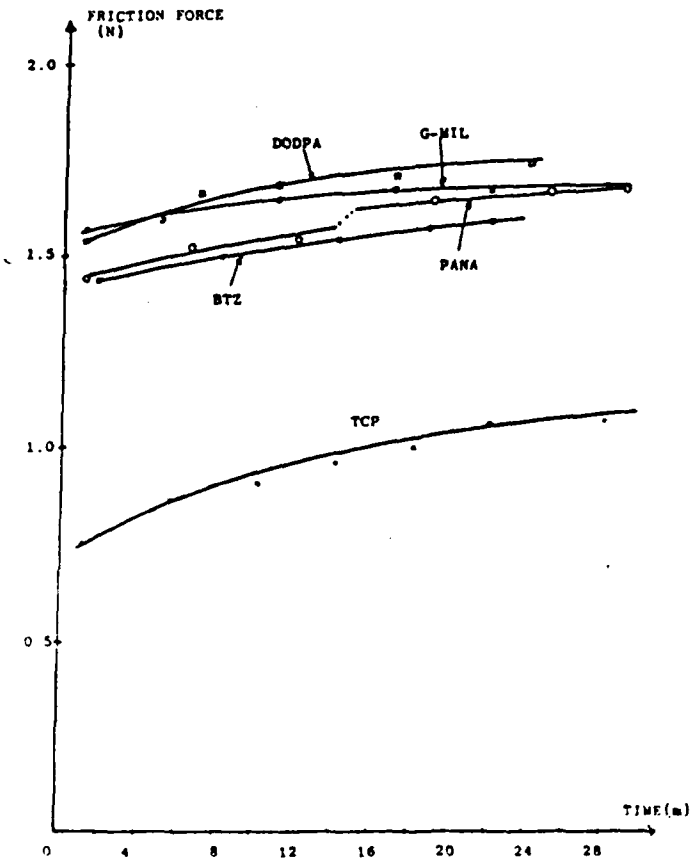

Fig. 9—Traction curves for the base oil after surfaces had been soaked in different additives

face layer are probably atmospheric contamination. They are present even in the reference.

2. TCP and GMIL (also containing TCP) have an oxide layer under the atmospheric contamination layer. BTZ is likely to have one as well. The reference, however, does not have such a layer within our error of measurement, but the other materials might have a weak oxide layer.
3. A carbide layer might also underly the atmospheric contamination layer.

Careful study of the original spectra did not show a higher Cr-concentration in the wear track than without. Buckley (*12*) noticed such an increase for 302 stainless steel.

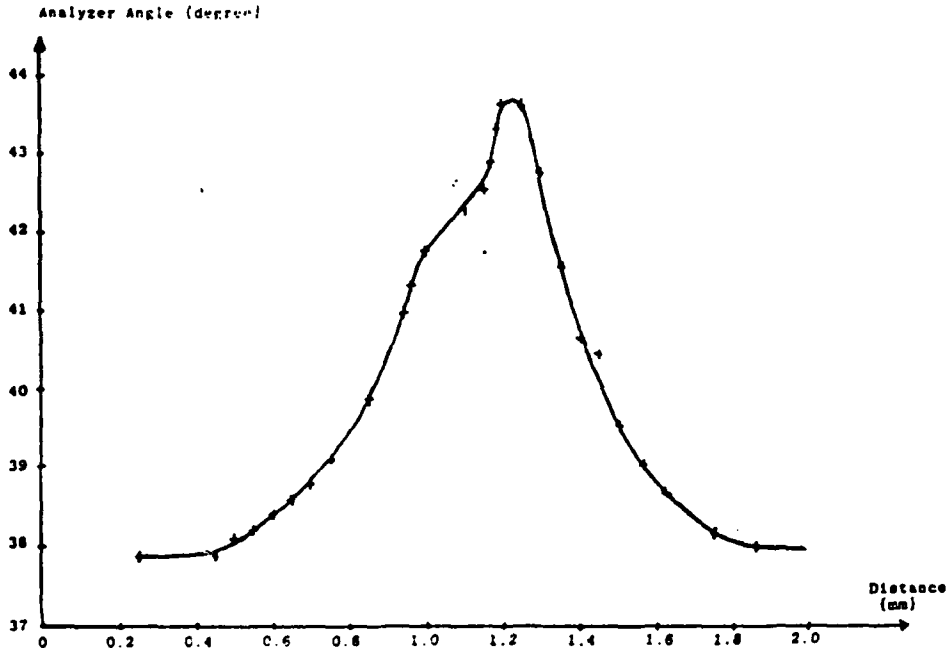

Fig. 10—Ellipsometry trajectory across a wear track produced with TCP in the ball/plate experiment

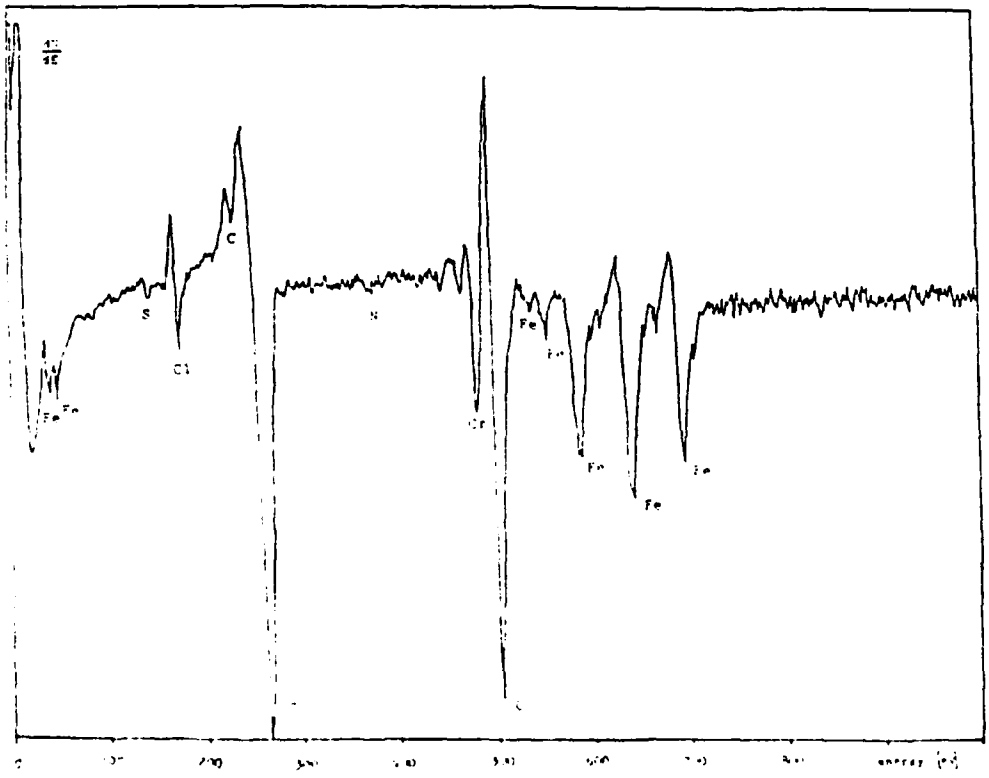

Fig. 11—Auger spectrum from an area within the wear track produced by the ball experiment with TCP soaking. *dN dE* (arbitrary units) is plotted against electron energy.

DISCUSSION AND CONCLUSIONS

In our previous publications (*1*), (*2*) the difference in the effect of dilute hydrochloric acid (our acid probe) on causing contour changes within and outside a wear track was described, this difference being especially great when scuffing conditions were approached. It was also found that the presence of the antiwear additive TCP in the lubricant would enhance this difference. Then the question was raised why scuffing could occur so suddenly, apparently without warn-

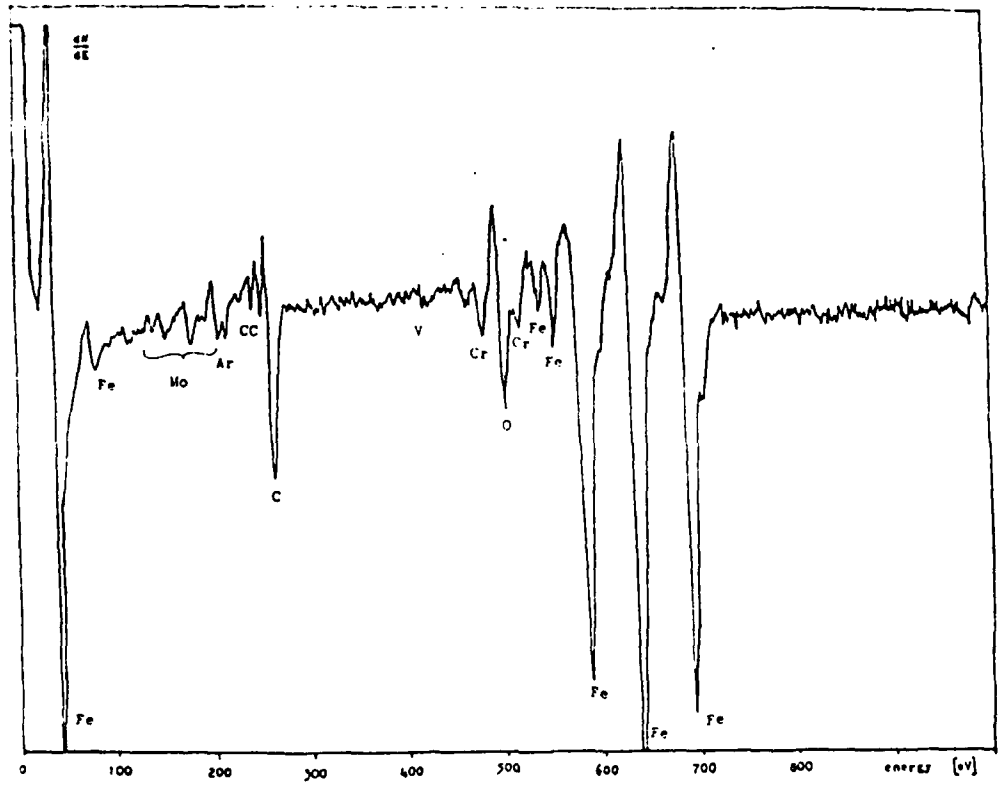

Fig. 12—Auger spectrum from the Fig. 11 sample after six months of ion bombardment. *dN/dE* (arbitrary units) is plotted against electron energy.

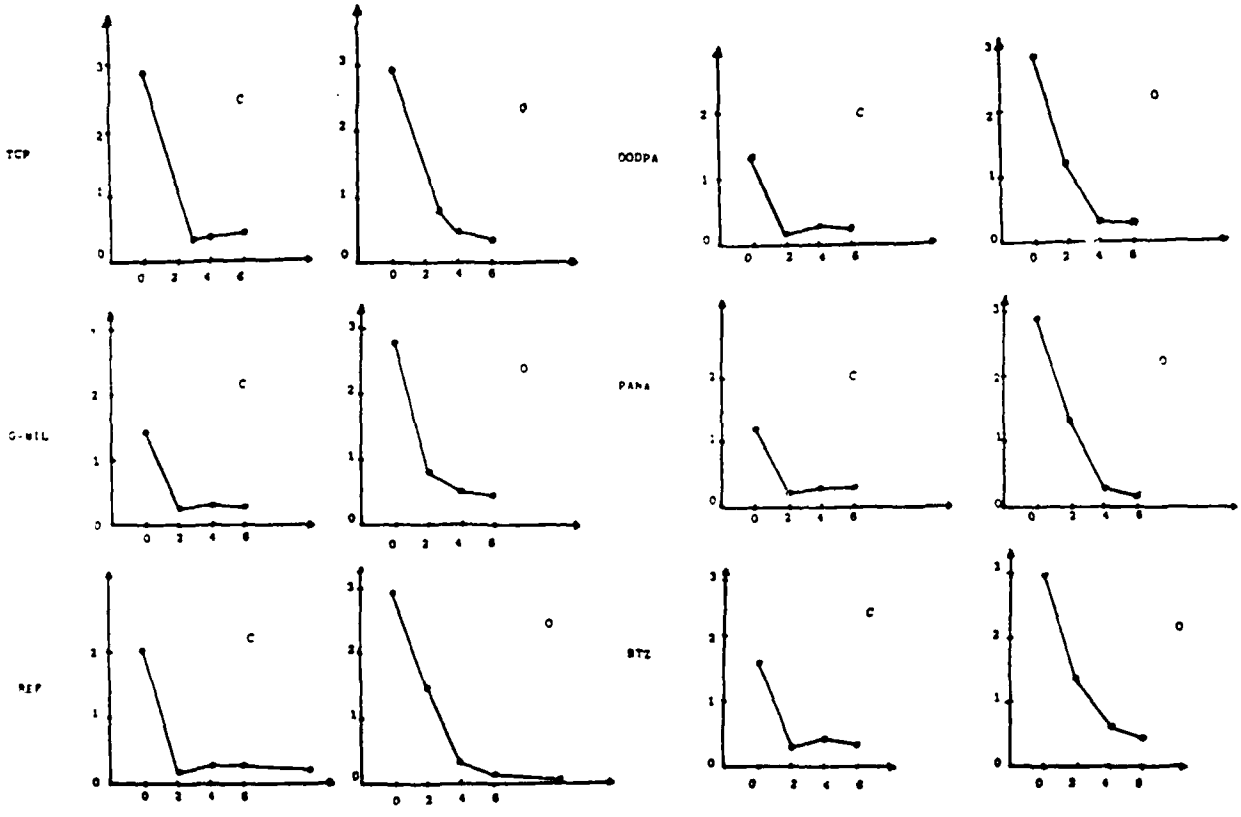

Fig. 13—Ratio of a carbon to an iron Auger peak and of an oxygen peak to the same iron peak for different additives as a function of ion bombardment time. An approximate calibration has shown that about 10 Å of depth are removed in a minute of ion milling. The units of the abscissa are milling time in minutes.

ing, even though operating conditions could have been far from those postulated by the Blok temperature criterion. A principal objective of this study was to try to explain the behavior of the acid probe in the hope that an answer there would also help toward arriving at an answer to the latter question.

Differences in the optical profile at different wavelengths, ellipsometry, and Auger electron spectroscopy have now been shown to discriminate between the surface within the wear track on M-50 steel and outside of it. The evidence points to a higher concentration of an oxide, most likely iron oxide, within the wear track than outside. Interestingly enough, it would seem that TCP promotes the formation of such an oxide. Our Auger spectra never showed phosphorus peaks as others had reported (*11*), but then this study used only dilute solutions of TCP while Shafrin (*11*) used the pure material. Such an oxide would react much faster chemically with acid then the alloy steel itself. Thus, the oxide would explain the behavior of the hydrochloric acid probe. The oxide is more likely to be formed in the wear track than outside of it because of the higher surface temperature in the wear track. It would also reduce friction at higher temperatures, though not at low ones and explain both our data of Fig. 9 and the results of Faut and Wheeler (*3*). Although such an iron oxide layer on the surface could conceivably promote the formation of friction polymer—whose formation was reported to be enhanced by TCP also—it is more likely that the same oxidizing conditions that lead to the formation of the oxide also lead to the formation of *friction polymer. Since friction polymer is, in turn, related* to acid sludge and the acid is likely to react quickly with the basic iron oxide, provided the temperature is high enough, a case could be made for a mechanism of scuffing, viz removal of the oxide layer by reaction with acids in the lubricant exposing the nascent metal and allowing metal-to-metal welds. Work now in progress in our laboratory will test this idea.

A new metallurgical phase for M-50 steel was also found and reported in our earlier publication (*2*). Its etching characteristics seemed to identify it as a carbide. The higher carbon contents found in the wear track below the surface, especially for TCP, are consistent with this identification.

The sharp initial decrease in the ball experiment of acid probe reactivity of the two amine antioxidants (Fig. 8) can be explained by the initial formation of an amine surface film and subsequent exposure of the original alloy steel surface, i.e. the lack of a surface oxide. Since the metal reacts more slowly than the oxide—which was prevented from forming—the probe reaction slows down. Once the amine antioxidant is exhausted, the reaction speeds up again, however, thus explaining the increased activity later. The amine surface film could also be instrumental in reducing traction.

The behavior of BTZ, the anticorrosion additive, has been found to be similar to TCP in some ways. Its low oil solubility requires its small concentration. By the same token, it is more likely to come out of solution and coat the bearing surfaces with an anodic (*13*) layer. However, as Parkins (*13*) admits, the behavior of these materials is still not well understood, even by electrochemists, though they have been used for a long time.

It would appear that the behavior of TCP with respect to oxide formation in the fully formulated oil is not altered by the other fuel additives as the fully formulated oil behaved similarly. However, there are mutual influences on traction. They should be the subject of further study.

Thus, it would seem that leads have been generated to help in the design of lubricating materials to reduce traction and scuffing failure. Their chemical interaction with the bearing surfaces, i.e. the formation of oxide and perhaps other layers is an important key.

ACKNOWLEDGMENT

This work was sponsored by a grant from NASA-Lewis Research Center, NAG 3-222. Additional funding was provided by the Air Force Office of Scientific Research, Grant No. AFOSR-81-0005 and by a grant from the Army Research Office, Grant No. DAAG 2483K0058.

We also want to take this opportunity to thank Simon Fung for the initial work, Michael Mailloux for construction of some of the circuitry, and H. P. Liechti for various improvements in both the PLIM and ESE circuitries. The development of the necessary software was made easier for us by the help of Dean Chandler-Horowitz from the National Bureau of Standards to whom we hereby express our thanks. Duncan T. Moore of the Institute of Optics, University of Rochester, provided us with most of the knowhow and circuitry of the ellipometer, for which we are most grateful. Without his continued assistance, our ellipsometer *would not be built.*

The Auger analyses were carried out for us by J. B. Hudson of our Materials Engineering Department and we are grateful to him for this work.

REFERENCES

(*1*) Lauer, J. L. and Fung, S. S., "Microscopic Contour Changes of Tribological Surfaces by Chemical and Mechanical Action," *ASLE Trans.*, **26**, pp. 430–436 (1983).

(*2*) Lauer, J. L., Fung, S. S., and Jones, W. R. Jr., "Topological Reaction Rate Measurements Related to Scuffing," ASLE Preprint No. 83-LC-2B-3. Presented at the ASME-ASLE Lubr. Conf. in Hartford, CT, October 18–20, 1983.

(*3*) Faut, O. D. and Wheeler, D. R., "On the Mechanism of Lubrication by Tricresylphosphate (TCP)—The Coefficient of Friction as a Function of Temperature for TCP on M-50 Steel," *ASLE Trans.*, **26**, 3, pp. 344–350 (1983).

Bowden, F. P. and Tabor, D., *The Friction and Lubrication of Solids*, Oxford, Clarendon Press, pp. 311–319.

(*4*) Anderson, A. K., Nagaki, H. S., Sanborn, D. M., and Winer, W. O., "Infrared Temperature Mapping of Elastohydrodynamic Lubrication," *Trans. ASME, F*, **98**, p. 236 (1976).

(*5*) Archuleta, J. A. and Ludema, K. C., "Ellipsometry of Rough Surfaces," *Wear*, **19**, pp. 561–573 (1980).

(*6*) Archuleta, J. and Bowers, G. A., "Concept, Realization and Performance of a New Ellipsometer," *Appl. Opt.*, **4**, pp. 1579–1603 (1973).

(*7*) Sallo, Nancy J., "Measurement of Absolute Refractive Index Profiles in Graded Index Materials Using Modulation Ellipsometry," M.S. Thesis, Inst. of Optics, Univ. of Rochester, supervised by Prof. Duncan T. Moore.

(*8*) Checkroughi, C. L. and Eastman, B., "An Optical Investigation of Oxide Films on Metals," *J. Opt. Soc. Am.*, **29**, pp. 59–66 (1939).

(*9*) Archuleta, K., *The Characterization of Materials in Research, Ceramics and Polymers*, J. J. Burke and V. Weiss, eds. Syracuse University Press, pp. 503–527 (1975).

(*10*) Buckley, D. H., *Surface Effects in Adhesion, Friction, Wear, and Lubrication*

Elsevier Scientific Publishing Co., Amsterdam, pp. 62–73 (1981).
(72) Buckley, D. H., *Surface Effects in Adhesion, Friction, Wear, and Lubrication*, Elsevier Scientific Publishing Co., Amsterdam, pp. 521–525 (1981).
(73) Parkins, R. N., *Corrosion Inhibition, in Comprehensive Treatise of Electrochemistry*, **4**, *Electrochemical Materials Science*, J. O'M. Bockris, B. E. Conway, E. Yeager, and R. E. White, eds., Plenum Press, New York, pp. 213–315 (1981).
(74) Shalom, E. G. and Morales, J. S., "Auger Compositional Analysis of Ball Bearing Steels Reacted with Tricresyl Phosphate," *ASLE Trans.* **21**, 1, pp. 029–036 (1978).

Presented at the ASLE/ASME Lubrication Conference, San Diego, California, October 22–24, 1984.

APPENDIX VI

Analysis of Patchy Microscopic Depositions from Jet Fuels on Stainless Steel or Aluminum by Infrared Emission

by

James L. Lauer and Peter Vogel

(Presented at the Third Conference on Infrared Physics, in Zurich Switzerland, July 23-27, 1984)

To be published in Infrared Physics

James L. Lauer and Peter Vogel

Analysis of patchy microscopic depositions from jet fuels on stainless steel or aluminum by infrared emission

Rensselaer Polytechnic Institute
Troy, New York 12181

Fuels used in aircraft jet engines also serve as coolants in heat exchangers. As they circulate past hot aluminum or stainless steel surfaces, they deposit decomposition products which, if allowed to accumulate, seriously reduce both heat transfer and flow rate at a given pressure drop. The deposit problem is aggravated by the presence of dissolved oxygen, a high aromatic content and the small amounts of nitrogen and sulfur compounds which are most prominent in fuels derived from shale oil. An accepted procedure for the testing of fuel stability makes use of a rig (jet fuel oxidation tester, JFTOT) in which air-containing fuel is pumped through the jacket of a "condenser" whose inner tube is made of 6 cm long aluminum or stainless steel tubing of 3 mm outside diameter, terminated at both ends by 4.5 cm long, 5 mm diameter, brass or steel cylinders to which electrical connections are made. The outer wall of the jacket is a glass tube which fits snugly around these cylinders, thus providing an annular space, 1 mm wide, for the flow of the fuel which enters and leaves by connecting tubes located at the ends of the test section and directed at right angles to the condenser axis. The inner tube is heated by electric current to a temperature monitored at the center of the test section by a thermocouple with leads along the tube axis. Typical temperatures range between 200 and 300°C. The standard flow rate is 3 ml per minute. The flow of cool liquid fuel over the tube surface causes the surface temperature to vary with distance from the inlet and the displacement of the position of maximum temperature from the tube center to the outlet side.

After several hours of operation deposits will have formed on the outside wall of the inner (JFTOT) tube of the "condenser," predominantly on the outlet side. In the standard test the deposit density and color is rated against empirical standards. In our study JFTOT tubes were located in a horizontal plane above an all-reflecting microscope objective lens, whose optical axis was in a vertical direction, in such a way that the deposits were in the focal plane of the objective. The enlarged image of the deposit was aligned at the focal position of the collimator mirror of an infrared Fourier spectrophotometer. This instrument, of our own design and construction, was described earlier [1]. Translation of the JFTOT tubes in an axial direction could be done precisely and accurately so that different deposit portions could be brought into the field of view and their infrared emission spectra analyzed. For this purpose JFTOT tubes were heated to 70°C by thermostatted water. A room temperature Golay detector was used in the spectro-

photometer. The spatial resolution was better than 0.5 mm. The deposit thickness ranged between 100 and 1000 A, as estimated by SEM.

With many fuels the JFTOT deposits formed in a series of brightly colored rings, shown schematically in Fig. 1 (bottom). These rings are not interference colors for they generally correspond to emission intensity maxima (Fig. 1, top). Most likely they were produced by instabilities of flow velocity similar to those observed by Knapp et al. [2] in their investigation of the flow pattern about the walls of a cylinder whose axis is located in the flow direction. At positions of low flow velocity in the boundary layer overheating is likely to occur, giving rise to fuel decomposition. The color of the rings is probably caused by light scattering.

Figure 2 shows emission spectra obtained at three positions indicated in Fig. 1. The deposits come from JP-4 fuel containing 10% of aromatics and were formed at a 285°C JFTOT temperature. The top spectrum corresponds to a peak of overall infrared emission--and a yellow ring--while the other spectra correspond to between-rings positions. Characteristically, the top spectrum shows apparently inverted emission and absorption peaks at the intersections with the broken lines because deposit thickness, substrate reflectivity and wavelengths resulted in the distortions described by Hvistendahl et al [3]. The middle spectrum is also partly distorted while the bottom spectrum is essentially undistorted. The distortions can be removed by computations, showing that all three spectra are very similar and permitting estimation of deposit thickness. Chemically the bands at the broken lines refer to aromatic rings, but the last one (1740 cm^{-1}) to carbonyl groups.

Figure 3 shows emission spectra from deposits of a jet fuel derived from shale oil, which were collected on aluminum and stainless steel JFTOT tubes. The upper spectrum is distorted, but both spectra can be shown to be essentially identical (by computer). The main carbonyl band is now at 1700 cm^{-1} (carboxyl). This band and others indicate the presence of metal carboxylates. A particularly outstanding difference between these spectra and those of Fig. 2 is the presence of strong bands around 1100 cm^{-1} (OH and unsaturation) and at 730 cm^{-1} (CH_2 rock).

It is clear that such analyses are difficult, but can yield a wealth of information. The JFTOT tubes containing the deposits were supplied by Mr. Robert Morris of Wright-Patterson AFB. His cooperation and the funding of the project by AFOSR Grant No. AFOSR-81-0005 are gratefully acknowledged.

REFERENCES

1. Lauer, J.L. and King, V.W., "Fourier Emission Infrared Microspectrophotometer for Surface Analysis-I. Application to Lubrication Problems," Infrared Physics, 19, 395-412 (1979).

2. Knapp, C.F., Roache, P.J., and Mueller, T.J., "A combined visual and hot-wire anemometer investigation of boundary layer transition," UNDAS-TR-866 CK, prepared by the Aerospace Engineering Department of the University of Notre Dame for the U.S. Navy, David Taylor Model Basin, Contract Nonr 1623-(17), August 1966.

3. Hvistendahl, J., Rytter, E., and Oye, H.A., "IR emission spectroscopy of molten salts and other liquids using thick samples as reference," Applied Spectroscopy, 37, 182-187 (1983).

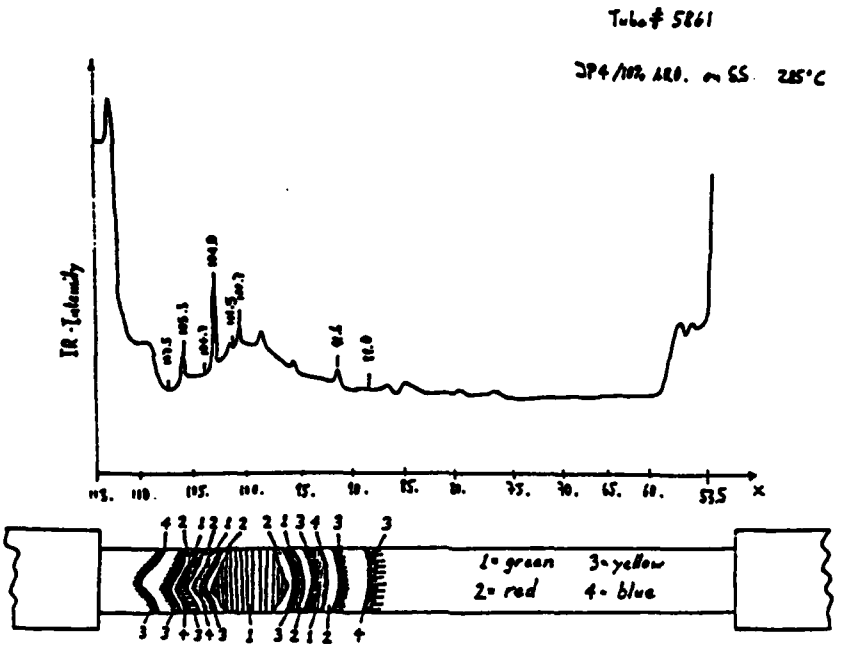

Figure 1

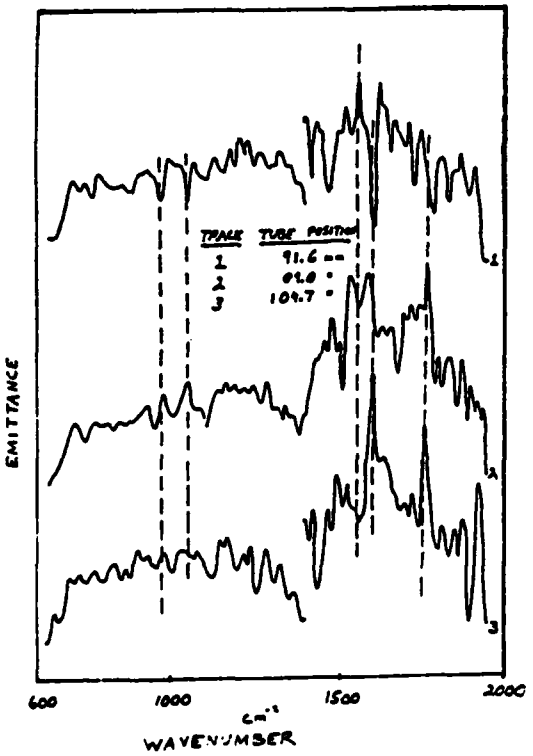

Figure 2

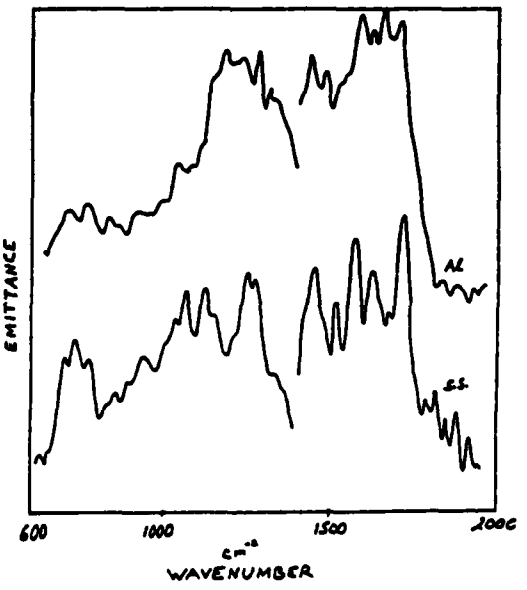

Figure 3

APPENDIX VII

Characterization of Lubricated Bearing Surfaces Operated Under High Loads

by

James L. Lauer, Norbert Marxer
and
William R. Jones, Jr.

(To be presented at the International Tribology Conference,
Tokyo, Japan, July 1985)

Characterization of Lubricated Bearing Surfaces Operated Under High Loads

James L. Lauer*, Norbert Marxer* and William R. Jones, Jr.**

The composition and surface profile of different bearing surfaces was determined after different periods of operation under various operating parameters. A variety of lubricating oils and additives such as tricresylphosphate antiwear agent, amine anticorrosive agents and antioxidants, water and oxidized oils (containing acidic components) were used. Optical surface profiles could be obtained to ± 30 Å depth resolution of 10 μm diameter areas within and outside the wear track and the optical constants and surface film thickness of the same areas could be found by a specially designed magnetically modulated scanning ellipsometer. Metal oxide formation was accelerated within wear tracks.

1. INTRODUCTION

Although lubrication has been recognized as a surface phenomenon for a very long time and is of enormous importance in modern civilian and military technology, the changes occurring on a microscale which must precede macroscopic changes, such as failure by scuffing, are still mostly unknown. Yet the identification and understanding of these changes offer much promise toward the solution or at least mitigation of bearing problems.

While many new methods of surface analysis have been developed in recent years, their requirements of ultrahigh vacuum and of electron bombardment make these methods destructive. Furthermore they mostly furnish only elemental analysis and then their spatial resolution is not high. For some of our work we have been fortunate in having access to a scanning Auger electron spectrophotometer (AES); its best spatial resolution of about 50 μm is rather high. However, most of our analyses were carried out with spatial resolutions better than 20 μm and they made use of (i) a phase-locked interference microscope (PLIM), (ii) an electronic Faraday-modulated ellipsometer (EFME), (iii) speckle-contrast (SC), and (iv) friction and lubricant thickness measurements with a ball-on-plate sliding contact. This apparatus was assembled and brought to bear in the search for significant surface changes of a loaded ball-plate sliding contact operated on its way to failure.

A realistic system was selected for these laboratory studies; an operating contact consisting of a loaded M-50 bearing steel ball-on-plate of the same material mock-bearing and lubricants simulating MIL 23699 and its additives, i.e. a most common heavily loaded bearing system. The mock-bearing had dimensions such that the width of the wear track was amenable to our surface analyses.

Significant changes were found (i) in the changes of the surface profile within the wear track over the course of bearing operation for different lubricants, (ii) in the rate of oxidation of the steel bearing surface within and without the wear track, (iii) in the rate of change of optical profile within and without the wear track after a brief exposure to dilute hydrochloric acid, and (iv) in the friction for different lubricants. Common surface additives in lubricants, such as tricresylphosphate (antiwear) and benzotriazole (anticorrosion), produced larger profile changes than other common lube additives. Invariably these changes could be associated with the more rapid formation of surface oxides within than without the wear track.

The hydrochloric acid probe reaction changing the surface profile could become a convenient and useful test for bearing surface reliability.

The PLIM and EFME instruments developed for this work will prove to be useful in many different applications, not only in the analysis of metal and metal oxide surfaces. The

*Rensselaer Polytechnic Institute
**NASA-Lewis Research Center

applicability of SC will, however, remain very limited.

2. MATERIALS

The lubricants were trimethylol propane triheptanoate base stock either alone or with one or all of the following (i) benzotriazole (0.0203% corrosion inhibitor, BTZ), (ii) dioctyldiphenylamine and (iii) phenyl-alpha-naphthylamine (both 1.036% and antioxidants, DODPA and PANA), and (iv) tricresylphosphate (2.55% TCP antiwear additive). The fully formulated oil is equivalent to MIL-L-23699 (G-MIL-99).

The probe solution was 0.04 M hydrochloric acid in ethanol.

The ball and the plate were hardened (62-63RC) martensitic M-50 steel (0.8% C, 4.1% Cr, 1.0% V, 4.25% Mo).

3. APPARATUS AND EXPERIMENTAL CONDITIONS

Ball/Plate Sliding Contact

In this rig an M-50 bearing ball of 20.6 mm diameter could be rotated by a horizontal shaft supported by two bearings and driven by an electric motor. The ball was loaded from the top by an M-50 plate supported by linear bearings on a horizontal loading platform in such a way that the friction force developed in the contact could be determined from the strain generated in a leaf spring connecting the plate with the loading platform. The load could be varied by hanging weights on the loading platform. The lubricants were injected into the contact from a reservoir at ambient temperature by a peristaltic pump.

The maximum Hertzian pressure was 0.1 GPa in all the experiments reported here. The ball speed was 220 revolutions per minute, corresponding to 0.2 m/s linear speed. The duration of every run was 30 minutes at which time the traction force had reached a near-steady value.

No attempt was made to control the contact temperature or to measure it. However, an estimate of the maximum surface temperature rise based on Winer's calculations [1] indicated that the temperature could have exceeded 220°C, the critical temperature for TCP/surface reaction according to Faut and Wheeler [2].

AC Phase-Locked Interference Microscope (PLIM)

This instrument, schematically shown in Fig. 1, is basically a Michelson interferometer with a laser source and microscope objectives facing two mirrors at almost equal distances from the beamsplitter. One of these mirrors is the reference mirror which is vibrated piezoelectrically at 20 KHz. The other "mirror" is the sample surface, which can be translated horizontally to bring surface features of different heights into the field of view. Reflected radiations from these mirrors are recombined at the beamsplitter and passed through another microscope objective to bring enlarged interference fringes onto a photodetector. If the two beamsplitter-to-mirror distances are equal the photodetector is "locked" into the peak of a fringe and the 20 kHz amplitude vanishes. If they are not equal, an error signal is generated, resulting in a d.c. potential on the piezoelectric crystal to shift its plane in such a way as to make the distances equal. A plot of d.c. potential against the horizontal sample position results in the "optical" profile of a surface. It is the optical profile rather than the true physical profile because in reality phases and not distances are compared and phases depend on the optical constants of the surface layer and its thickness as well as on the optical properties of the substrate. For this reason the profiles obtained with different laser wavelengths are different when different surface layers, e.g. oxides on steel, are present. From these differencies the nature and thickness of the oxides can be deduced provided some of the optical constants are independently known, e.g. ellipsometrically.

Faraday-Modulated Electronic Recording Scanning Ellipsometer (ESE)

A schematic diagram of the Faraday-modulated ellipsometer is shown in Fig. 2. This is the ellipsometer originally designed by Monin and Boutry [3], which was modified first by Sullo and Moore at the University of Rochester [4] and now by us. Radiation from the laser source S is polarized by the polarizer P, whose azimuth of vibration with respect to the plane of incidence is θ. On reflection from the sample surface M the plane-polarized radiation has become elliptically polarized. The angle of the semi-major axis of the ellipse and the plane of incidence is γ. CF is a Faraday modulator consisting of a solenoidal coil with a Faraday glass cylinder at its axis. The magnetic field generated by the coil causes the azimuth of polarized radiation of the light traveling along the axis of the cylinder to be changed proportionally to the magnitude of the magnetic field and to the length of the cylinder, the proportionality constant being called the Verdet constant. This phenomenon is known as the Faraday effect. The coil is driven by a 500 Hz oscillator, causing the magnetic field to vary with that frequency. By the Faraday effect the inclination angle

of the polarization ellipse with respect to the plane of incidence is also varied with the same frequency. The radiation from the Faraday modulator is passed through the polarization analyzer A of azimuth β and is finally detected by the photocell or photomultiplier PM.

Our instrument uses a 10 cm long, 0.6 cm diameter Faraday glass cylinder (three times as long as Sullo's) in order to obtain a large amplitude of modulation. The current in the coil is modulated with a 500 Hz frequency. If the analyzer angle β is equal to the true azimuth γ, the radiation detected at the 500 Hz frequency by phase-sensitive electronic detector is zero and the electronic system is "locked". At the same time, the amplitude of the first harmonic (1000 Hz) is monitored to make sure it is non-zero. If, however, the amplitude detected at 500 Hz is nonzero, an error signal is used to turn the analyzer by an angle appropriate to make it zero. This is done by an electro-optic transducer and control circuiting capable of resolving 0.01 degrees of arc.

Scanning of a sample surface is done by moving the sample M parallel to its plane while the polarizer is rotated at an essentially constant speed with a DC motor and the analyzer is being continuously reset at corresponding azimuths. Plots of polarizer versus analyzer angle look like the curve of Fig. 3. One method of obtaining the ellipsometric parameters ψ and Δ from this curve is graphically as shown in the figure. However, our computerized curve fitting program is much more accurate, because all the data points on the curve are used, not just a few selected ones. Furthermore, many such curves can be traced and averaged in a short time. Once Δ and ψ are known, the index of refraction n and the film thickness can be calculated, but since n is complex, consisting of two variables, more than two measurements are needed, e.g. at more angles of incidence (not just at 45°), different wavelengths, etc. The computations can become quite extensive, but are easily performed on a small laboratory computer.

By placing a microscope objective forming a real image of the sample surface ahead of the detector, sample areas as small as 20 μm in diameter can be resolved ellipsometrically. Most of the energy reflected of the surface is lost, but sufficient energy remains to make the measurements.

4. RESULTS

Tractions and Surface Roughness. Effect of the Acid Probe

Figure 4 shows traction curves for the different lubricants after the ball and plates were soaked in them for three hours at ambient temperature. The operating conditions were such that scoring or scuffing would occur very soon for the fully formulated oil, thereby allowing us to maximize the differences with respect to scoring or scuffing for the additives. Differences between the bearing surfaces for the antioxidants and TCP with and without soaking were found. The surface roughnesses (standard CLA roughness) were determined from the optical profiles and plotted in Fig. 5. The antioxidants DODPA and PANA show the least change over the measured time period within the error limits. DODPA and PANA are also the only lubricants giving a significant reduction of roughness in the initial phase of operation when the acid probe was applied Since these measurements were made in separate experiments, the consistency of the traction, roughness, and acid probe data must be significant. Another interesting observation is the sharp increase in relative roughness change after acid treatment for both BLZ and TCP in the final stage of the ball plate run, while the roughness change remained about constant during most of the run.

A closer examination of Fig. 5 reveals some interesting correlations. Since the vertical scale is arbitrary and the curves were displaced by arbitrary amounts to avoid confusion, only trends are significant. The fully formulated oil (G-MIL-99) and the two amine additives PANA and DODPA gave rise to roughness peaks at about 20 seconds. The fully formulated oil, the base oil and BTZ, the anticorrosion additive, had roughness peaks at about 80 seconds. Only TCP shows a descending slope beyond 100 seconds. These differences might be related to the formation of different surface oxides.

The two surface additives TCP and BTZ had the highest traction while the antioxidants had the lowest. All the surfaces were soaked for three hours in the respective lubricants, cleaned and dried, and then immediately used in the traction test with clean base oil (Fig. 4).

Ellipsometry of Wear Tracks

In Fig. 6, the changes of slope, $\cos \Delta / \tan \psi$, were plotted across the wear track for the samples of Fig. 4. It will be noted that TCP, which had the highest traction in Fig. 4, also shows the greatest variation over the traverse. The sharp positive and negative peaks correspond to a spot on the wear track (between 100 and 500 μm on the abscissa), which is clearly visible under the microscope. The half-widths of these peaks is about 20 μm. The slope changes for the other materials

inside the wear track were much smaller. Outside the wear track the slope variations were minimal; the bottom curve for DODPA shows the characteristic behavior there. Clearly, the nature of the surface is different inside the wear track. The change is not caused by a change of reflecting angle for the reflected laser beam is very restricted by apertures. When the angles and corresponding azimuths were changed in order to compute the film thickness and the optical constants, the former came out to be about 60 Å at the maximum and the latter correspond roughly to Fe_2O_3 by comparison with the data of Laberknight and Lustman [5]. The identification is tentative and not unique for lack of reference data, which will be obtained later.

The preferential production of a thin oxide layer on wear tracks would seem to be general, but is strongest for those produced in the presence of TCP.

It should be pointed out that the collection of data such as those of Fig. 6 persents problems different from those encountered when ellipsometry is used with dielectric substrates [6]. Most ellipsometric work today refers to dielectrics and semiconductors. The most important difference is reflectivity - high for metals and low for dielectrics and semiconductors. Furthermore, metals have a complex index of refraction (two optical constants), dielectrics only a real index of refraction.

Auger Electron Spectrograms

The plates were analyzed after the ball experiments with every lubricant. Three areas were selected, two within the wear track and one outside of it for reference. After the ball experiment, the specimens were washed with lots of alcohol and allowed to dry and not handled or treated prior to their introduction into the Auger spectrometer. As a control, a polished M-50 plate not used in a ball/plate experiment was included in the set of Auger analyses.

All the lubricants and the reference gave about the same spectra in the asreceived condition. However, after six minutes of ion bombardment, all the spectra from outside the wear scar as well as from the reference plate were essentially free of O and C while those from inside the wear scar, notably those from TCP and perhaps also from BTZ had a higher O and C content.

In order to show the effect of ion bombardment on elemental composition, the plots of Fig. 7 were drawn for two position within the wear scar. They present the ratios of the O and C peaks to one of the Fe peaks as a function of time. A sharp change of slope after two-to-four minutes probably signifies the removal of a surface layer.

From these observations, the following deductions would seem to be reasonable:

1. The high C-ratios and O-ratios in the outermost surface layer are probably atmospheric contamination. They are present even in the reference.
2. TCP and GMIL (also containing TCP) have an oxide layer under the atmospheric contamination layer. BTZ is likely to have one as well. The reference, however, does not have such a layer within our error of measurement, but the other materials might have a weak oxide layer.
3. A carbide layer might also underly the atmospheric contamination layer.

5. DISCUSSION AND CONCLUSIONS

In our previous publications [7],[8] the difference in the effect of dilute hydrochloric acid (our acid probe) on causing contour changes within and outside a wear track was described, this difference being especially great when scuffing conditions were approached. It was also found that the presence of the antiwear additive TCP in the lubricant would enhance this difference. Then the question was raised why scuffing could occur so suddenly, apparently without warning, even though operating conditions could have been far from those postulated by the Blok temperature criterion. A principal objective of this study was to try to explain the behavior of the acid probe in the hope that an answer there would also help toward arriving at an answer to the latter question.

Differences in the optical profile at different wavelengths, ellipsometry, and Auger electron spectroscopy have now been shown to discriminate between the surface within the wear track on M-50 steel and outside of it. The evidence points to a higher concentration of an oxide, most likely iron oxide, within the wear track than outside. Interestingly enough, it would seem that TCP promotes the formation of such an oxide. Such an oxide would react much faster chemically with acid than the alloy steel itself. Thus, the oxide would explain the behavior of the hydrochloric acid probe. The oxide is more likely to be formed in the wear track than outside of it because of the higher surface temperature in the wear track. It would also reduce friction at higher temperatures, though not at low ones and explain both our data of Fig. 4 and the results of Faut and Wheeler [2]. Although such an iron oxide layer on the surface could conceivably promote the formation of friction polymer--whose formation was reported to be enhanced by TCP also--it is more likely that the same oxidizing conditions that lead to

the formation of the oxide also lead to the formation of friction polymer. Since friction polymer is, in turn, related to acid sludge and the acid is likely to react quickly with the basic iron oxide, provided the temperature is high enough, a case could be made for a mechanism of scuffing, viz. removal of the oxide layer by reaction with acids in the lubricant exposing the nascent metal and allowing metal-to-metal welds. Work now in progress in our laboratory will test this idea.

A new metallurgical phase for M-50 steel was also found and reported in our earlier publication [8]. Its etching characteristics seemed to identify it as a carbide. The higher carbon contents found in the wear track below the surface, expecially for TCP, are consistent with this identification.

The sharp initial decrease in the ball experiment of acid probe reactivity of the two amine antioxidants (Fig. 7) can be explained by the initial formation of an amine surface film and subsequent exposure of the original alloy steel surface, i.e., the lack of a surface oxide. Since the metal reacts more slowly than the oxide--which was prevented from forming--the probe reaction slows down. Once the amine antioxidant is exhausted, the reaction speeds up again, however, thus explaining the increased activity later. The amine surface film could also be instrumental in reducing traction.

The behavior of BTZ, the anticorrosion additive, has been found to be similar to TCP in some ways. Its low oil solubility requires its small concentration. By the same token, it is more likely to come out of solution and coat the bearing surfaces with an anodic [9] layer. However, as Parkins [9] admits, the behavior of these materials is still not well understood, even by electrochemists, though they have been used for a long time.

Thus, it would seem that leads have been generated to help in the design of lubricating materials to reduce traction and scuffing failure. Their chemical interaction with the bearing surfaces, i.e., the formation of oxide and perhaps other layers is an important key.

6. ACKNOWLEDGEMENT

This work was sponsored by a grant from NASA-Lewis Research Center, NAG 3-222. Additional funding was provided by the Air Force Office of Scientific Research, Grant No. AFOSR-81-0005 and by a grant from the Army Research Office, Grant No. DAAG 2483K0058.

7. REFERENCES

1. Ausherman, V.K., Nagaraj, H.S., Sanborn, D.W., and Winer, W.O., "Infrared Temperature Mapping in Elastohydrodynamic Lubrication," Transactions ASME, F, 98, 236 (1976).

2. Faut, O.D., and Wheeler, D.R., "On the Mechanism of Lubrication by Tricresylphosphate (TCP) - The Coefficient of Friction as a Function of Temperature for TCP on M-50 Steel," ASLE Transactions, 26, 3, 344-350 (1983).

3. Monin, J., and Boutry, G.-A, "Concept, Realization and Performance of a New Ellipsometer," Nouv. Rev. Optique, 4, 159-169 (1973).

4. Sullo, Nancy J., "Measurement of Absolutue Refractive Index Profiles in Gradient Index Materials Using Modulation Ellisometry." M.S. Thesis, Institute of Optics, University of Rochester, supervised by Professor Duncan T. Moore.

5. Leberknight, C.E., and Lustman, B., "An Optical Investigation of Oxide Films on Metals," J. Opt. Soc. Am., 29, 59-66, (1939).

6. Vedam, K., The Characterization of Materials in Research: Ceramics and Polymers. J.J. Burke and V. Weiss, Eds. Syracuse University Press, 1975, pp. 503-537.

7. Lauer, J .L., and Fung, S.S., "Microscopic Contour Changes of Tribological Surfaces by Chemical and Mechanical Action," ASLE Transactions, 26, 430-436 (1983).

8. Lauer, J.L., Fung, S.S., and Jones, W.R. Jr., "Topological Reaction Rate Measurements Related to Scuffing," ASLE Preprint No. 83-LC-2B-1. Presented at the ASME/ ASLE Lubrication Conference in Hartford, CT, October 18-20, 1983.

9. Parkins, R.N.: Corrosion Inhibition, in Comprehensive Treatise of Electrochemistry, Vol. 4, Electrochemical Materials Science, J. O'M Bockris, B.E. Conway, E. Yeager, and R.E. White, eds., Plenum Press, New York, 1981, pp. 313-315.

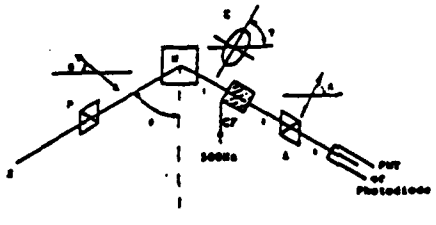

Fig. 2 - Schematic drawing of ellipsometer.

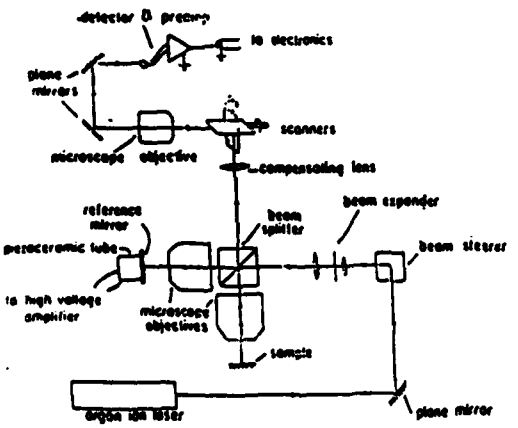

Fig. 1 - Schematic drawing of laser interferometer.

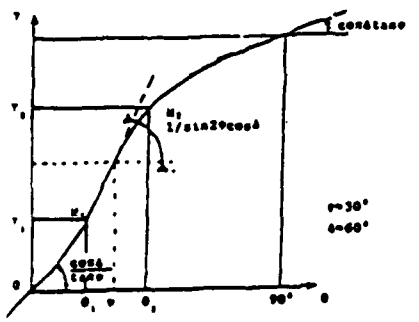

Fig. 3 - Determination of the ellipsometer parameters.

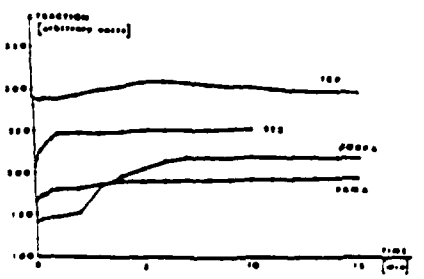

Fig. 4 - Tractions for different lubricants.

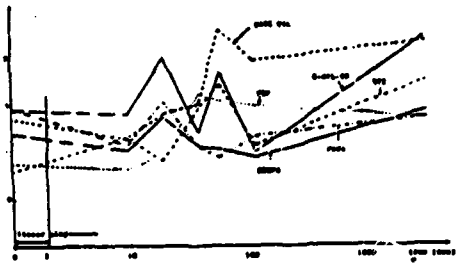

Fig. 5 - Roughness changes with operating time

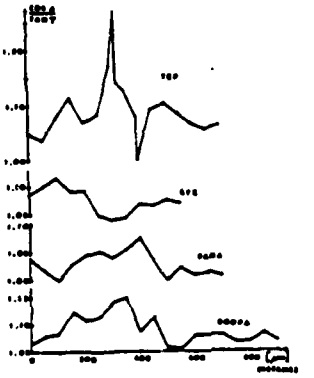

Fig. 6 - Ellipsometric slopes over a wear track traverse for different lubricants.

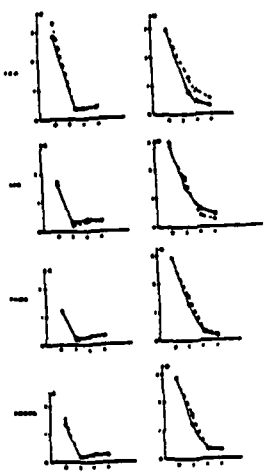

Fig. 7 - Ratio of a carbon to an iron Auger peak (left) and of an oxygen to the same iron peak (right) for ion bombardment times of zero to six minutes (10 Å are removed per minute). The solid and broken lines refer to two different spots within the wear track.

END

FILMED

1-85

DTIC